U.PORTO

FEUP FACULDADE DE ENGENHARIA
UNIVERSIDADE DO PORTO

IMPACT OF CFRP ADHESIVE JOINTS FOR THE AUTOMOTIVE INDUSTRY

Submitted by
Joana Filipa Dias Varajão

MSc THESIS

Supervised by: Lucas Filipe Martins Silva
Co-supervised by: Rodrigo Avendaño Mata

Mestrado Integrado em Engenharia Mecânica

July 2015

Impact of CFRP adhesive joints for the automotive industry

Joana Filipa Dias Varajão

Mestrado Integrado em Engenharia Mecânica

July 2014

“Se puderes olhar vê, se puderes ver repara”

José Saramago

À minha família

ACKNOWLEDGEMENTS

First of all, I would like to express my gratitude to Prof. Lucas da Silva, my supervisor, for the opportunity to collaborate in this work.

I would like to thank the help and valuable patience provided by Rodrigo, my co-supervisor, during the development and execution of this dissertation.

I also would like to thank my colleagues for their support, especially Mariana and Sofia and all the personnel in the FEUP Adhesives Group, Tânia and Daniel, for the help and company in the long hours spent studying adhesives and developing this dissertation.

Special thanks to Mr. Miguel Figueiredo from the *Laboratório de Ensaios Tecnológicos (LET)* for his help while performing the impact tests.

Lastly and the most important I would like to express my gratitude to my family and friends, specially my parents and boyfriend, for all the support, encouragement and patience for helping me going through all these years.

ABSTRACT

In the recent years there has been an increasing interest in the automotive industry in applying adhesive bonding in structural components of vehicles. Adhesive joints permit to join complex shapes and can provide exceptional strength while reducing the weight of structures. Moreover, other mechanical fastenings such as bolts or rivets are not suitable for fiber-reinforced composites due to the stress concentrations that occur in the vicinity of the bolts and rivets. When adhesive joints are used in this area, some factors such as impact loading have a decisive factor. Under impact conditions, the joints must provide enough strength to transmit the load without fracturing, and thus assure the car's integrity.

The main objective of this study was to characterize the impact strength of carbon fibre reinforced plastics (CFRP) single lap joints using a brittle and a ductile epoxy adhesive. To achieve this, SLJs were tested in a drop weight impact machine, in order to simulate real situations. Quasi static-tests were also performed for obtaining the comparison between static and impact conditions.

In order to determine the properties of adhesives, tensile bulk tests were performed to get the tensile properties as a function of strain rate. The standard thick adherend shear test (TAST) was performed so that to measure the shear properties at two different strain rates. Finally, the end-notch flexure (ENF) tests were carried out with the purpose of determining the mode II critical strain energy release rate (G_{IIc}).

The numerical models of adhesively bonded joints using cohesive zone models were developed in ABAQUS ® and the numerical results were validated with experimental results.

The overall results of this dissertation show that different overlap lengths affect considerably the impact response of the composite SLJs. From quasi-static to impact conditions an increase in the joint strength was perceptible. The results obtained by the use of analytical and numerical predictions are in a good agreement with the experiments.

RESUMO

Recentemente tem havido um crescente interesse na industria automóvel em aplicar as juntas adesivas em componentes estruturais dos veículos. As ligações adesivas permitem ligar formas complexas e podem providenciar resistências mecânicas exceptionais e ao mesmo tempo reduzem o peso das estruturas. Para além disso, outro tipo de ligações mecânicas que usam parafusos ou rebites não são adequadas para compósitos devido à concentração de tensões que estes elementos criam. Quando as juntas adesivas são utilizadas na indústria automóvel, alguns factores como o impacto tem um factor decisivo. Em condições de impacto, as juntas tem que garantir resistência suficiente de forma a transmitir a carga sem fracturar à junta e desta forma assegurar a integridade do veículo.

O principal objectivo deste trabalho foi caracterizar a resistência ao impacto das juntas de sobreposição simples com substratos em CFRP utilizando para o efeito um adesivo ductil e um adesivo frágil. Deste modo, SLJs foram testadas numa máquina de impacto de forma a simular as situações reais. Os testes estáticos também foram realizados para se obter a comparação entre as condições estáticas e de impacto.

Para determinar as propriedades dos adesivos, testes de tração foram realizados de forma a obter as propriedades de tração em função de velocidade de deformação. As propriedades de corte foram determinadas com testes TAST a diferentes velocidades. Finalmente, testes ENF foram levados a cabo com o propósito de determinar a tenacidade à fractura em modo II.

Modelos númericos de juntas adesivas usando elementos coesivos foram desenvolvidos no software ABAQUS e os resultados numéricos foram validados com os resultados experimentais.

Os resultados apresentados nesta dissertação mostram que diferentes comprimentos de sobreposição afectam consideravelmente a resposta ao impacto das juntas de sobreposição simples. De condições estáticas para condições de impacto, um aumento na resistência da junta foi perceptível. Os resultados obtidos através do uso de previsões numéricas e analíticas tiveram boa concordância com o trabalho experimental realizado.

CONTENTS

LIST OF ACRONYMS

DCB Double cantilever beam

ENF End notched flexure

SLJ Single lap joint

CBBM Compliance based beam method

RT Room temperature

CFRP Carbon fiber reinforced polymer

CZM Cohesive zone models

TAST Thick adherend shear test

FEA Finite element analysis

FEM Finite element method

UTS Uniaxial tensile strength

NOTATION

b Joint width

l Overlap length

t Adherend thickness

P Load applied

$\bar{P}$ Applied load per unit width

M Bending moment

V Transverse force

k Bending Moment Factor

k' Transverse Force Factor

τ Shear stress

ε Strain

E Young's Modulus

δ Displacement

G_{Ic} Critical strain energy release rate or fracture toughness in pure mode I

G_{IIc} Critical strain energy release rate or fracture toughness in pure mode II

T_g Glass transition temperature

P_a Failure load of the joint

τ_y Adhesive yield adhesive s

σ_t Direct tensile stress

σ_s Stress at the inner adherend surface

P_Y Maximum load which only creates adherend yield

σ_Y Yield strength

P_s Maximum load which only creates adherend yield

$\dot{\varepsilon}_e$ Elastic deformation

$\dot{\varepsilon}_p$ Plastic deformation

t_a Adhesive thickness

LIST OF FIGURES

LIST OF TABLES

Chapter 1

INTRODUCTION

This dissertation presents results of impact and static tests performed on adhesive joints with CFRP. Experimental and numerical studies were carried out during this work and comparisons between them were also done.

In this chapter, a brief introduction to adhesive bonding and composite materials is presented as well as the motivation and objectives behind this thesis. Finally, the organization of the work is also presented.

1.1 Background and motivation

Adhesively bonded joints are increasingly used in the automotive industry. In this industry, an essential factor to considerer when joining different parts of a vehicle by adhesion is the resistance to impact loads. Therefore, the adhesives need to provide high impact resistance and deform significantly without breaking, absorbing enough energy to keep the parts together.

The need to reduce the weight of vehicles is also increasing the use of composites. Composite materials are combinations of two or more different materials and are characterized by their constituent mechanical properties, owning generally high stiffness, high strength and low density. Their behaviour when bonded is completely different from metals and very few studies can be found in literature, especially under impact loads. The automotive industry mainly focuses on the delamination resistance of CFRP laminates and/or the fracture behaviour of joints. Different impact tests have been used to quantify the maximum load and energy absorbed in adhesive joints with composite adherends. This dissertation has therefore the main goal of studying the impact response of CFRP adhesive joints. To do so, experimental tests were performed and observations were made to quantify and to describe the behaviour of these adhesive joints in terms of their impact response.

1.2 Objectives

The main objective of this thesis is to investigate the CFRP adherends bonded with two different adhesives (a ductile and brittle adhesive) in order to show the importance of the

adhesive on the joint impact behavior. For that, CFRP adhesive joints were tested under impact load at room temperature.

1.3 Research methodology

To achieve the main aim of this work, partial objectives needed to be completed and are described in this section. The following tasks were conducted in the respective order to assure the success of the research:

(a) Carry out a bibliographic review of adhesive bonding, composite materials, as well as impact testing methods.

(b) Manufacture of CFRP laminates in order to produce the SLJs and perform the static and impact tests.

(c) Perform tensile tests of the CFRP used for the adherends to determine the mechanical properties in two different directions and two different strain rates (longitudinal and transverse).

(d) Perform bulk tests of adhesive at two different strain rates (1 mm/min and 100 mm/min) in order to understand the influence of strain rate on adhesive properties.

(e) Perform the ENF test to determine the G_{IIC}.

(f) Perform the impact and quasi-static tests at room temperature (RT).

(g) Accomplish SLJs numerical analysis using Cohesive Zone Models (CZM), predicting the maximum values of load and displacement in order to compare with experimental results.

1.4 Dissertation outline

This dissertation is organized in six chapters, including the introduction and conclusions. The first chapter introduces the work that was developed and that will be described in the following chapters. This is where the motivation and the objectives of this work are described.

Chapter 2 of this dissertation reports the literature review. An introduction to adhesive bonding is done, starting by describing the general properties of adhesives and due to its importance, a description of the structural adhesives is also presented. The studies of adhesives under impact load and the high strain rate properties of adhesives are described here. A brief description of composite materials is presented as well as the more relevant properties of CFRP. Moreover, the main failure modes in composite materials are referred. Finally, the joints with composite adherends are described along with some examples of works using them.

Chapter 3 describes the experimental details where the fracture, tensile and shear tests were conducted to characterize the adhesives and adherend at different strain rates. The joint

geometry and manufacture process is presented as well as all the information relative to the joint testing.

Chapter 4 emphasizes on the numerical details. Here, a 2D Finite element model was built and the static and impact conditions were simulated using a CZM.

Chapter 5 presents the experimental results for quasi-static and impact tests. The load displacement curves are shown as well as the values comparison and analyse is done. In addition, the joint strength prediction by CZM is presented. The discussion performed concerning the experimental and numerical results is also shown.

Chapter 6 presents the main conclusions regarding the carried out work. Finally, future works are suggested in order to continue the research of this study.

Chapter 2

In this chapter, the more relevant concepts of adhesive joints are introduced, as well as the properties of adhesive joints. Due to its importance, a description of analytical models is also presented as well as a brief reference to impact load. Composite materials are also described including the failure modes and the high strain rate dependence of these materials.

LITERATURE REVIEW

2.1 Adhesive joints- an introduction

There are many ways to define an adhesive. According to [1] "an adhesive may be defined as a material that when applied to surfaces of materials can join them together and resist separation. The materials being joined are commonly referred to as substrates or adherends".

The adhesives which can resist substantial loads are called structural adhesives. A structural adhesive is responsible for the strength and stiffness of the structure. Their shear strength can vary from 5MPa for polyurethanes to 50MPa for an epoxy adhesive. They have been used within different fields, for example in the automotive industry, adhesive bonding techniques are applied to bond elements to the cars' body and to assemble structural parts. On the other hand, the non-structural adhesives are used to hold lightweight materials and are not required to support substantial loads [2], [3].

The main structure of an adhesive joint consists in two substrates, also denominated adherends (the term generally used after bond). Their function is to bind two surfaces by applying adhesive to attach them. The region between the adhesive and the adherend is referred to as the interphase. Inside this region there is the interface, defined as the plane of contact between the surface and two materials [2]. The use of adhesive bonded joints in engineering applications is increasing compared to other joining techniques due to advantages such as:

- More uniform stress distribution along the bonded area when compared with bolted or riveted connections. Consequently, they enable to have a higher stiffness and load transmission (see Figure 1);

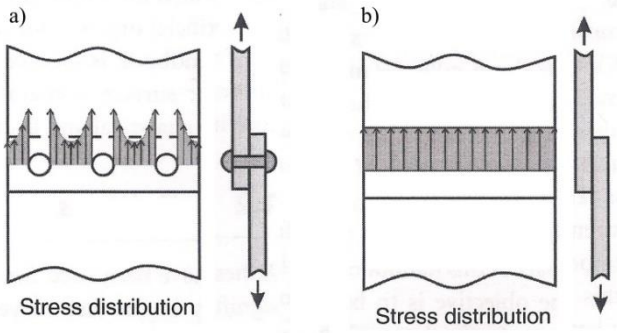

Figure 1- Illustration of the stress distribution comparison between the riveted joints and adhesively bonded, respectively. [2]

- Reducing the weight and thus the cost;
- Adhesives can bond dissimilar materials with different coefficients of thermal expansion since the adhesive flexibility can compensate the difference;
- They are highly efficient since it is easy to create an automatic process to apply them;
- High fatigue resistance [4],[6].

On the other hand, adhesives are also associated to some **disadvantages,** which opens doors for more technological research and development:

- It is necessary to reduce the peeling and cleavage stresses because they concentrate the load in a small area, resulting in a poor joint strength;
- Lower resistance to temperature and humidity conditions due to the polymeric nature of the adhesive;
- A careful surface preparation is necessary such as solvent cleaning, mechanical abrasion, or chemical treatments;
- Difficulty in the detection of defects related to poor adhesion in adhesive bonds without the use of destructive methods;
- To attain long service-life from adhesive joints in very severe and hostile environments may often require the use of a surface pretreatment process for the substrates being joined [1], [4], [5].

Concerning the failures modes, there are two possibilities that can occur on the adhesive joint: adhesion and cohesion. It is necessary to understand these two concepts.

Adhesion is defined as the attraction between two substances resulting from intermolecular forces that are established between them. Adhesion failure, usually characterized by interfacial failure, can occur due to inadequate or ineffective surface preparation [4], [7].

This concept is different from that of **cohesion,** which only involves intermolecular forces inside one substance. Thus, various factors can be enumerated for cohesion failure such as:

- ✓ Inadequate overlap length;
- ✓ Thermal stresses;
- ✓ Gross void defects (production)[8].

After understanding the terms of adhesion and cohesion, it is necessary to understand the main differences between cohesive and adhesive failures. Thus, the Figure 2 illustrates that the adhesive joint can break by cohesion, adhesion or a combination of the two [2], [4].

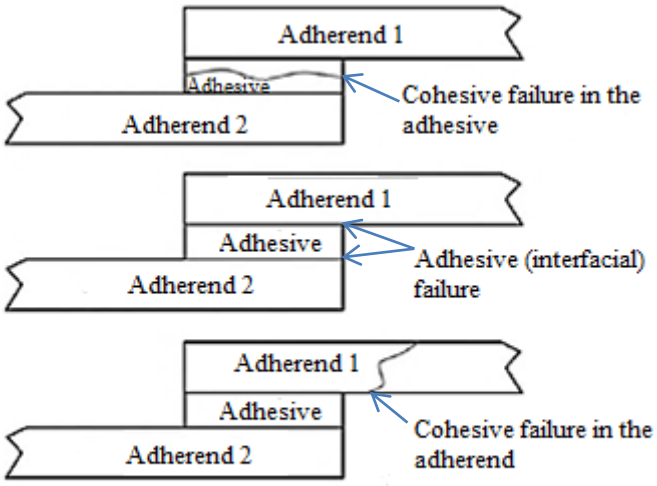

Figure 2- Examples of cohesive and adhesive failures (adapted from [4]**).**

When considering adhesive bonded joints there are various types of stresses which are normally reffered to as shown in Figure 3.

- Normal or direct stresses (these are normal to the plane on which they act and can be compressive or tensile);
- Shear stress (it is parallel to the plane on which they act);
- Peel stress (which appears if one or both of the substrates are flexible)
- Cleavage (which typically appears as the result of an offset tensile force or bending moment).

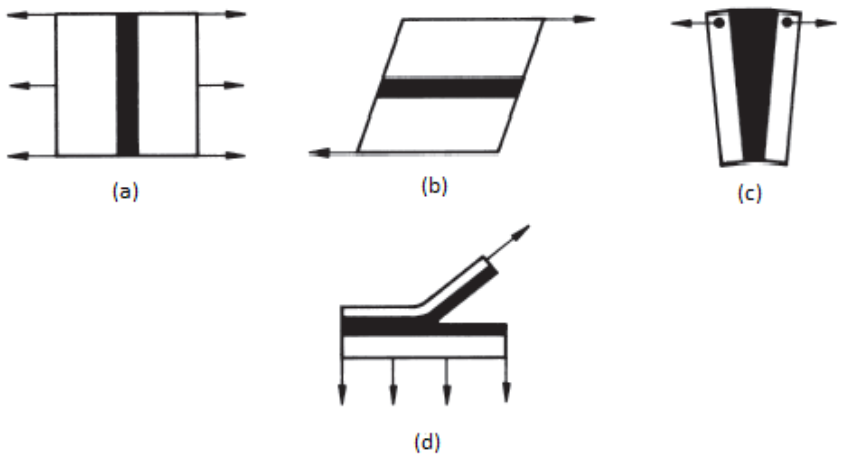

Figure 3-Types of stresses in adhesive joints. (a) normal (or direct) stress, (b) shear stress, (c) cleavage, (d) peel stress (Adapted from [1])

It is important to mention that a joint needs to be designed to avoid peel. Nevertheless, if peel and cleavage forces are inevitable, then some means of distributing the load must be found. An example of a way to suppress these forces is the use of local mechanical restraints, such as rivets, bolts or spot welds [9].

According to [10] "Joints represent one of the greatest challenges in the design of structures in general and in composite structures in particular since they entail discontinuities in the geometry of the structure and/or material properties and introduce high local stress concentrations". There is a vast amount of adhesive joint configurations that can be found in literature. However, the more common joint configurations (see Figure 4) that have been deeply analyzed in the literature are:

- Single-lap joints;
- Double-lap joints;
- Scarf joints;
- Stepped-lap joints.

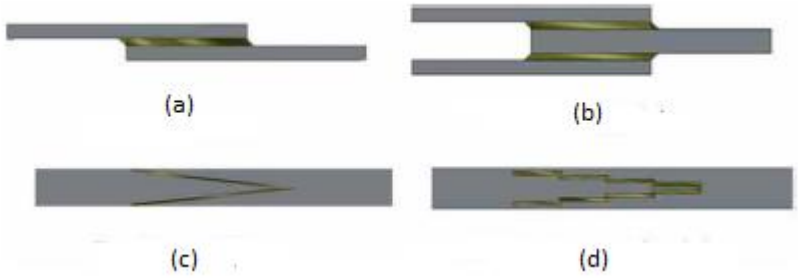

Figure 4- Adhesive bonded joints configurations. (a) single lap joint, (b) double lap joint, (c) double scarf joint, (d) double stepped-lap joint (adapted from [10])

In addition, other types of configurations have also been studied, such as:

- strap joints;
- butt joints,
- butt strap joints;
- corner joints;
- stepped-scarf joints;
- T-shaped joints;
- L-shaped joints. [10]

As for the single lap joint (sometimes, denominated by SLJ), this is one of the most representative joints according to reality, which is why it is the configuration used more often for testing adhesives. However, the stress state is complex [5].

There are many reasons why the single lap joint is the most popular geometry. One of them is that a lap joint has simple and convenient geometry for evaluating adhesive joints as can be proven by its frequent use in the standard test methods [1].

Depending on the approach, each component of the adhesive joint can be regarded as either a simplified 2D representation or a full 3D model of the joint [11].

There are two ways to predict the stress distribution in an adhesive joint. The first one is by using a numerical simulation (numerical method) such as the finite element analysis (FEA) and the second solution is to use a closed-form model. The last one is more appropriate for a fast and easy answer [12].

2.1.1 Adhesive joint properties

Adhesives have been classified in different ways. The most general classification is to differentiate them between natural and synthetic adhesives. Natural adhesives are produced from the natural resources such as starch, casein glues or natural rubber. The synthetic adhesive group corresponds to those which are designed and manufactured by man, such as polymers. These types of adhesives are the most commonly used due to their mechanical, physical and chemical properties which are superior to natural ones [2], [13] . However, the classification in synthetics and natural adhesives is not specific enough for the many applications. Therefore, in the industry more factors are considered to assort the adhesives, such as: function, chemical composition, physical form and reaction method.

Regarding to the function there are two important groups that we can distinguish such as: structural and non-structural adhesives. Engineering and structural adhesives are distinguished from other adhesives by being high strength materials that are designed to support loads, often substantial loads. On the other hand, non-structural adhesives are divided in other groups depending on their application, as pressure sensitive tapes, hot melts, or packaging adhesives [2], [14].

Classification based on chemical composition describes adhesives as thermoplastics, thermosets, elastomers or hybrids adhesives. One of the main differences in their behavior lies on their glass transition temperature (T_g). Thermosetting adhesives cannot be heated and melted repeatedly after the initial cure. Some of these adhesives require pressure and others need only contact pressure. They are provided as one-part or two-part systems. In case of thermoplastic adhesives, they do not cure with heat and are not recommended for working temperatures above 66℃. Elastomers adhesives can be divided in thermosetting and thermoplastic adhesives. Curing varies, depending on the type and the form of adhesive. Finally, hybrid adhesives are made by combining thermosetting, thermoplastic, or elastomeric resins into a single adhesive formulation. These hybrid adhesive systems possess high peel, impact, and shear strengths without sacrificing high temperature or chemical resistance properties [2], [4], [6].

Finally, other adhesive classifications exist based on the physical form (liquid, paste, powder and film), their type of reaction method (by chemical reaction, loss of solvent and water, cooling from a melt) [4].

2.1.2 Structural adhesives

By definition a structural adhesive is one used when a substantial load is required to cause separation [5].

In the beginning of this chapter a brief definition about structural adhesives was done. In this section, they are analyzed with more detail. Thus, the more important situations generally associated with a structural adhesive joint are listed in the following topics:

- High-strength adherends are involved;
- The adhesive is capable of structural integrity, within the design limits for the bonded structure;
- The bonded structure maintains integrity over long periods of time in typical service environments [15].

The most common structural adhesives properties in the automotive industry are shown in Table 1.

Table 1- Comparative values of some mechanical properties of common structural adhesives (adapted from ([4])).

Adhesive type	Relative density	Young's modulus (GPa)	Shear modulus (GPa)	Tensile strength (MPa)
Epoxy	1.3	3	1.2	60
Polyurethanes	1.1	0.02	0.008	40

Considering this, it is essential to know more detailed information for each adhesive which is given below.

❖ Epoxies

Generally, toughened, single-part paste epoxies are used for structural bonding of car body shells due their strength and stiffness. This type of adhesives has an improved impact and peel strength compared to the previous generation of brittle epoxy adhesives. They are possibly the most versatile family of adhesives because they bond well to many substrates and form strong and durable joints. A list of information is presented in Table 2 [14], [16], [17].

Table 2-Typical properties and comments of epoxies adhesives (adapted from [2], [10]).

Physical forms	Available in one or two parts
Service temperature	-40 to 100 ℃ for one-part, 40 to 180 ℃ for two-part
Comments	High strength and temperature resistance, good corrosion resistance, easy to use and relatively low cost
Applications	Aircraft, helicopters, trains, cars, sports equipment

❖ Polyurethanes

Polyurethane is described as “one of the most versatile chemistries for adhesives and sealants”. Moreover, these adhesives can cure at room or elevated temperature and they are flexible and have both relatively high shear and peel strength. They have important advantages in terms of damping, impact, fatigue, and safety which are critical factors in the automotive industry. The typical properties of polyurethanes adhesives are shown in Table 3 [14], [16].

Table 3- Typical properties and comments of polyurethanes adhesives.

Physical forms	One-part and two-part systems
Service temperature	-40℃ to 80℃
Comments	Excellent flexibility at low temperatures and resistant to fatigue, high toughness and durability, cure occurs at room temperature
Applications	Automotive industry, cryogenic applications and shoe industry

The values and properties presented above are only indicative and the variety of adhesives in each group is very wide. The adhesive selection process is difficult and includes many others factors such as: type and nature of substrates to be bonded, costs, adhesive application method and stresses that the joint will face in service.

2.1.3 Adherend properties

Focusing on the adherend material, although new materials like plastics and composites have replaced metals in many industries, metals will continue to be used where their unique combination of properties such as high strength and high temperature resistance are coupled with low cost. In the automotive industry, a mix of mild, high- and highest-strength steels are prevalent in vehicle bodyshells. During vehicle assembly, carbon fibre composite materials are increasingly used in attachment parts such as roofs and flaps (see Figure 5). The lightweight construction potential of these materials becomes evident in the density differences as compared to steel. Table 4 shows the more commons adherend materials and their main mechanical properties [18].

Figure 5- Potential application areas of bonded hybrid composites [18].

Table 4- Common adherends indicative mechanical properties (adapted from [4]).

Material	Relative density	Young's modulus (GPa)	Shear modulus (GPa)	Tensile strength (MPa)
Mild steel	7.5	210	80	450
Aluminium	2.6	70	26	550
Carbon fiber reinforced composite	1.55	110	45	800

2.1.4 Single Lap Joints mechanics - analytical approach

This simplest approach to study a SLJ assumes that the substrates are rigid. In this case, the adhesive is considered to deform only in shear and the adherends to be rigid, and the shear stress is considered constant along the overlap. Figure 6 shows a uniform shear stress distribution that is generated [19], [20].

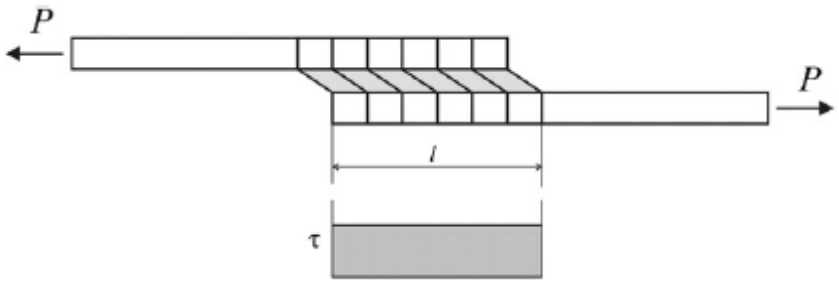

Figure 6-Uniform adhesive shear stress.

The adhesive shear stress (τ) is given by:

Where:

$$\tau = \frac{P}{bl} \quad \text{(eq. 1)}$$

P - Load applied;

b - Joint width;

l- Overlap length.

This analysis is not very accurate due to many simplifications. However, it is still used to easily determine the adhesive shear strength in many test situations [12].

2.1.4.1 Volkersen's shear lag analysis

This approach was developed by Volkersen and assumes that the adhesive deforms only in shear but that the adherends can deform in tension (elastic). This happens because they are considered elastic and not rigid. Figure 7 shows the differential shear in adherends [12].

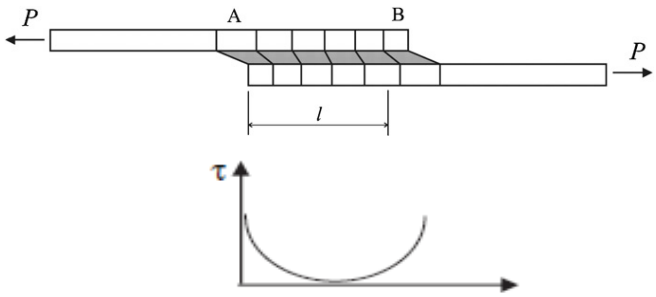

Figure 7- Deformation occurred in a Single Lap Joint with elastic adherends and shear stress distribution along the overlap. (adapted from ([19]))

However, the Volkersen solution does not reflect the effects of the adherend bending and shear deformations. These are significant for composite adherends with a low shear and transverse modulus [10].

Thus, this analysis is more suitable for double lap joints (DLB) than single lap joints (SLJ) since in a DLJ the bending of the adherends is not as significant as in the SLJ [12].

2.1.4.2 Goland and Reissner's analysis

The analysis developed by Goland and Reissner in 1944 [21] for the single lap joint can be applied to an arbitrary end loaded single overlap configuration. Thus, this analysis can be applied to single overlap joints but also to many other configurations.

In this model, the bending moment is considered as well as the transverse force that occurs due to the non-collinearity of the applied load, which causes the joint to rotate until the end of the load application, as shown in Figure 8.

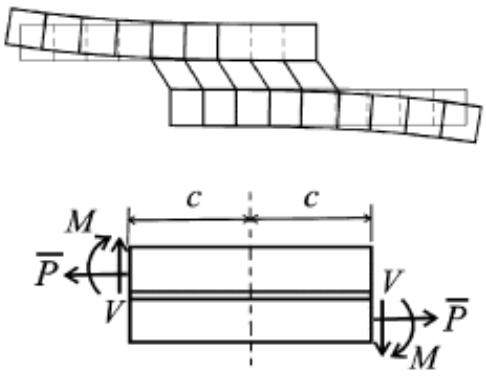

Figure 8- Goland and Reissner's model.

Because of this rotation of the joint, the bending moment will decrease, making way for a nonlinear geometric problem where the effects of the large deflections of the adherends must be accounted [20].

In this method a bending moment factor (k) is used as well as a transverse force factor (k') that relates the applied tensile load per unit width $(\bar{P})$ to the bending moment (M) and the transverse force (V) at the overlap ends. If the joint does not rotate, the value of the factors will be approximately equal to 1.

Figure 9 shows the adhesive shear and peel stress distributions for aluminium alloy adherends and an epoxy adhesive proposed by Goland and Reissner.

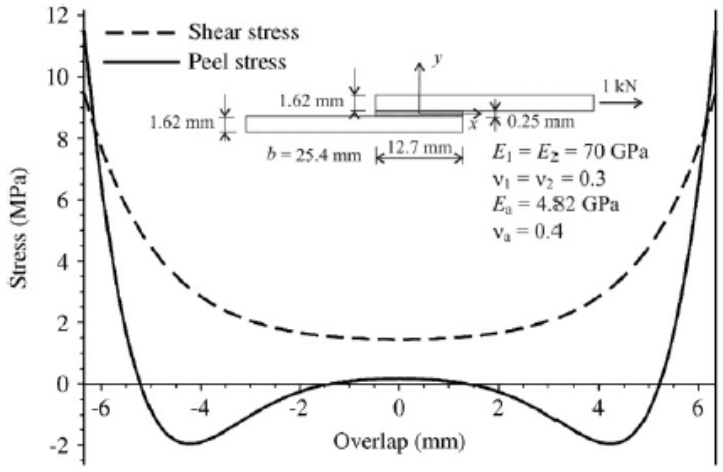

Figure 9-Goland and Reissner's adhesive shear and peel stress distributions for aluminium alloy adherends and an epoxy adhesive [12].

2.1.4.3 Hart-Smith's analysis

The analysis done by Volkersen, Reissner and Goland are based on an elastic behavior. However, the adhesive and adherend may become non-linear or plastic.

Thus, in 1973, Hart-Smith [22] accounted for adhesive plasticity, using an elastic-plastic shear stress model. As shown in Figure 10, Hart-Smith chose an elasto-plastic model such that the ultimate shear stress and strain in the model are equal to the ultimate shear stress and strain of the adhesive, the two curves having the same strain energy. The maximum lap joint strength was calculated by using the maximum shear strain as the failure criterion [5], [12].

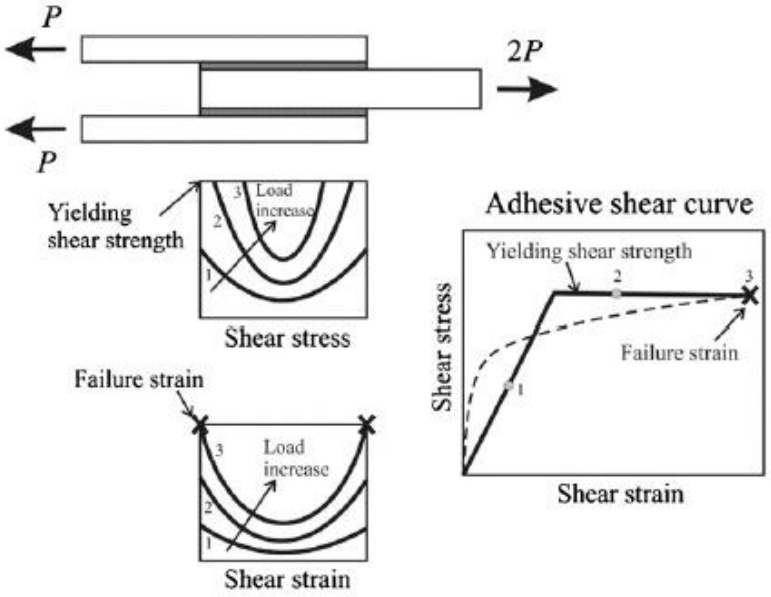

Figure 10- Schematic explanation of shear plastic deformation of the adhesive according to Hart-Smith.

However, the Hart-Smith analysis exhibits some mistakes. The model neglected the large deflection in the overlap and considered deflection only in the outer adherend. Therefore, this model is limited to the case of short overlaps and thin flexible adhesives. In that sense, Oplinger included large deflections in the overlap region and considered the effect of bond layer thickness on stress distribution in the adhesive [23].

2.1.4.4 Adams

For the many cases in which the substrates will yield (e.g. aluminium or low strength steel), Adams developed a simple methodology to predict the joint strength.

If the adhesive is very ductile, typically with more than 20% shear strain to failure and the adherends are elastic, the joint strength is given by the load corresponding to the total plastic deformation.

For the adherends that yield, a constant level is reached for a certain value of overlap corresponding to the yielding of the adherend. For a brittle adhesive and elastic adherends, the methodology can't be used and the author suggests using the finite element method (FEM) [5], [24].

As shown in Figure 11, the failure load of the adhesive joint corresponds to the total plastic deformation of the adhesive and it is designated by P_a :

$$P_a = \tau_y \text{bl} \quad \text{(eq. 2)}$$

Where P_a represents the failure load of the joint, τ_y is the adhesive yield strength, b is the joint width and l the overlap length. The formula above is used when we have elastic adherends and ductile adhesives.

The direct tensile stress σ_t acting in the adherend due to the applied load P is given by:

$$\sigma_t = \frac{P}{bt} \quad \text{(eq. 3)}$$

where t is the adherend thickness. When a bending moment (M) appears, the stress at the inner adherend surface (σ_s) is

$$\sigma_s = \frac{6M}{bt^2} \quad \text{(eq. 4)}$$

Where $M = kPt/2$ (according to Goland and Reissner's model). The variable k represents the bending moment factor that is reduced from unity as the lap rotates under load. The stress acting in the adherend is calculated as the sum of two stresses. Therefore, the maximum load that can be carried which only creates adherend yield (P_Y) is given by:

$$P_Y = \sigma_Y bt/(1 + 3k) \quad \text{(eq. 5)}$$

where σ_Y represents the yield strength of the adherend. For low loads and short overlaps, the value of bending moment factor (k) is approximately 1. For this case,

$$l/t \geq 20, P_Y = \sigma_Y bt/4 \quad \text{(eq. 6)}$$

If the relation was verified, the value for k is considered 0.

On the other hand, P_s represents the maximum load that can be carried which just creates adherend yielding.

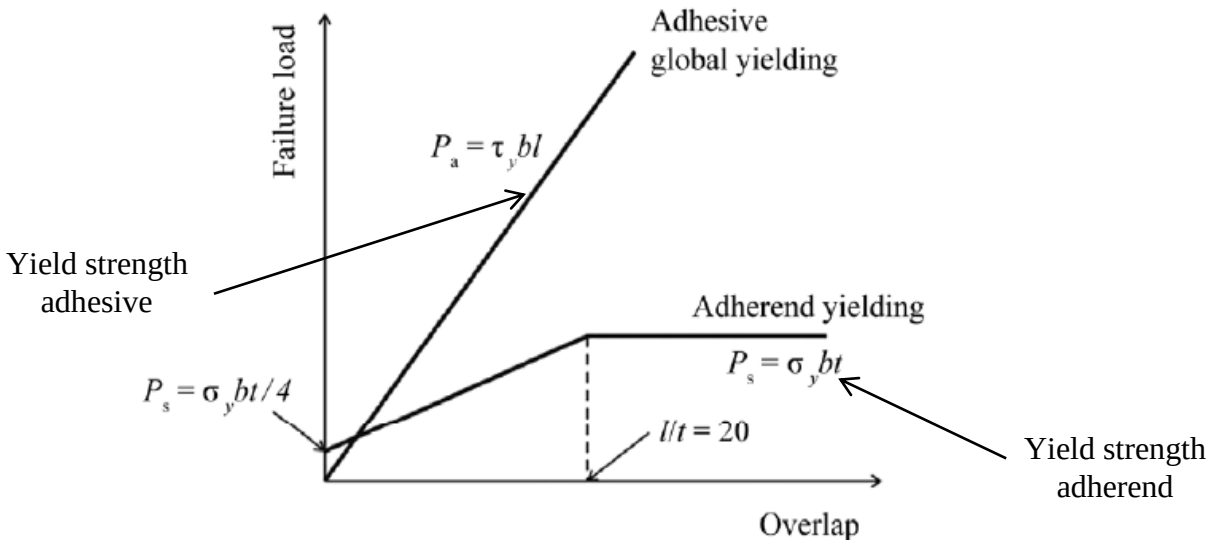

Figure 11- Single Lap Joints methodology based on the adherend yielding [4].

For the global yielding criterion in the adhesive, the failure load is calculated by a simple formula:

$$P_a = \tau_y bl \quad \text{(eq. 7)}$$

Where τ_y represents the shear failure strength of the adhesive, b is the width of the joint and l the overlap length [5], [25].

2.1.5 Failure criteria for adhesively bonded joints- numerical approach

As previously stated, a numerical method is also used to predict the strength of the joints. The use of this method requires knowledge of the mechanical properties of the adhesives. For that reason, it is necessary to previously characterize them by performing bulk tensile tests.

2.1.5.1 Cohesive damage model

Fracture mechanics have been used to predict the joint strength by many researchers. However, this approach is only valid under elastic deformations and it is not appropriate when there is plastic deformation before failure.

CZM has been used to simulate and predict the failure behavior of bonded joint when using linear elastic material properties in the adhesive layer. In this method it is assumed that the energy is dissipated as the crack grows and if we have single mode propagation (Mode I, II or III) the area under the stress/relative displacements curve can be equated to the critical fracture energy (see Figure 12) [26].

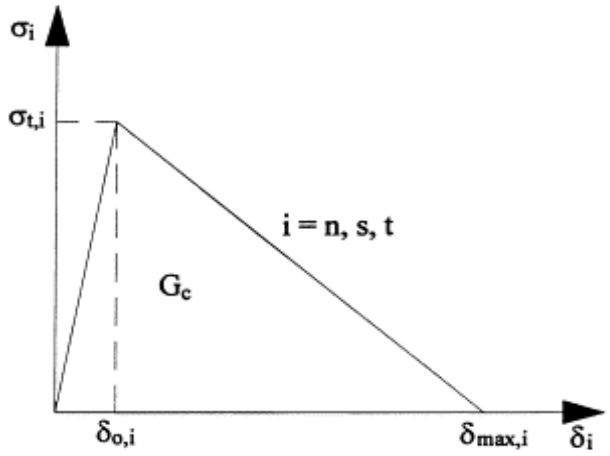

Figure 12- Softening stress/relative displacements relationship for pure mode (I, II or III) [27].

Failure initiates once the defined strength $\sigma_{t,i}$ which corresponds to a critical relative displacement ($\delta_{0,i}$) has been exceeded. The maximum relative displacement (δ_{max}) can be obtained by the strength ($\sigma_{t,i}$) and the critical fracture energy (G_c) which are material properties determined experimentally [27], [28].

Figure 13 shows the combination of mode I and mode II as well as pure-mode (tension and shear).

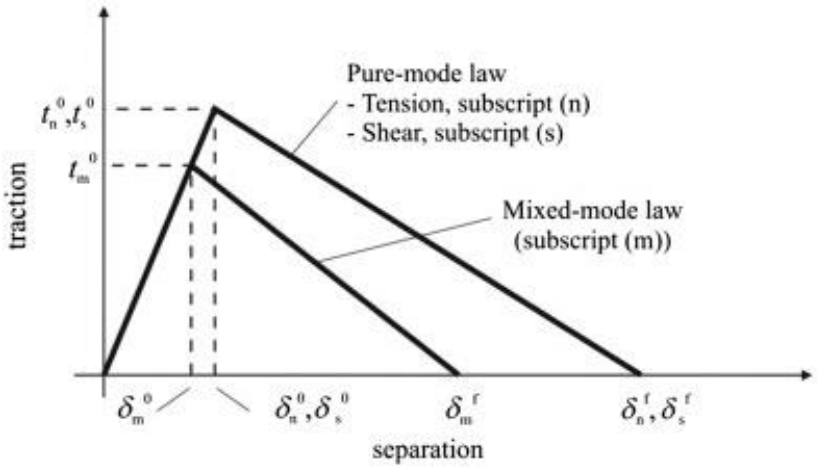

Figure 13- Traction-separation law with linear softening law available in Abaqus® [29].

In general, the shape of the cohesive laws can be adjusted to conform to the behaviour of the material. As previously stated, the values of G_n and G_s, representing the areas under the traction-separation laws in tension or shear, respectively, allow to define the normal or shear maximum relative displacements (δ_n^f and δ_s^f). Under mixed mode, stress and energetic criteria are often used to combine tension and shear.

The traction-separation laws assume an initial linear elastic behavior followed by linear evolution of the damage. In the case of elasticity, this is defined by an elastic constitutive matrix:

$$t = \begin{Bmatrix} t_n \\ t_s \end{Bmatrix} = \begin{bmatrix} K_{nn} & K_{ns} \\ K_{ns} & K_{ss} \end{bmatrix} \begin{Bmatrix} \varepsilon_n \\ \varepsilon_s \end{Bmatrix} = K\varepsilon \qquad \text{(eq. 8)}$$

Where the matrix K contains the stiffness parameters of the adhesive layer. A suitable approximation for thin adhesive layers is provided with: $K_{nn} = E, K_{ss} = G$ and $K_{ns} = 0$.

Complete separation and mixed-mode failure displacement are predicted by a linear power law form of the required energies for failure in the pure modes [29]:

$$\frac{G_n}{G_n^c} + \frac{G_s}{G_s^c} = 1 \qquad \text{(eq. 9)}$$

2.2 Impact load

It is essential to clarify that the impact conditions can be categorized in three ranges: low velocity, medium velocity and high velocity. Therefore, in the laboratory, impact can be simulated using essentially three tests: pendulum type, where tests rates are below 10 m/s, drop-weight tests, with rates up to 10 m/s and the split Hopkinson pressure bar, where we have the highest rates of up to 100m/s.

In the last few decades, researchers have identified the importance of studying the behaviour of CFRP at high strain rates in order to observe the damage and mechanisms of failure in impact conditions. Many studies [30], [31] and [32] concluded that the interlaminar shear strength of carbon fibre/epoxy composites increases with strain rate. So, Hosur et al. [30] suggested that this behaviour can be attributed to the time-dependent deformation of the material, which is a product of the visco-elastic behaviour of the matrix in the composite. Under impact conditions, it is necessary that the adhesive layer retains sufficient toughness to induce the damage mechanisms that might occur in composite or layered materials.

The behavior of adhesives under impact has also been studied. Adams and Harris [33] obtained results with a pendulum impact machine. They show that for a range of adhesives, joint strength is not significantly affected by high rates of loading. The second conclusion obtained was the existence of a relation between adherend strength, joint strength and energy absorption. Results of energy absorbed and failure load for different combinations of adhesive and adherend materials are shown in Figure 14. They noticed that using rubber-toughned adhesive with ductile aluminum alloy adherends provided the highest energy absorption, while for a high-strength aluminum alloy, the joint strength increased with a reduction of the energy absorption due to the high yield strength of the aluminum. When the adhesive used is strength enough to keep the adherends together under impact load, it is also the adherend yielding that controls failure.

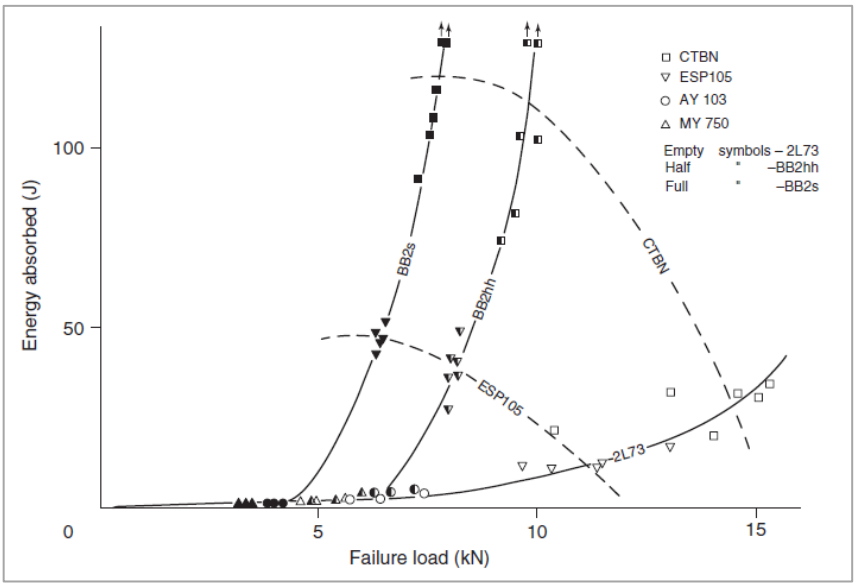

Figure 14- Impact results for lap shear alluminum alloy specimen [34].

For conclusion of their study is that the energy absorption comes not from the adhesive, but from the deformation of the adherend material and a joint having a high strength does not necessarily have optimum energy absorbing capabilities. When a ductile and strong adhesive is used, the sensitivity of the adherend material to the high strain-rate is what determine the failure.

When the SLJs are submitted to high strain-rate conditions, their material properties tend to be different from the ones reviewed in quasi-static conditions. In literature experimental results for impact tests can be found but if the materials have the same properties as obtained in static conditions, it is possible extrapolate the materials properties in order to predict failure [35].

Results were found for impact load tests on SLJs with an epoxy adhesive, a very ductile polyurethane and mild steel adherends. The results showed that the adhesive joints with the epoxy adhesive (AV138) are stronger than those with the polyurethane adhesive (Sikaflex) and there is an increase in joint strength in both the static and impact tests (see figure 15) [16].

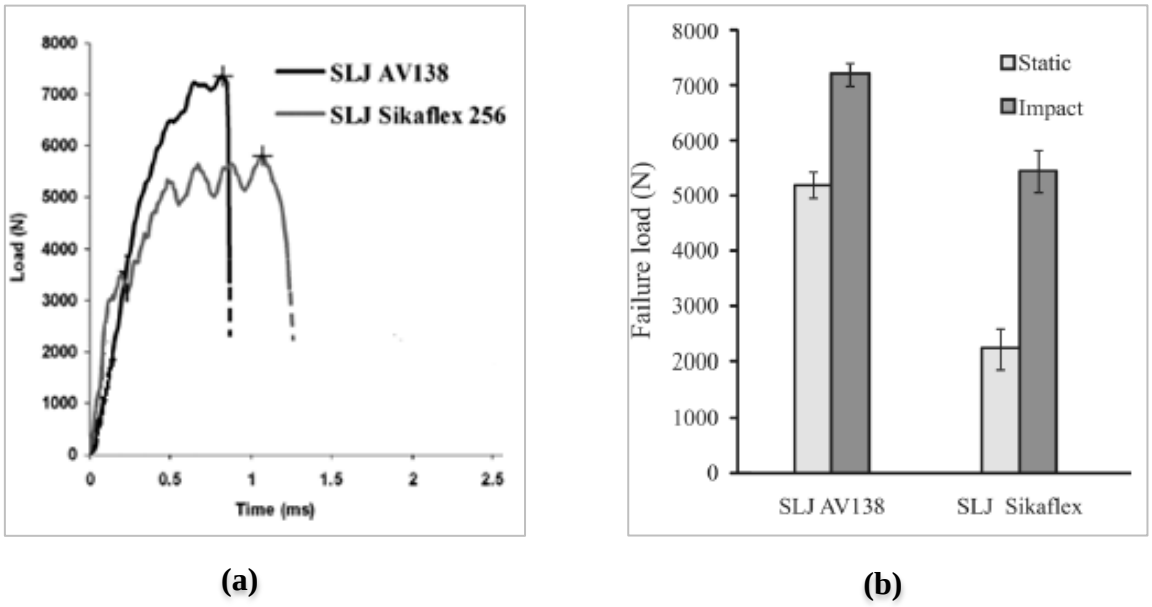

Figure 15- (a) Load variation of impact tests as function of time; **(b)** comparison between failure load values of static and impact tests [16].

Other results [36] show that in the case of the steel adherends and due to the high adherend yielding, the steel strength determines the failure of SLJs at room temperature.

Other results found for drop impact load tests in SLJs with a high elongation epoxy adhesive and ductile adherends show that the failure mode obtained under high strain-rate was almost the same as the one obtained in quasi-static. However, some differences in the behavior of joints were referenced - the adherends deformed less than in quasi-static tests and absorbed less energy. Consequently, the failure load increased but the adhesive experienced similar damage as in the quasi-static tests, as shown in Figure 16 [37].

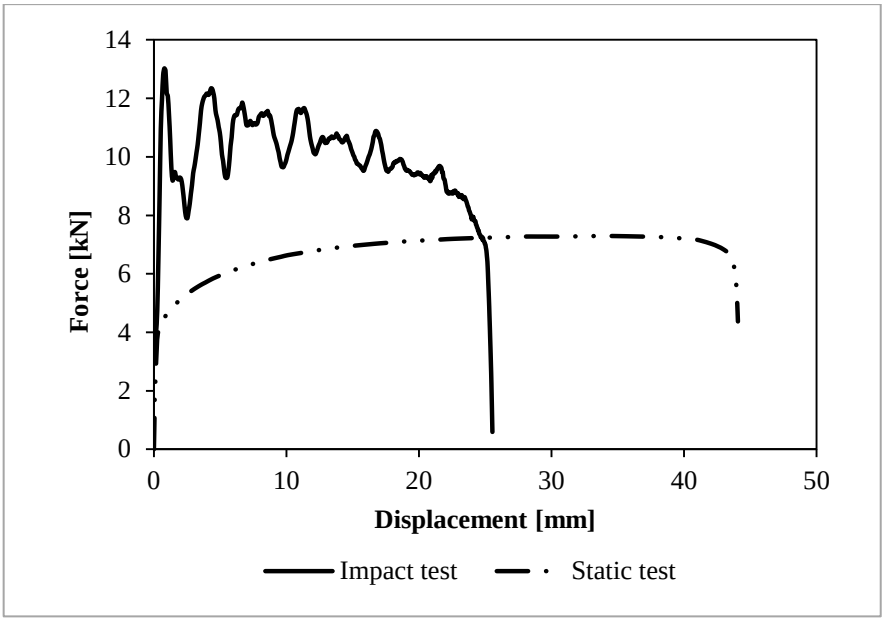

Figure 16- Comparison of SLJ with mild steel adherends under different strain rates (1mm/min and 4.47 m/s) [37].

2.1.1.1 Impact in the automotive industry

In the automotive industry, under impact load it is crucial to transfer the load to the material (steel, composite and others) without fracturing the joint thus assuring the integrity of the car under a crash situation. The adhesives used have impact resistance and deform significantly without breaking, absorbing enough energy to keep the parts together. These adhesives combine the high toughness of polyurethanes and the high strength of an epoxy. However, pure epoxy adhesives are very brittle. This type of adhesives become crash durable via special polymeric additives or the use of rubber-like particles [4], [38].

In Figure 17 three sections which a crash-suitable adhesive must have in its stress-strain representative curve are illustrated. Section 1 represents the linear behavior where the strength and the deformation of the bond can be predicted for the lifetime. Section 2 shows the adhesive resistance against short time high load without damage. As you can see, the maximum load in this section is 40 MPa. Sections 1 and 2 are typical for both high strength structural adhesives and brittle type adhesives. Section 3 shows the additional benefit of a crash-suitable adhesive starting to deform significantly without breaking, absorbing enough to keep the parts together [4].

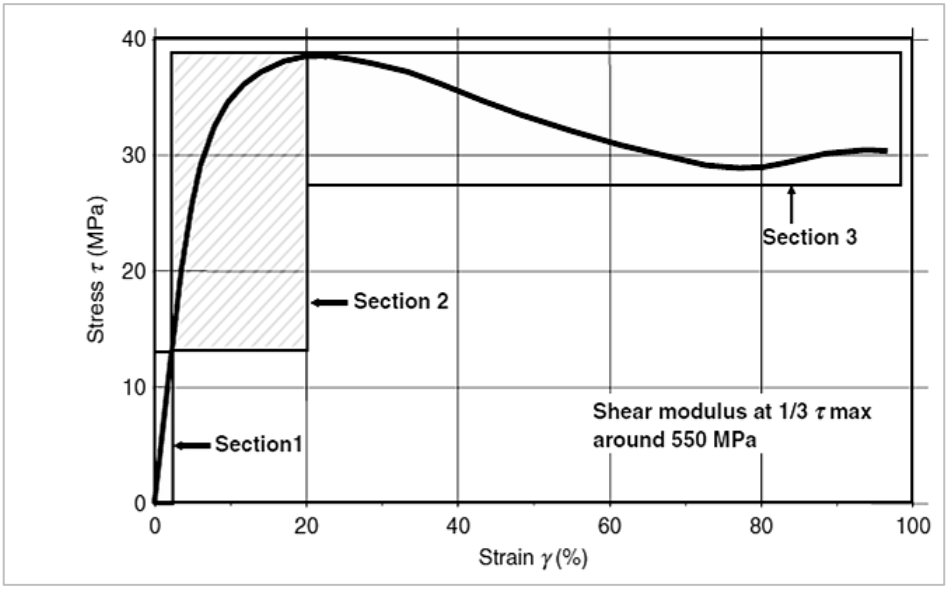

Figure 17- Stress-strain diagram of a crash-suitable adhesive [4].

2.1.2 High strain rate properties of adhesives

As mentioned in the previous section, it is necessary to understand the performance of adhesive joints under different rates of loading. This is of particular importance since adhesives for automotive applications (adhesives which are toughened epoxy polymers) exhibit rate-dependence deformation.

In Figure 18, we can see the strain rate dependence values of the young's modulus (*E*) and the uniaxial tensile strength (UTS). As you can see, the dependence of E and UTS with high strain rate is not very significant.

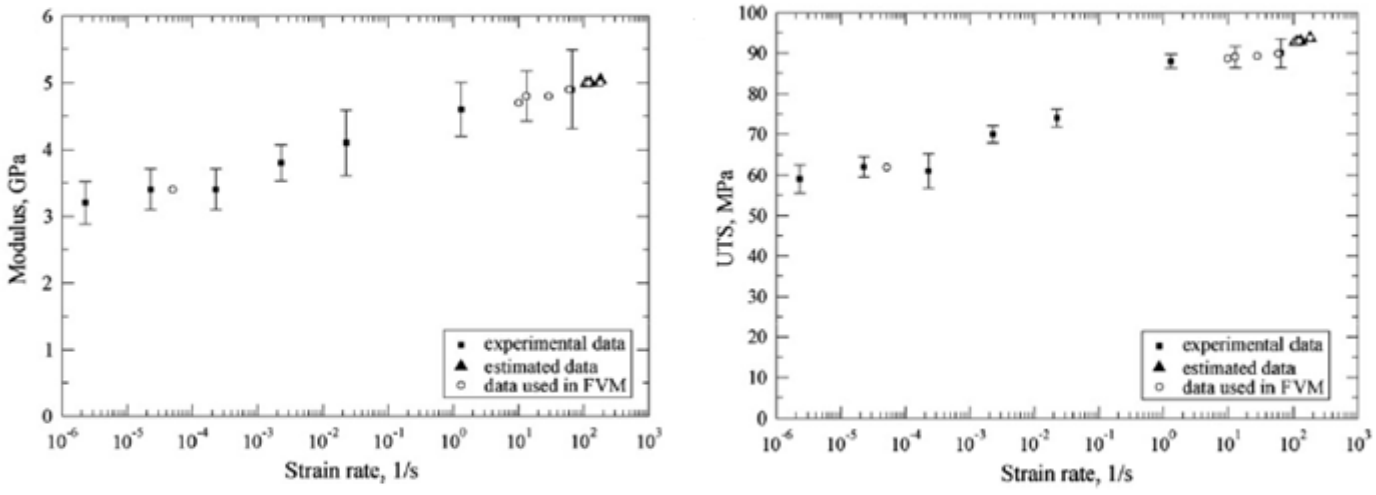

(a) **(b)**

Figure 18-Mechanical properties of the adhesive as a function of strain-rate: (a) Young's modulus and (b) UTS. [54]

Other studies showed the influence of strain rate on cohesive parameters of a structural epoxy adhesive (DOW-Betamate XW1044-3). These experiments are performed in peel mode using the double cantilever beam (DCB) specimen and in shear mode, using the ENF specimen. They concluded that in the peel mode, the fracture energy increases slightly with increasing strain rate and in shear mode the fracture energy decreases (see Figure 19) [39].

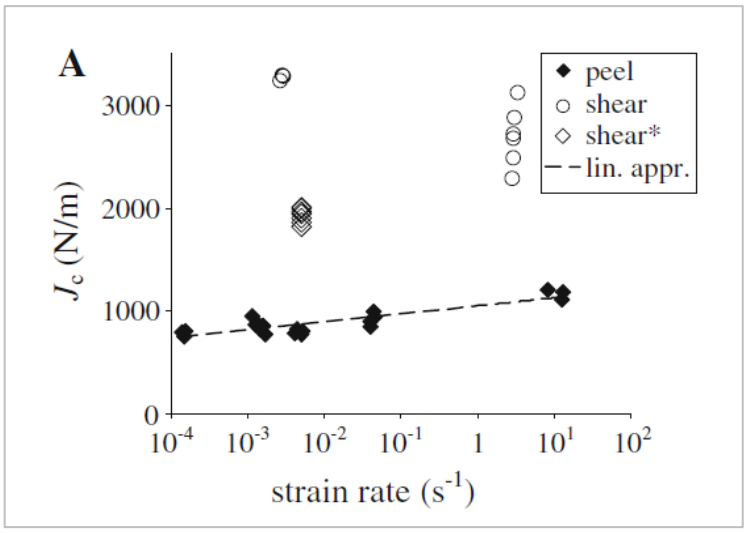

Figure 19- Fracture energy as function of strain rate.

In many cases it is necessary to predict the values at a larger range of strain rates which can be done by extrapolating to strain rates beyond the experimental ones. Moreover, the adhesive materials exhibit a non-linear relationship between stress and strain and cannot be modelled using young's modulus and poisson's ratio alone. Figure 20 shows the experimental tensile testing carried out on bulk samples of the adhesive at three crosshead speeds.

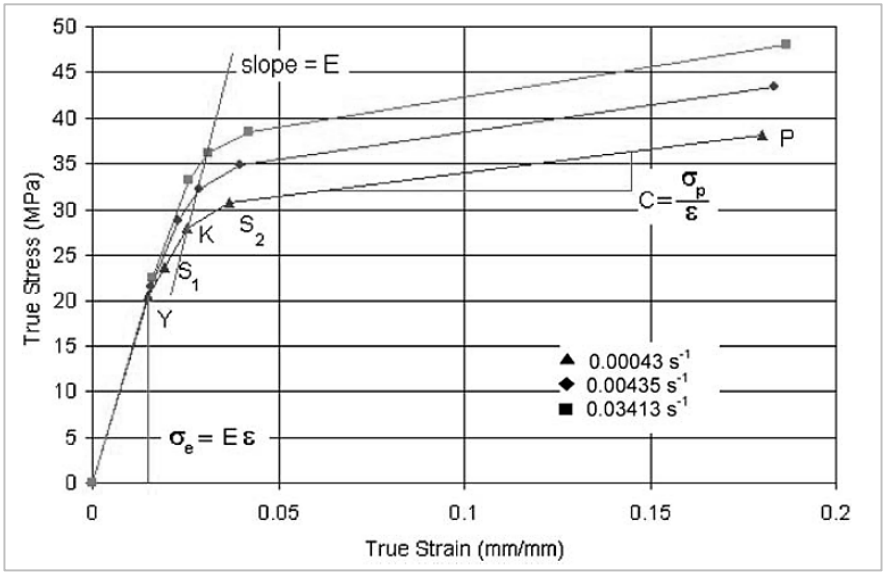

Figure 20-Typical true stress–strain curves for the bulk adhesive [35].

The plastic deformation that we can find is given by:

$$\dot{\varepsilon}_t = \dot{\varepsilon}_e + \dot{\varepsilon}_p \quad \text{(eq. 10)}$$

Where $\dot{\varepsilon}_t$, $\dot{\varepsilon}_e$, $\dot{\varepsilon}_p$ are the total, elastic and plastic strain rates, respectively. The values of $\dot{\varepsilon}_p$ and ε_p are also required and given by:

$$\varepsilon_p = \varepsilon_t \left(1 - \frac{C}{E}\right) \quad \text{(eq. 11)}$$

.

$$\dot{\varepsilon}_p = \dot{\varepsilon}_t \left(1 - \frac{C}{E}\right) \quad \text{(eq. 12)}$$

The relationship between stress and plastic strain rate at each of the five characterising points found to be logarithmic:

$$\sigma = A\ ln\left(\dot{\varepsilon}_p\right) + B \quad \text{(eq. 13)}$$

Where A and B are constants found from experimental data for each stress point.

2.3 Composites materials -an overview

The use of composite materials in structures has significantly increased during the last years. This trend is mainly because composite materials have properties which are very different from conventional isotropic engineering materials, namely high strength-weight and high stiffness-weight ratios, thermal stability, corrosion resistance and fatigue resistance, making them suited for structures in which the weight is a fundamental variable in the design process. A schematic classification of composite materials is shown in Figure 21 [40].

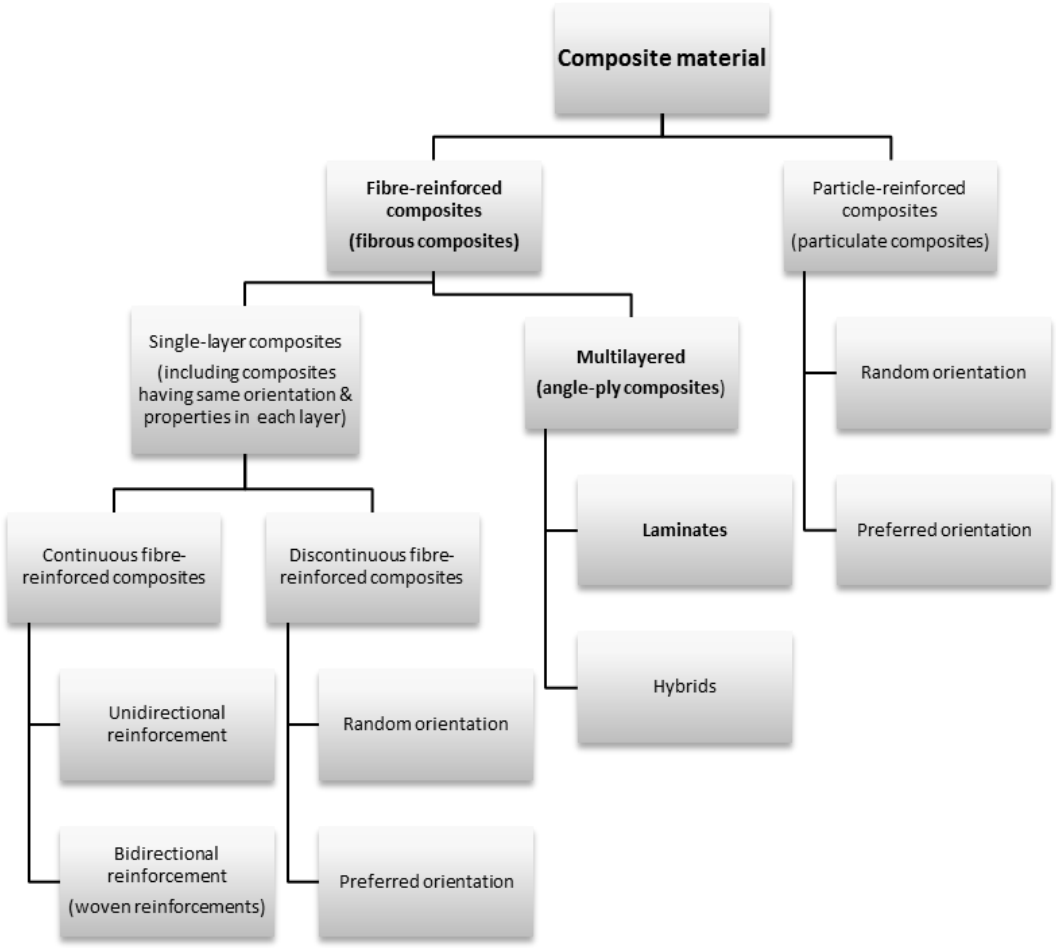

Figure 21- Classification of composite materials (adapted from [41].

Composites are very anisotropic: in the fibre directions, unidirectional composites can be very strong and stiff, whereas the transverse and shear properties are much lower. The composite lamina consists in two or more plies of composite with the same or different orientations. The lamina of unidirectional composite material is orthotropic with the axis in the direction of the fibers (direction 1), normal to the fibers in the lamina plane (direction 2) and normal to the lamina plane (direction 3), as shown in Figure 22 [42].

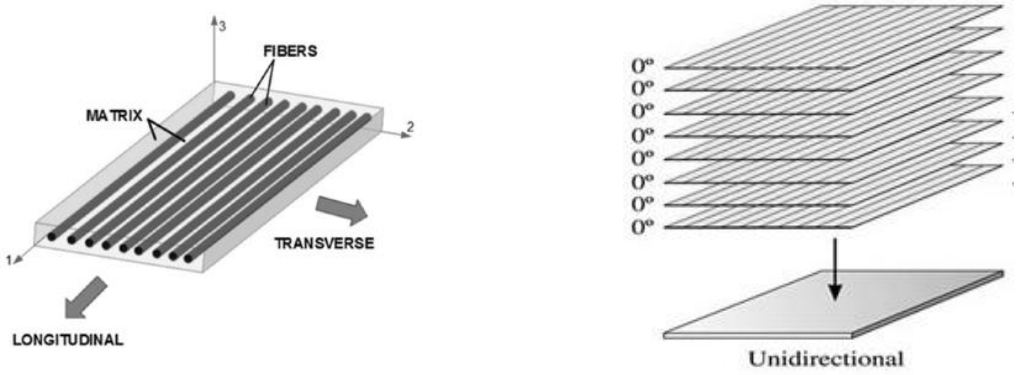

Figure 22- Schematic representation of unidirectional lamina with plies orientation to 0º degrees [44].

In the most general case, the laminas can have different thicknesses and consist in distinct types of fibers (unidirectional or woven), as well as being different materials. Many stacking of plies and orientations of composite can be study and some examples are shown in Figure 23.

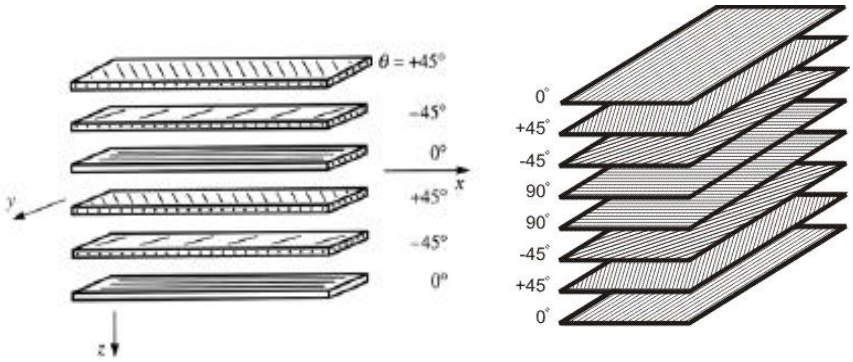

Figure 23- Plies stacking examples.

The analysis techniques are essentially the same as when isotropic adherends are used, although attention must be paid to the low longitudinal shear stiffness of unidirectional composites. Therefore, in the case of metallic adherends, the shear modulus is in the order of 25-38 % of their young´s modulus. On the other hand, with unidirectional composites, this modulus ratio may be as low as 2% and so the adherend shears become extremely important [5].

2.1.1 CFRP properties

CFRP are composite materials. In this case the composite consists of two parts: the matrix and the reinforcement. In CFRP the reinforcement is carbon fiber, which provides the strength. The matrix is usually a polymer resin, such as an epoxy, to bind the reinforcements together. Therefore, since CFRP consists of two distinct elements, the material properties depend on these two elements [43].

CFRP laminates are being increasingly used in structures that require high specific strength and light weight. This material has specific properties such as much higher stiffness/weight and strength/weight ratios than those of metallic materials [44].

However, these materials have some disadvantages such as:

- Prone to suffer damage;
- Specific delamination between plies due to, for example, low velocity impact which can easily occur in a structure's lifetime. This phenomenon can highly reduce the strength of these structures which, associated to the recycling difficulties and replacement costs, makes repairing very advantageous;
- Lack of confidence on the use of available design criteria on using these materials.

2.1.2 Failure modes in composite materials

Fibre reinforced plastics have a low strength epoxy resin matrix and adherend failure is more likely in composite joints than in metal to metal joints. According to [5] there are three possible modes of failure in the composite (see Figure 24):

- tensile failure in the fibre direction;
- tensile failure perpendicular to the fibre direction;
- interlaminar shear failure.

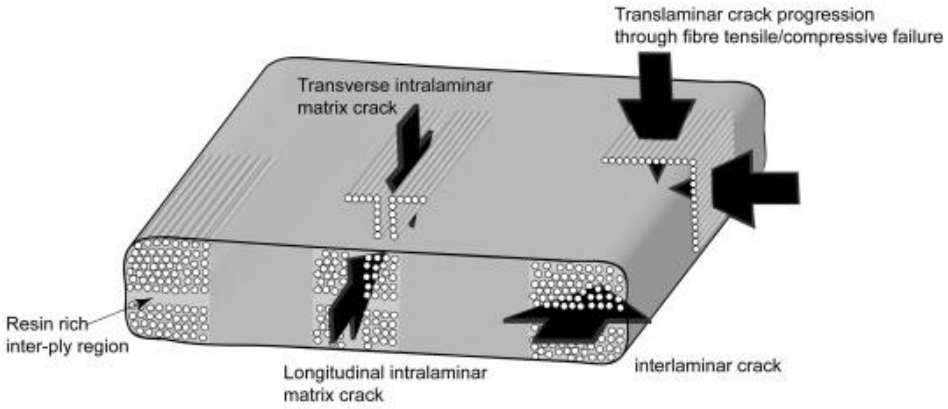

Figure 24- Overview of ply-level failure modes [45].

To be more precise, failure in composites is governed by three mechanisms: matrix cracking, delamination, and fibre debonding and pull-out. Normally, delamination is defined as the separation of two plies of a laminated composite [46].

Composite laminates are expected to absorb low velocity impacts either during assembly or in use. When a laminate is subjected to even barely visible impact damage, micro-damage is incurred, which can have a significant effect on its strength, durability and stability [47].

2.1.3 Joints with composite adherends

When studying and working with composites, there are other parameters that need to be considered and the models presented above do not contemplate that. In the case of these materials, the adherend constitutive model is more complex because of the anisotropic nature of composites. The possible failure modes in composite bonded joints are shown in Figure 25.

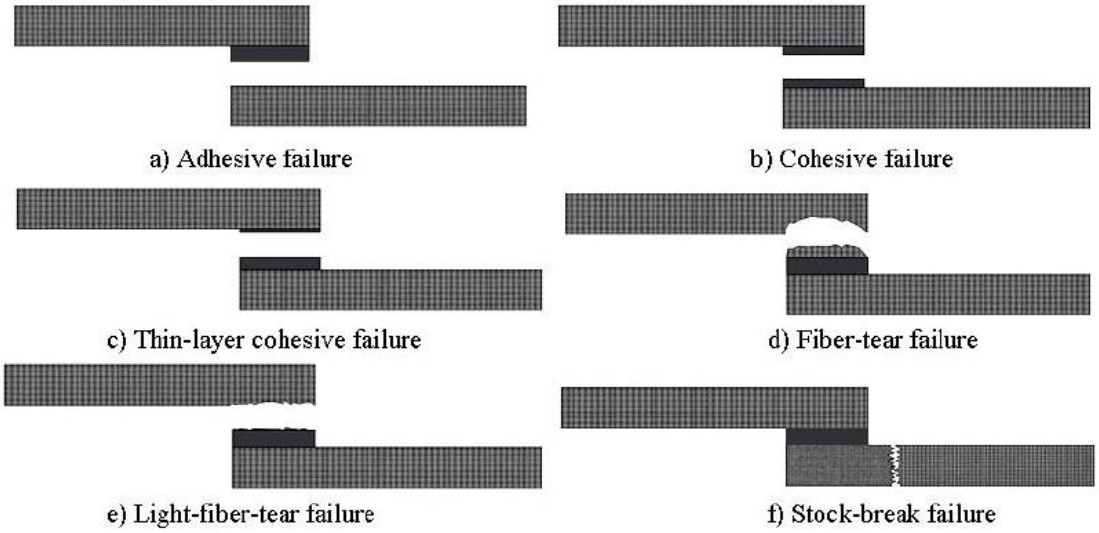

Figure 25- Possible failure modes in bonded joints between composite adherends [10].

Numerous studies considered the composite laminated, but Wah in 1973 was the first to investigate this subject and considered the laminated composite adherends. His analysis considered the laminated adherends as symmetrical along their midsurface. In this case, the peel stress at the interface must be related to the composite through-thickness strength. However, few models account for interface stresses [12], [20].

As previously mentioned, the analyses of Wah were limited to composite adherends that are symmetrical along their midsurface. The analysis of non-symmetric composite adherends was more recently considered by Yang, Pang, Mortensen and Thomsen. Their analysis concluded that the use of asymmetric laminates can provide more flexibility in design. However, in this case it is more difficult to manufacture asymmetric composite laminates [12]. However, other authors such as Grimes, Dickson, Hsu and McKinney have also concentrated on composite adherends [22].

Several works have been proposed for studying the behaviour of composite joints and Nascimento [48] studied the adhesive thickness's influence in joints with CFRP adherends. For that, different thicknesses (t_a=0.2, 0.5, 1 and 3 mm) and different overlap lengths (l_0=10, 20, 30, 40, 50, 60 mm) were used. The joints were tested in static tests and the results showed that for the biggest adhesive thickness, the joint only supported 50% of the failure load. Concerning the studies where the overlap length varied, he concluded that composite

delamination can occur for some overlap lengths (l_0=30mm), but generally the failure modes were cohesive and the maximum load for each length was higher in proportion.

Neto [49] also concluded in his work that with the use of two adhesives (a ductile and a brittle adhesive), with ductile adhesives the failure load increases as function of the overlap length.

Normally what experiences show is that a bonded joint's peel loading results in transverse tension composite fail before the adhesive fails. The inner composite adherend splits apart locally due to these peel stresses, thereby destroying the shear transfer capacity between the inner and the outer adherends (see Figure 26). Other authors have studied the problem of peel stresses in adhesive joints with composites and found designs to reduce these peel stresses. Da Silva et al. [46] proposed some techniques to reduce the peel stress in adhesive joints with composite adherends. They propose an internal taper and an adhesive fillet to reduce this problem. With this technique the adhesive joints with composites have a higher failure load than that of adhesive joints with no taper and fillet. Nevertheless, an internal taper and fillet are not easy to manufacture.

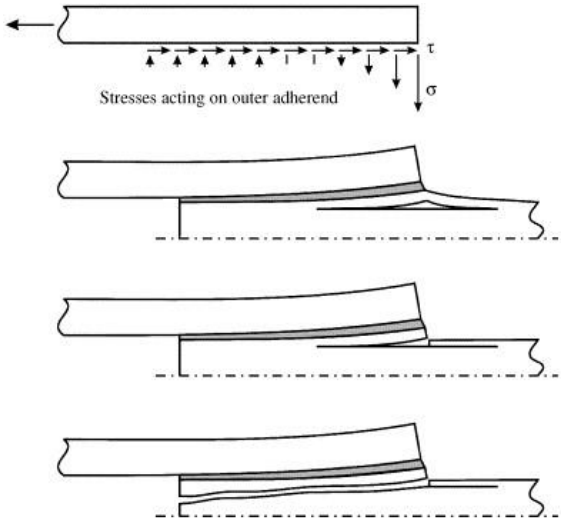

Figure 26- Peel stress failure of composite adherend [46].

2.1.4 Impact resistance of composite materials

In recent years many research programs have been undertaken in an attempt to better understand the impact response of these materials. The manner in which composite materials respond to impact loading is very different than that of metals.

Therefore, for low and intermediate energies, metals absorb energy through elastic and plastic deformation. However, in the case of composites, the ability to undergo plastic deformation is extremely limited, resulting in absorbed energy creating large areas of fracture with ensuing reductions in both strength and stiffness. While metal structures collapse under impact by buckling involving extensive plastic deformation, composites fail through a sequence of fracture mechanisms. The actual mechanisms and sequence of damage are highly

dependent on the geometry of the structure, lamina orientation, crush speed, all of which can be suitably designed to develop high-energy absorbing mechanisms.

2.1.5 Mechanical response of composites under high strain rates

As previously stated, the mechanical properties of composites, like other materials, are sensitive to the rate at which they are loaded and deformed. In comparison to metals, the damage and failure mechanisms of composite materials are not fully understood, in particular for the case of high strain rate loading. The rate effect on composite tensile properties has been studied. Harding [50] was the first to study the high strain rate longitudinal tensile behavior of unidirectional carbon-epoxy laminates using a tension split-Hopkinson bar apparatus, and found no significant strain rate effects. The same was concluded in a recent study by Taniguchi et. al. [51]. In the case of Transverse modulus and strength, the differences with the increase of strain rate are more significant (see Figure 27 b) and c)), because it is the resin which controls failure and, as explained in the literature review, the effect of strain rate variations is much higher than for the carbon fibers. Figure 27 shows the strain rate effects on composite tensile properties from previous results found in literature.

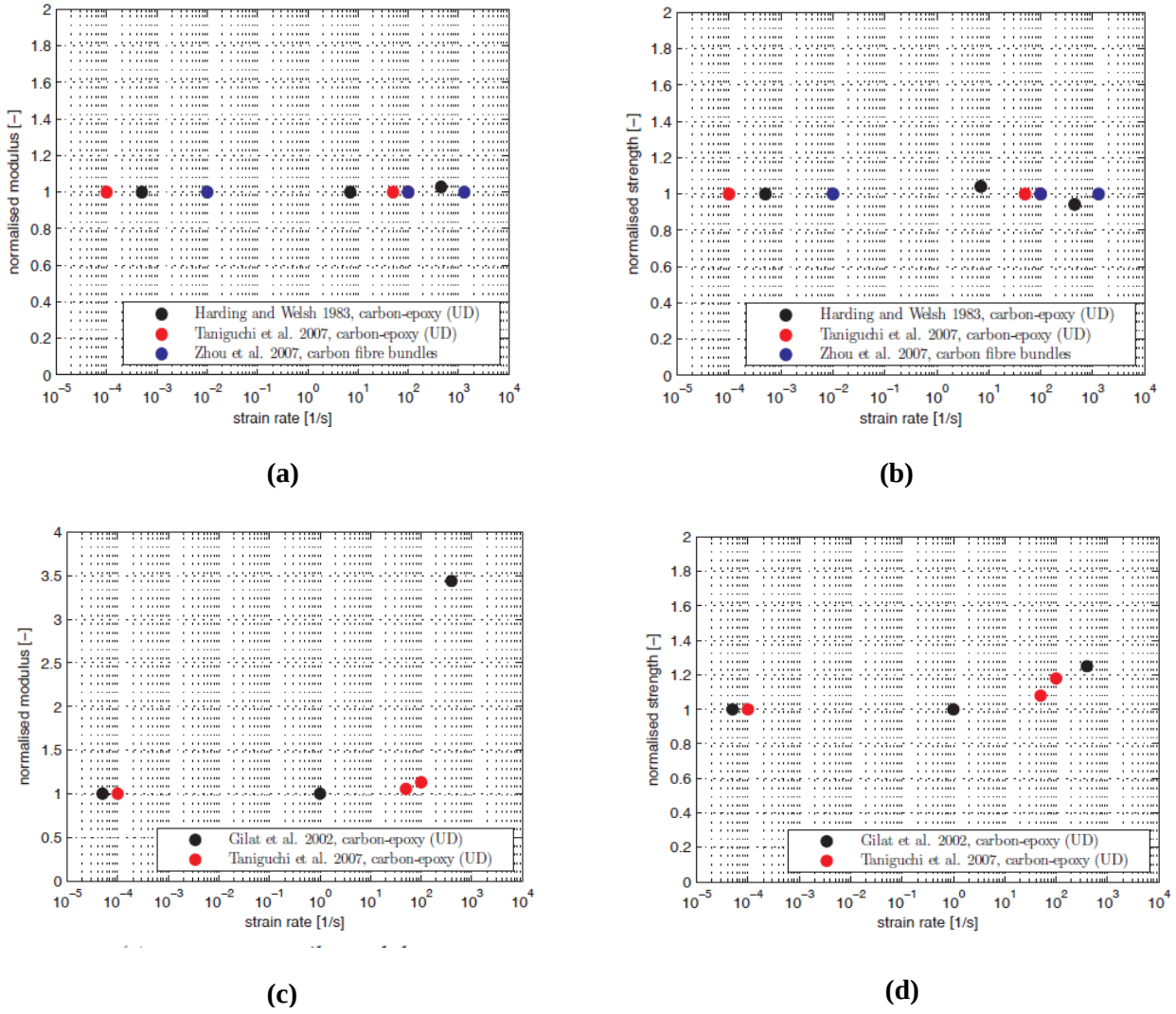

Figure 27- Comparison of literature results regarding the strain rate effect in the tensile properties of polymer composites (a) longitudinal tensile modulus (b) longitudinal tensile strength (c) transverse tensile modulus (d) transverse tensile strength [55].

Chapter 3

A set of experimental tests were performed during this work in order to study the static and impact behaviour of single-lap joints with composite adherend. In this chapter, the experimental procedure is described as well as the results obtained with these tests.

EXPERIMENTAL DETAILS

3.1 Material characterization and experimental procedure

3.1.1 Adhesives

Two adhesives were selected: a one-component epoxy adhesive, Nagase-Chemtex XNR6852E-2, supplied by Nagase Chemtex ® (Osaka, Japan) and a brittle adhesive, two-components, epoxy SikaPower 4720 developed and supplied by Sika Portugal, SA ® (Porto, Portugal). Adhesive SikaPower 4720 needs 1 day curing at room temperature and Nagase XNR 6852 E-2 cures at 150 °C for approximately 4h. The representative curves for each adhesive are shown in Figure 28.

The collected data of the adhesives properties is presented in Tables 5 and 6, where all of them were obtained in this work. An extended explanation of the procedure and the experimental results carried out in this thesis can be found in the following section.

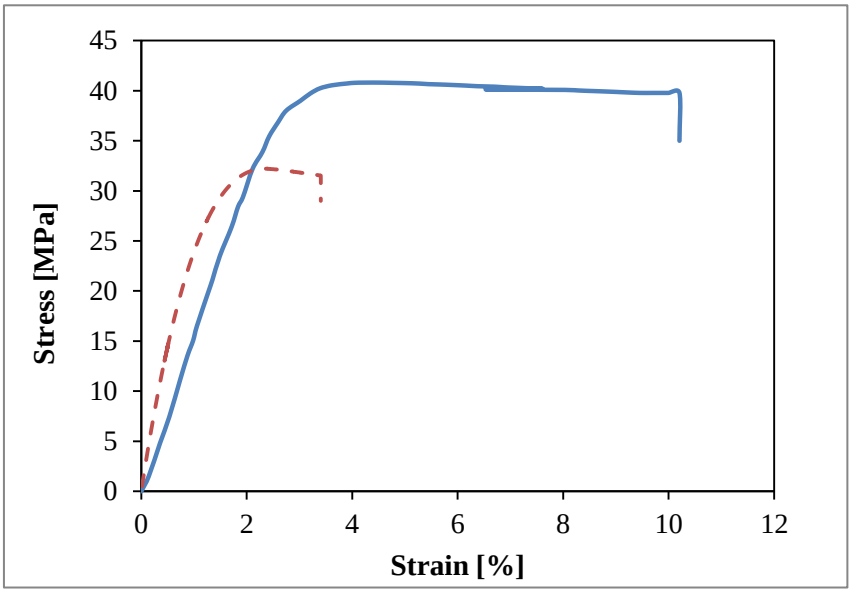

Figure 28- The representative curves of stress vs strain for the two adhesives studied**.**

Table 5- Properties of the adhesives, Nagase XNR 6852 E-2 ® and Sika Power 4720® at 1 mm/min.

Property	XNR 6852 E-2	SikaPower 4720
Young's Modulus, *E* [GPa]	1742	2170
Tensile strength, σ_{max} [MPa]	42.9	32.0
Strain to failure , ε_f [%]	9.95	3.1
Shear strength, τ_{max} [MPa]	28.7	22.9
Toughness in tension, G_{IC} [N/mm]	1.7	1.6
Toughness in tension, G_{IIC} [N/mm]	18	-*

*Property has not been determined and is not available in literature.

Table 6- Summary of adhesives properties at 100 mm/min.

Property	XNR 6852 E-2	SikaPower 4720
Young's Modulus, *E* [GPa]	1802	2431
Tensile strength, σ_{max} [MPa]	45.7	35.7
Strain to failure , ε_f [%]	12.9	3.4
Shear strength, τ_{max} [MPa]	33.6	-*
Toughness in tension, G_{IC} [N/mm]	-*	-*
Toughness in tension, G_{IC} [N/mm]	-*	-*

* Properties has not been determined and is not available in literature.

.

In order to determine the some important properties of adhesives, which were not determined, three different tests were performed. Bulk tensile tests were tested in a servo-hydraulic machine to obtain E, σ_{max} and ε_f at two different strain rates. The ENF was selected to obtain G_{IIC}. Finally, TAST was used for the purpose of obtaining the adhesive's shear properties.

❖ Tensile properties Results-Nagase XNR 6852 E-2

The more common test to determine the strength properties of adhesives is the tensile test on bulk specimens. The properties are intrinsic to the material and can be obtained under a uniform and uniaxial state of stress, with no influence of the adherends. Nevertheless, the properties determined may vary from the in situ (in a joint) tests. The test geometry should provide a uniformly distributed stress across the contact surface as to minimize the stress concentrations. In general, the geometry used for the tensile specimens is the dogbone-shaped specimen that follows the EN ISO 527-2 standard [34].

The tensile properties at different displacement rates of Nagase XNR 6852 E-2 and SikaPower 4720 adhesives were determined using dogbone specimens, produced from bulk adhesive plates cured in a steel mould, using a silicone rubber frame (see Figure 30). This last material was used to avoid the adhesive from flowing out. Curing of the bulk plates was carried out in a hot press for approximately 4h at 150ºC. Then, dogbone specimens were machined from the bulk sheet plates (see Figure 31). The specimen geometry used is showed in figure 29.

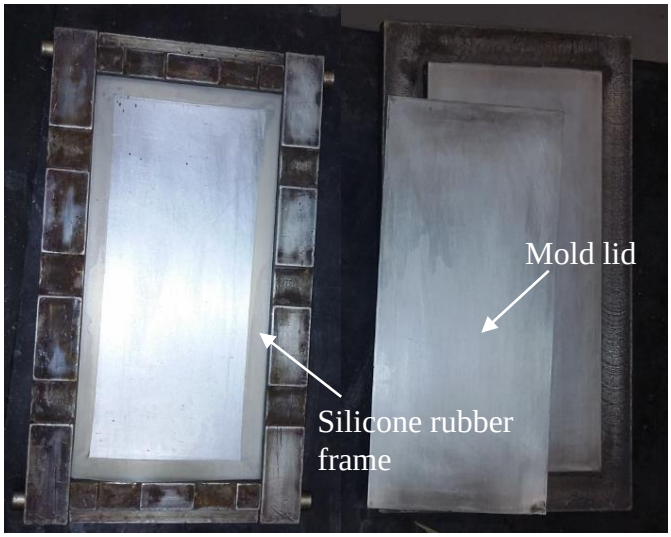

Figure 30- Mould for producing the bulk specimens with steel plates and silicone rubber frame.

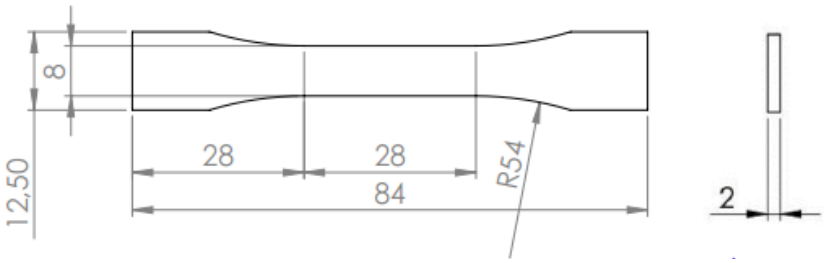

Figure 29- Geometry of the bulk tensile test specimen (dimensions in mm) [37].

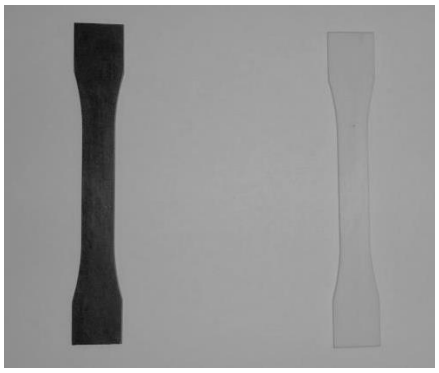

Figure 31- The tensile bulk specimen after machining**.**

The bulk tensile tests were performed in an INSTRON® model 3367 universal test machine (Norwood, Massachusetts, USA) with a capacity of 30 kN. The dogbone adhesive specimens were tested at room temperature, under a constant displacement rate of 1mm/min and 100 min/min. Three tests were performed for each condition. An optical method with a digital camera was used, monitoring the separation of the two lines inscribed on the test specimen (see Figure 32). This camera takes the pictures of the gauge length recording the change in separation of the two lines throughout the test. Therefore, we can record the various stages of specimens to failure. Then, the digital images were analysed using an image processing and analysis software and in the end, we could extract the strain for each specimen.

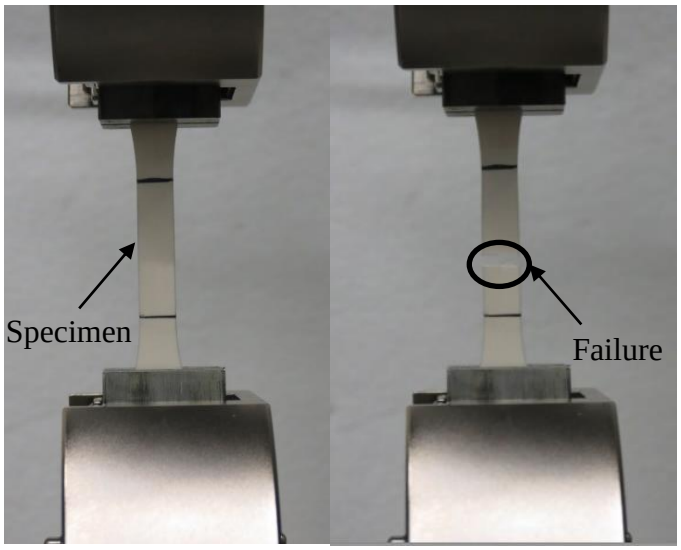

Figure 32-The dogbone specimen in the machine (a) during the test (b) after failure.

For each specimen, a tensile stress-strain curve was produced based on specimens dimensions and the values of stress and strain obtained by the software used. From the stress-strain curves, the mechanical properties were calculated and the results are summarized in Table 7. The values of young´s modulus can be obtained from the tangent to the tensile stress-strain curve at the origin.

Table 7-Properties of Nagase XNR 6852 E-2 at two different rates obtained in bulk specimens.

Strain rate (mm/min)	Tensile strength (MPa)	Young's modulus (MPa)	Strain to failure (%)
1	42.9 ± 1.9	1742 ± 134.1	9.95 ± 4.0
100	45.7 ± 1.8	1802 ± 9.8	12.9 ± 6.2

As you can see in Table 7 and as expected, there is an increase in the young's modulus and tensile strength with the high strain rate. However, a decrease in the adhesive ductility was not expected. Figure 33 shows the comparison of tensile stress-strain curves of Nagase adhesive at two different rates.

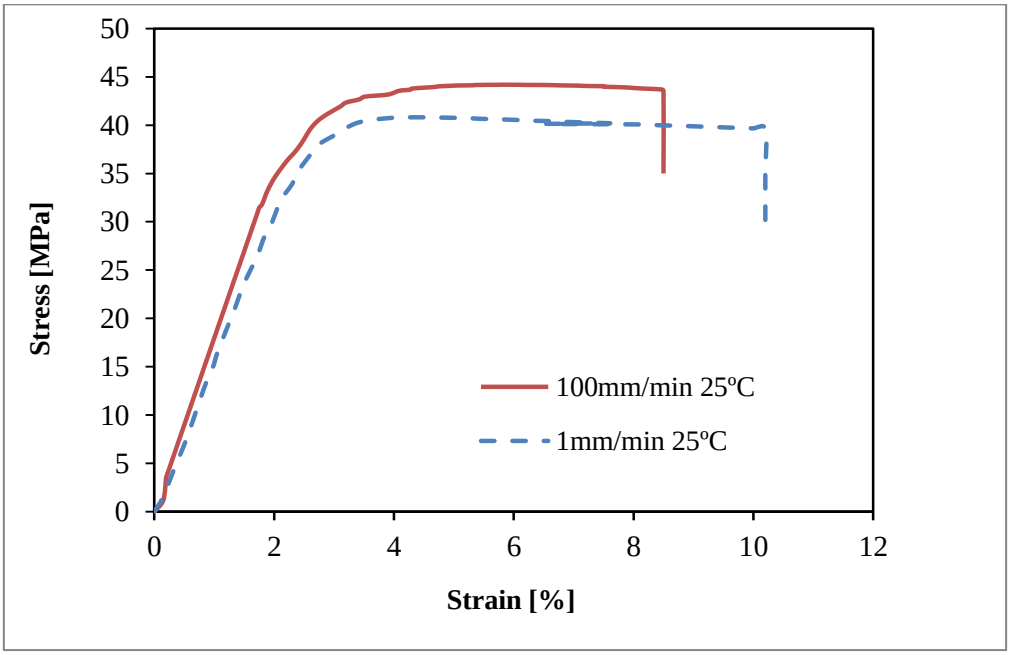

Figure 33- Stress vs. Strain curves for Nagase XNR 6852 E-2 bulk tensile tests at two different strain rates.

Figure 34 shows the fracture mode obtained after the tensile test of the Nagase XNR 6852 E-2 bulk specimens. In this case, the adhesive showed lower ductility when compared with the previous version (Nagase XNR 6852 E-1) [36].

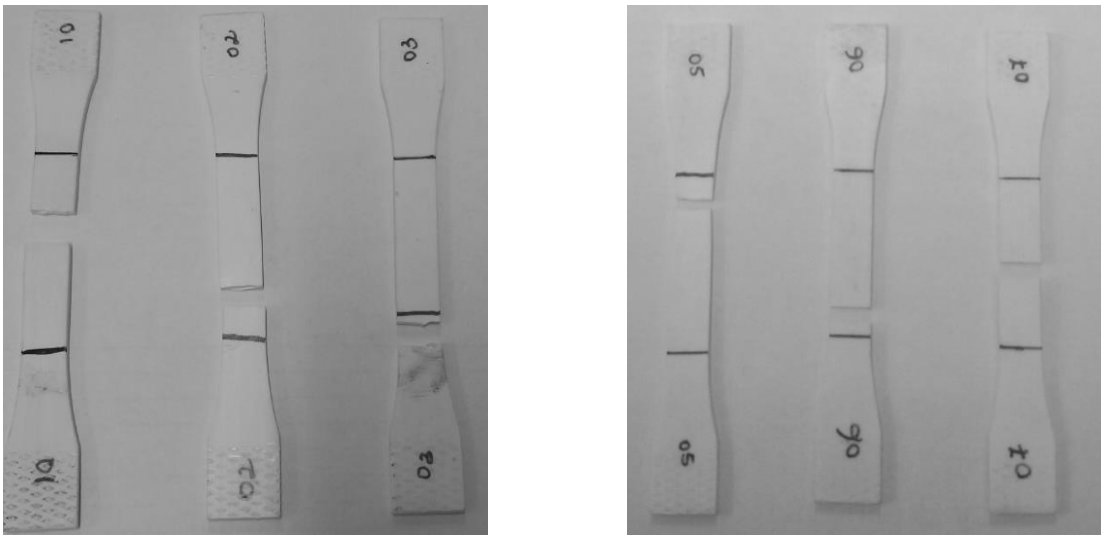

Figure 34- Bulk specimens after the tensile tests at 1 and 100 mm/min, respectively.

❖ Tensile properties- SikaPower 4720

The procedure for producing the SikaPower 4720 bulk specimens is the same as the previous described for Nagase XNR 6852 E-2 adhesive. In this case, the properties of this adhesive were determined with a displacement rate of 100 mm/min and four tests were performed. The geometry of "dogbone" tensile specimens is the same used in the case for Nagase adhesive. For each specimen, a tensile stress-strain curve was obtained based on the specimen dimensions and the values of stress and strain were obtained by the software used. The main properties of the SikaPower 4720 at 100 mm/min are shown in Table 8. This adhesive was characterized in bulk tension at 1 mm/min in previous works and a comparison between the experimental curve obtained at 100 mm/min and 1 mm/min are presented in the Figure 35.

Table 8- Mechanical properties of SikaPower 4720 at 100 mm/min**.**

Strain rate (mm/min)	Tensile strength (MPa)	Young's modulus (MPa)	Strain to failure (%)
1*	32	2170	3.4
100	35.7 ± 1.7	2431 ± 90.9	3.1 ± 0.4

*Results obtained in previous work.

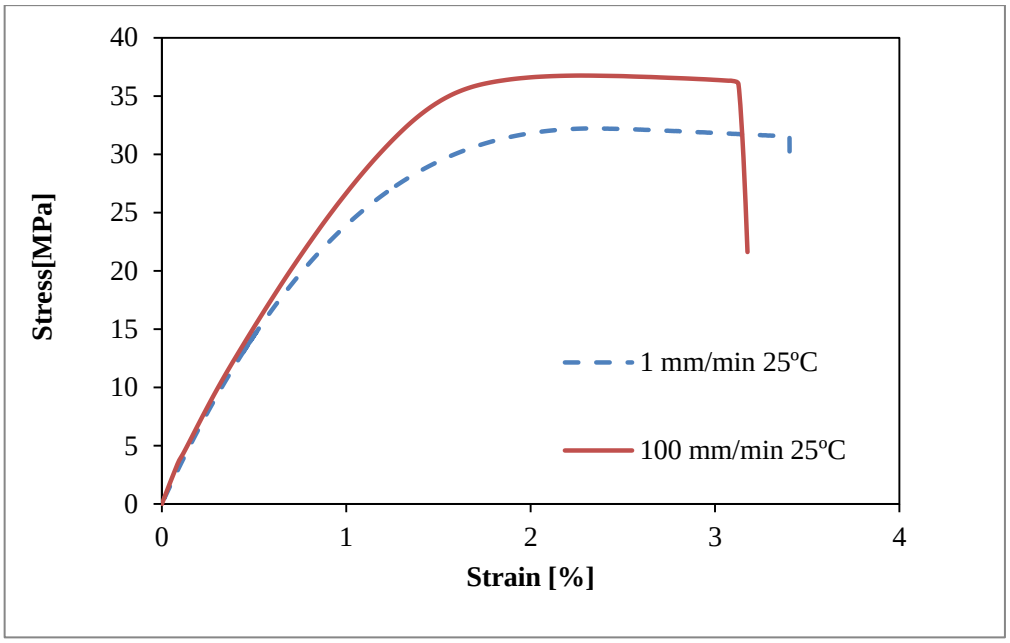

Figure 35- Comparison of results between at 1 mm/min and 100 mm/min for SikaPower 4720 adhesive.

In the figures above an increase of adhesive tensile strength at 100 mm/min is observed, as well as an insignificant variation in average young's modulus was found when compared with the properties of adhesive at 1mm/min. In the case of this adhesive, the ductility at 100 mm/min was lesser when compared with the properties obtained at 1 mm/min which is consistent with the literature.

Dogbone adhesive specimens before and after tests can be seen in Figure 36.

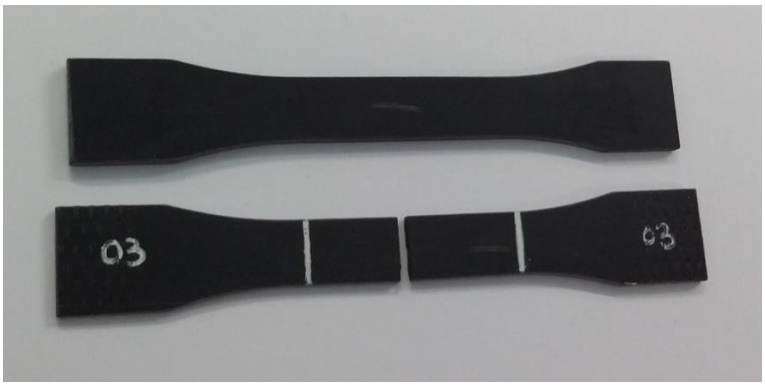

Figure 36- SikaPower 4720 bulk specimens before and after of the tensile test.

❖ End-Notched Flexure (ENF)- Nagase XNR 6852 E-2

The mode II fracture testing of adhesive joints is significantly more complex than mode I testing and is yet to be standardized. However there are tests based on interlaminar fracture of composites in mode II which can be adapted to the adhesive joint study [52].

In this context, one the most popular tests used to measure the mode II fracture toughness (G_{II}) is ENF. The test consists in a simply supported beam loaded at midlength, with a pre-crack at one of the edges (see Figure 37). One of the disadvantages of the ENF test is the unstable crack propagation [34].

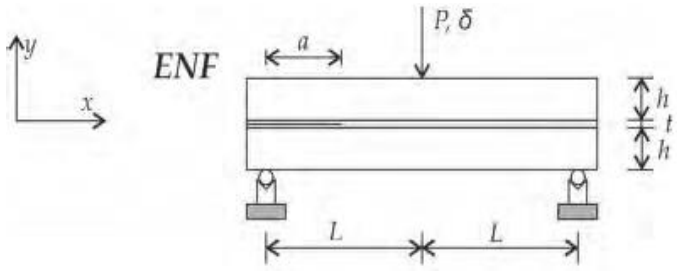

Figure 37- Schematic representation of the end notched flexure (ENF) [56]**.**

The strain energy release rate is determined from an experimental load-displacement curve by means of the compliance-based beam method (CBBM). CBBM allows the determination of the resistance curve (R-curve), without the requirement of measuring the crack length during the test. In this case the concept of equivalent elastic crack length (*aeq*) is introduced [53].

Therefore, in order to obtain G_{IIc} of Nagase adhesive, the ENF test was realized. The heat-treated steel DIN 40CrMnMo7 was used for the substrates. It is a high strength steel with a yield strength of 900 MPa. The specimen geometry is represented in Figure 38. The geometry used for the ENF test is the one used for the double cantilever beam (DCB) test, where the length between the supports was 283 mm and the initial crack length was 60 mm. The bondline thickness used was 0.2 mm.

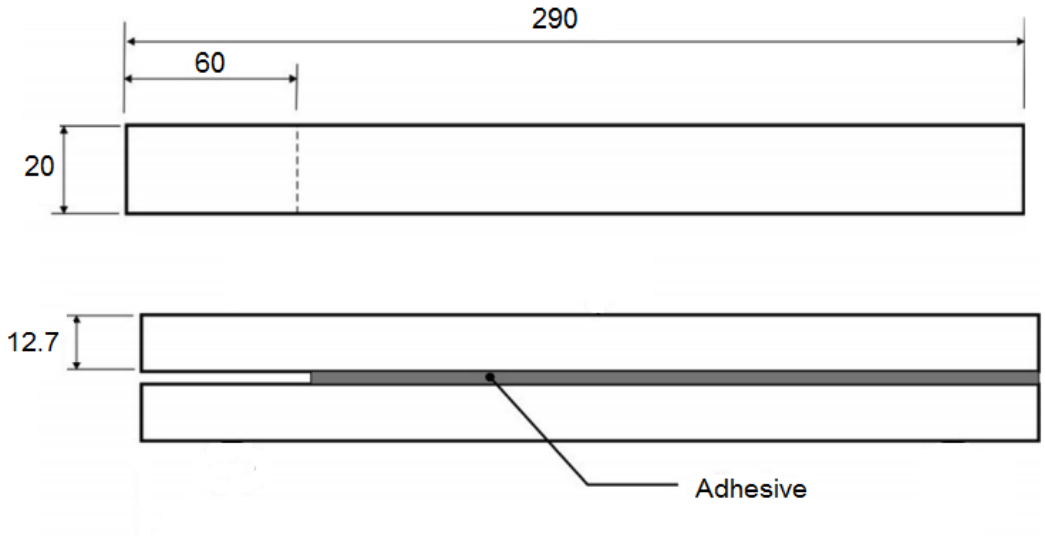

Figure 38- Geometry of the end notched flexure (ENF) test specimen.

Relatively to the specimen manufacture, the joint surfaces were grit blasted and degreased with acetone prior to the application of the adhesive. Spacers were inserted between the adherends before the application of the adhesive in order to control the bondline thickness. The ENF specimens with Nagase XNR 6852 E-2 were cured at 150 °C for approximately 4 h. A jig with spacers for the correct alignment of the adherends was used and is shown in Figure 39.

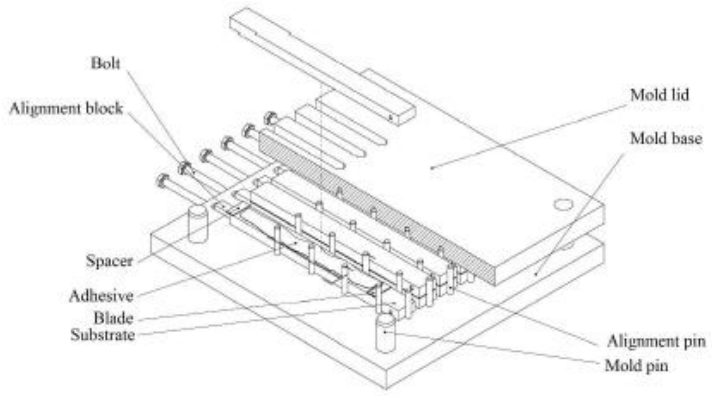

Figure 39- Schematic representation of the mold used to cure the DCB specimens.

The ENF specimens were tested using an INSTRON® model 3367 universal testing machine, under a constant crosshead rate of 0.5 mm/min. During the test, a load-displacement curve ($P-\delta$) was registered and the pictures were recorded at 5s intervals using a digital camera. This procedure allows the crack length measuring during its growth. The three tested specimens were marked with a white paint to facilitate the crack length reading. In order to minimize the friction effects concentrated at the region of the pre-crack above the support, two sheets of teflon with a thin pellicle of lubricator were included in the pre-crack region (see Figure 40).

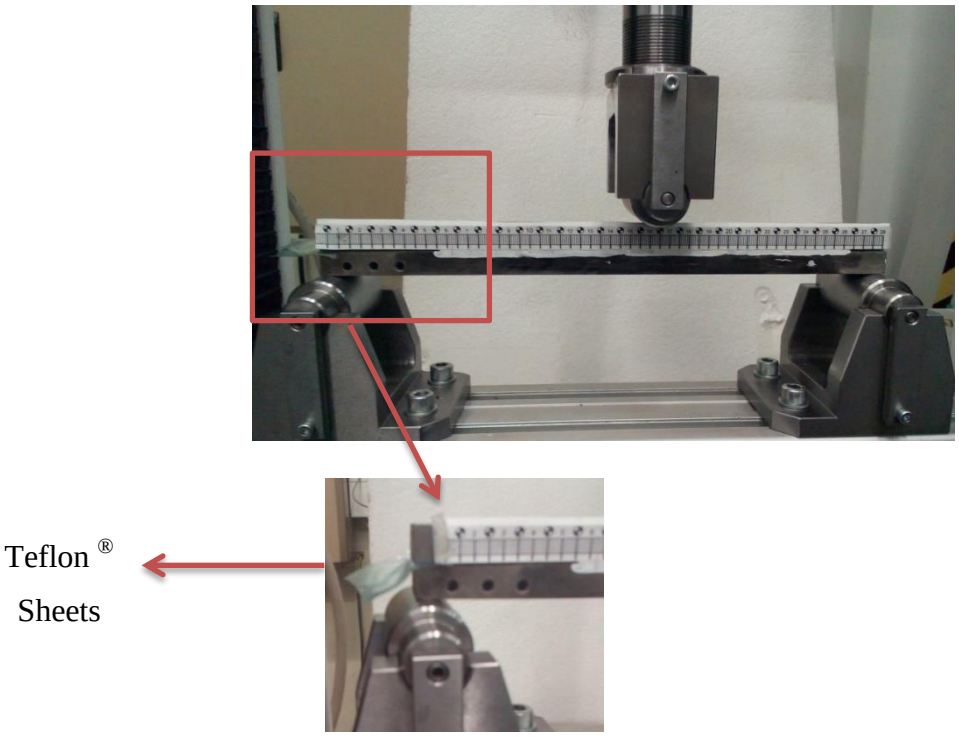

Figure 40- Experimental Set-up of the ENF test.

The results show that all specimens failed cohesively in the adhesive (see Figure 43). The $P-\delta$ curves for three specimens are presented in Figure 41.

Experimental R-curves obtained for the adhesive are shown in Figure 42. R-curves are used to identify the fracture energy from the plateau corresponding to the self-similar crack propagation. The fracture toughness was determined using the CBBM.

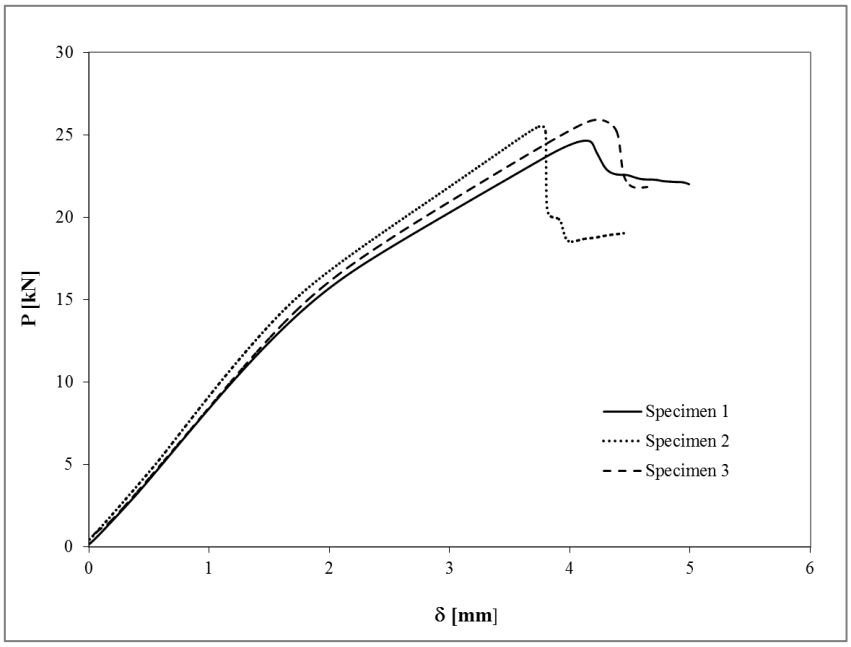

Figure 41- A representative experimental $P-\delta$ curves for three specimens tested.

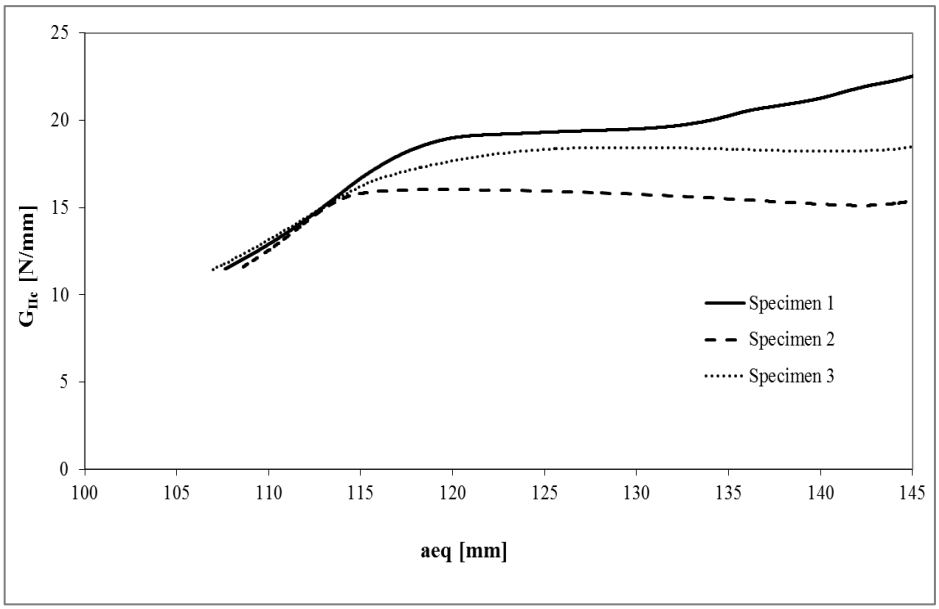

Figure 42- Typical experimental R-curves obtained for the Nagase XNR 6852 E-2 adhesive.

Table 9 shows the value of fracture toughness for three specimens and the corresponding average.

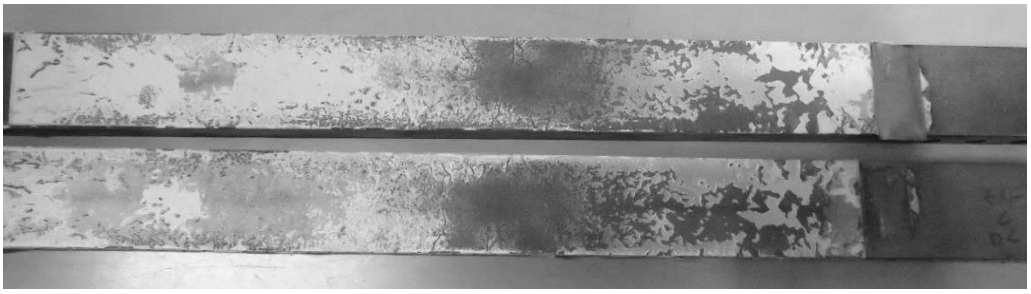

Figure 43- Fracture surface obtained after the ENF test.

Table 9- Fracture Toughness in Mode II determined using the CBBM method for Nagase XNR 6852 E-2.

Specimen	G_{IIC} (N/mm)
1	19.4
2	18.4
3	15.9
Average	**17.9**

As concluded from the table 9, G_{IIc} for the adhesive Nagase XNR 6852 E-2 is approximately 18 N/mm.

❖ Thick adherend shear test (TAST)- Nagase 6852 E-2

TAST is one of the most popular types of failure strength test because it is easy to make and test the specimens in order to obtain the adhesive's shear properties. Two forms of TAST are used: Krieger (ASTM D3983) in the United States and Althof and Neumann (ISO 11003-2), in Europe. These two tests have a main difference between them: the size of the specimen (the Althof specimen is half the size of Krieger's). An important point of this test and that can be considered an disadvantage is the fact that specimens produced by this method cannot be reused. Adams and al. have proposed that the solution is to machine the adherends to correct dimensions before bonding with the geometry shown in Figure 44a) [4], [34].

The bondline thickness used was 0.5 mm for the Nagase XNR 6852 E-2 and 1 mm for SikaPower 4720. The length of overlap test was 5 mm. Before the application of the adhesive, the joint surfaces were grit blasted and degreased with acetone .Spacers were inserted in the gaps between the adherends after the application of the adhesive and prior to curing, in order to provide the necessary spacing between the two adherends. A mould with spacers for correct alignment of the specimens was used and can be seen in Figure 44b). The SikaPower 4720 adhesive was cured at RT for one day and in the case of Nagase XNR 6852 E-2, the adhesive cured for approximately 4h at the hot press.After curing the adhesive, the spacers can be removed. The tests were performed at room temperature and a constant crosshead rate of 1mm/min and 100 mm/min for Nagase XNR 6852 E-2 and 1 mm/min for SikaPower 4720. The TAST test for SikaPower 4720 at 100 mm/min was not possible, because the adhesive is too brittle. The displacement was measured with an extensometer which is mounted in the metallic substrate. Three joints were tested for each adhesive. As the extensometer is mounted in the metallic substrate, the extensometer measures not only the displacement of the adhesive, but also the displacement of the adherend. Therefore, it is necessary to apply a correction to the measured displacements.

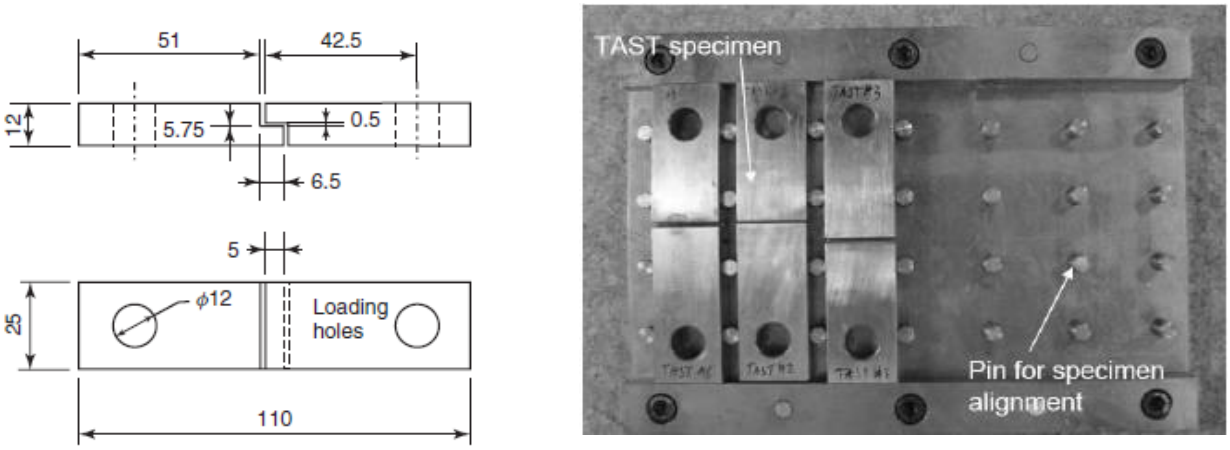

Figure 44- (a) Specimen geometry used for TAST tests. (b) Mould for TAST specimens fabrication [34].

Typical shear stress-strain curves for the Nagase XNR 6852 E-2 and SikaPower 4720 tested at RT are shown in Figures 45 and 46. From the shear stress-strain curves, the shear

modulus and shear strength were calculated. The values of shear modulus were calculated from the tangent to the shear stress-strain curve at the origin.

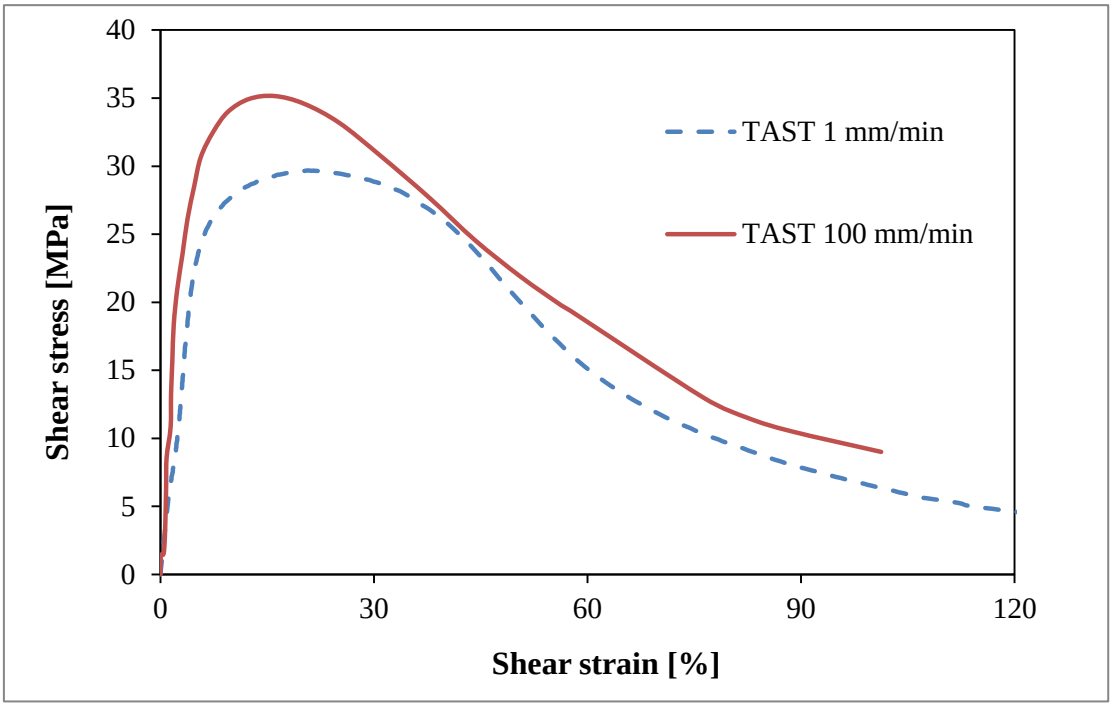

Figure 45- TAST shear stress-strain curves of Nagase XNR 6852 E-2 adhesive at two different strain rates.

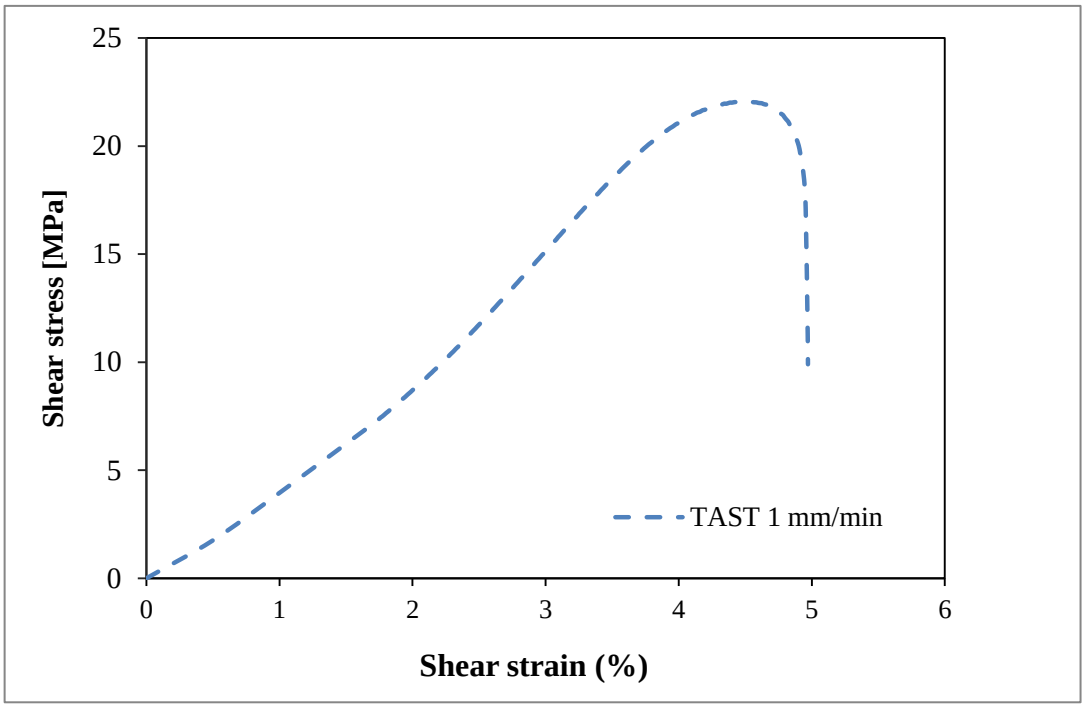

Figure 46- Shear stress-strain curve of SikaPower 4720 at 1 mm/min.

The shear strength and strain data for the adhesives XNR 6852 E-2 and Power 4720 are presented in Table 10.

Table 10- Results for two adhesives obtained from the TAST.

Adhesive	Shear strength (MPa)	Shear strain (%)
Nagase XNR 6852E-2 at 1 mm/min	28.7 ± 0.7	125 ± 17
Nagase XNR 6852E-2 at 100 mm/min	33.6 ± 7.4	92 ± 10
SikaPower 4720 at 1 mm/min	22.8 ± 0.7	5.2 ± 0.3

Typical failure modes of the TAST specimens are presented in Figure 47. The failure was essentially cohesive.

(a) **(b)**

Figure 47- Failure mode in TAST specimens: (a) XNR 6852 E-2 (b) Sika Power 4720.

3.1.2 Adherend

3.1.2.1 Characterization of adherend

The adherends material used to manufacture the SLJ consisted on unidirectional laminates of CFRP *(Carbon Fibre Reinforced Plastics)*. The properties of unidirectional 0º lay-ups of carbon/epoxy pre-preg (SEAL® Texipreg HS 160 RM) were determined in previous work of Campilho et al. (2005) and are presented in Table 11.

Table 11- Properties of the CFRP elastic orthotropic used for the SLJ adherends at according axes system represented [11].

Elastic modulus (MPa)	Poisson's ratios	Shear modulus (MPa)
E_1= 1.09E5	ν_{12} = 0.342	G_{12} = 4315
E_2 = 8819	ν_{13} = 0.342	G_{13} = 4315
E_3 = 8819	ν_{23} = 0.380	G_{23} = 3200

3.1.2.2 Specimens preparation

The specimens consisted on unidirectional laminates of CFRP were produced by hand lay-up and cured in a hot plates press. The plates with dimension of 300x300 mm were fabricated from a unidirectional 0° lay-up of fourteen plies of carbon/epoxy pre-preg (SEAL® Texipreg HS 160 RM) with 0.15 mm of ply thickness. In order to obtain better properties in the solicitation direction, the unidirectional layers were disposed at 0º. Then, the laminate manufacturing process involves the following steps:

(a) Unfreezing the carbon/epoxy composite for some minutes.

(b) Cutting the pre-preg in squares of 300 mm x 300 mm.

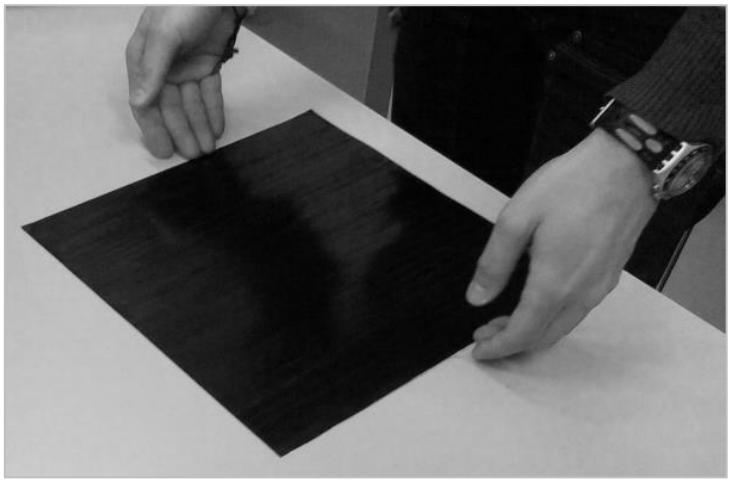

Figure 48- The pre-preg cutted in square**.**

(c) Stacking the laminate by hand lay-up, respecting the 0º sequence. The plies are piled one at a time, after heating in order to promote an easier adhesion. Then, the pressure is applied with a small weight.

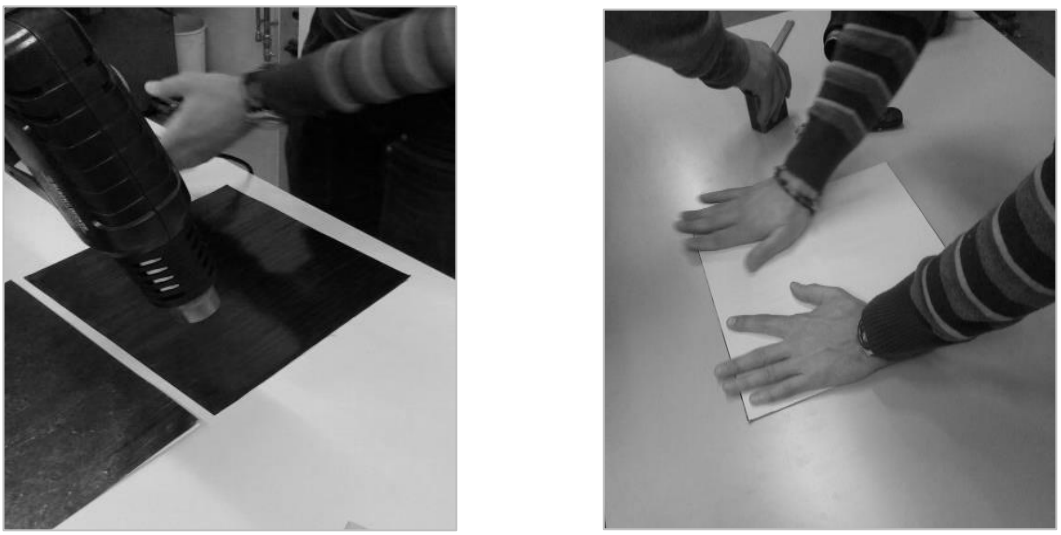

(a) **(b)**

Figure 49- (a) Heating the plies (b) application of pressure

(d) Squares shapes and various bars are used to ensure the pretended thickness of plate.

(e) The release agent is applied to ensure that the plates are removed with facility.

Figure 50- Application of release agent in the metallic sheets.

(f) The laminate is cured in a hot plates press (see Figure 51) under the defined thermal cycle recommended, under a pressure of 4 bar.

Figure 51- Hot plates press used to cure the CFRP plates.

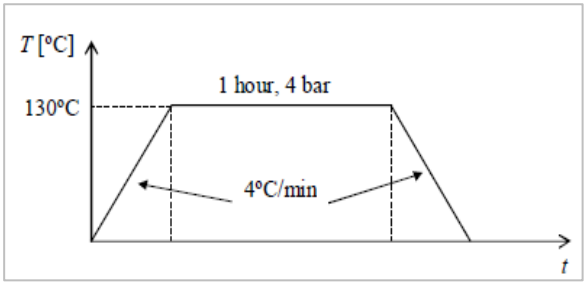

Figure 52- Thermal cycle applied to the laminate.

(g) After removal from the hot press, the laminate was cut into small specimens. The machine used was a diamond disc cutting (model DV 25 Batisti Meccanica).

Figure 53- Machine used to cut the CFRP plates.

3.1.2.3 Results of the composite properties

The young's modulus in the transverse and longitudinal directions was measured again in order to obtain the stress vs. strain curves at 1 mm/min and 100 mm/min. For that, two specimens geometry were manufactured: longitudinal and transverse laminates. The specimen geometry used is shown in Figure 54a) and follow the standard D638-03, corresponding to ISO 572-1. The test was performed in an INSTRON® model 3367 universal test machine (Norwood, Massachusetts, USA) the the displacement was measured with an extensometer which is mounted in the middle of specimen.

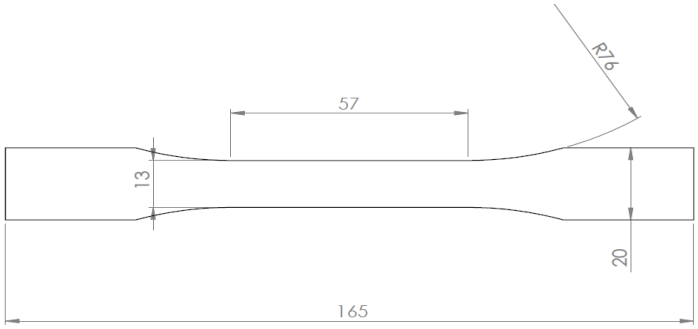

(a)

(b)

Figure 54- (a) Geometry Composite specimen according ASTM D638-03(dimensions in mm**)** (b) Dog-bone specimen after machining with fibers on longitudinal direction.

The representative stress-strain curves for the composite obtained in the tensile test are shown in Figure 55. In the longitudinal direction, the stress vs. strain curve only was measured at 1mm/min, because of the stiffness in this direction is very high and the properties at 100 mm/min will not change significantly, as reported in the literature review (see section 2.3). The specimens for longitudinal direction were not tested to failure because only wanted to check the elasticity. Therefore, the curves presented in figures above, only the elastic part is represented. As can be seen, the stiffness of the fibers is the most effective along its longitudinal axis (see Figure 55 a)) and the lowest strength is obtained when the fibers are perpendicular or transverse to the loading direction (see Figure. 55 b)).

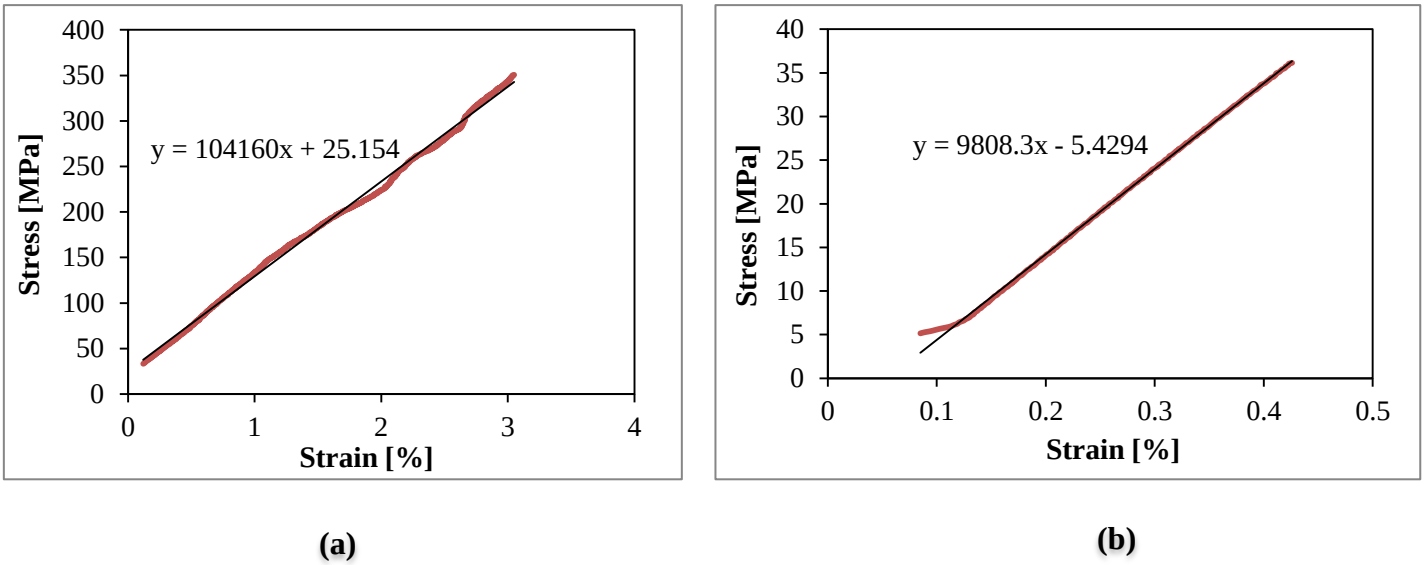

Figure 55-Strain vs strain curve for CFRP dog-bones at 1 mm/min. **(a)** longitudinal direction **(b)** transverse direction

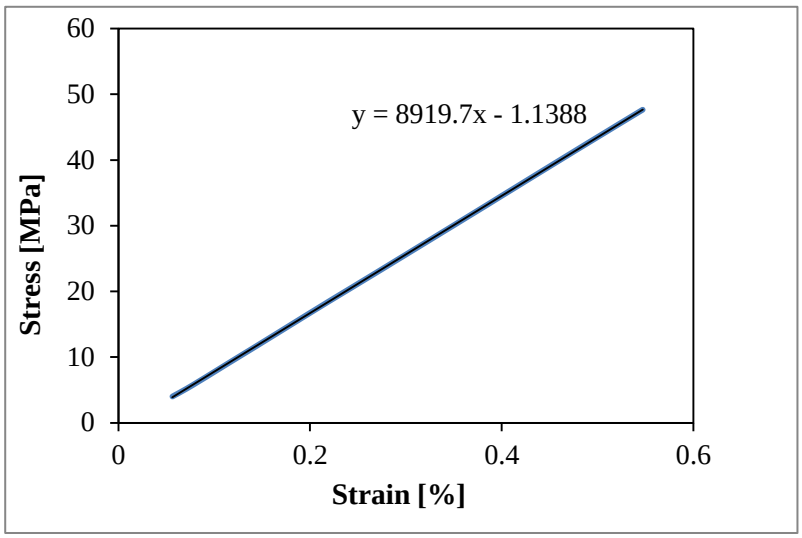

Figure 56- Strain vs strain curve for transverse direction at 100 mm/min.

The properties obtained for the composite in the two directions are presented in Table 12. As can be seen from Table 12, the young's modulus in the direction xx is about 13 times higher than the direction yy. With high speed rate, the Young's modulus and the tensile strength in transverse direction increase.

In order to check the displacement of the Instron machine, two types of equipment's were used for measuring: an extensometer coupled to the dog-bone specimen and only machine without measure equipment. The results obtained for young's modulus in the longitudinal direction are presented in Figure 57. A strain error factor of approximately 104/30 can be applied for the purpose of correcting the differences.

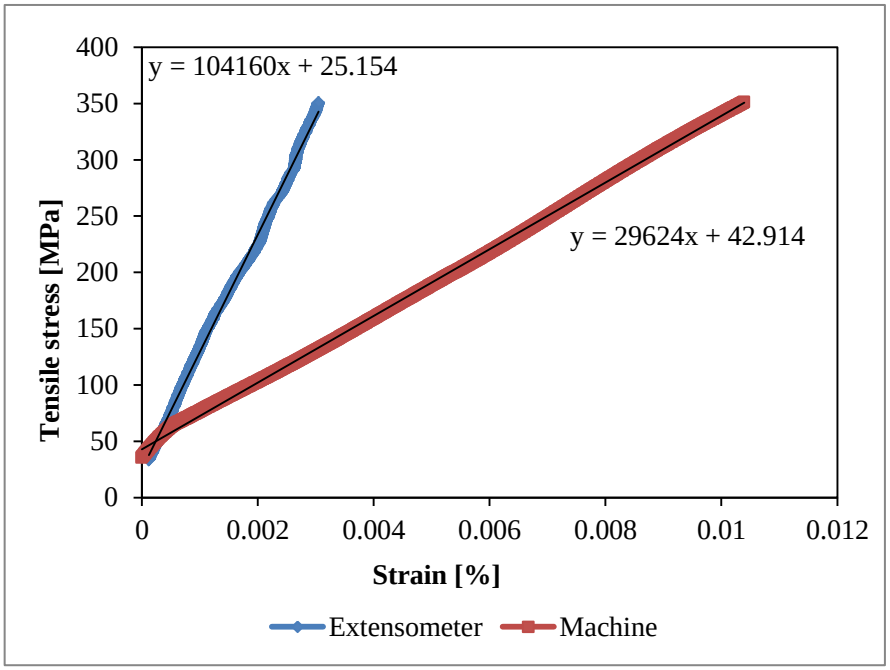

Figure 57- Young's modulus measured with the extensometer and machine.

Table 12- Properties obtained of the composite tensile tests.

Property	Property value
E_x at 1 mm/min	105 ± 1.5 GPa
E_y at 1 mm/min	8.2 ± 1.271 GPa
E_y at 100 mm/min	8.8 ± 0.77 GPa
σ_y at 1 mm/min	42.6 ± 5.1 MPa
σ_y at 100 mm/min	54.0 ± 4.6 MPa

3.2 Joint geometry

Two groups of SLJs were used, with a single difference between them lying in the overlap lengths, which were 12.5 mm and 25 mm. Other different aspect is the presence of aluminum and steel tabs which were bonded in the ends for the impact tests. In this way, it is avoided the holes failure in the impact tests are avoided, where a special assemble is needed. The composite adherends thickness was 2.1 mm and the adhesive thickness used was 0.2 mm. The geometry used for static and the impact tests was chosen because it is a faithful representation of the adhesive joint in the automotive industry. The specimen geometry can be seen in Figure 58.

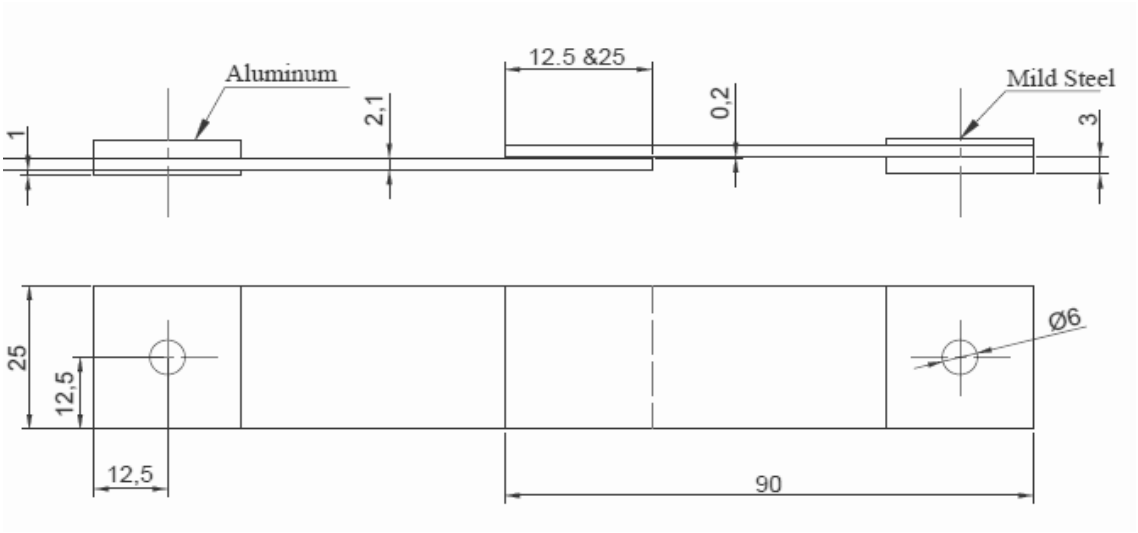

Figure 58- SLJ geometry used in static and impact tests (dimensions in mm).

3.3 Joint manufacture

The joint surfaces were grit blasted and degreased with acetone in the overlap zone prior to the application of the adhesive.

It was used a mould with spacers for correct alignment of the substrates (see Figure 59). The substrates were bonded and then the Nagase XNR 6852 E-2 joints were cured at 150ºC for approximately 4 hours in a hot-press. In the case of SikaPower 4720 adhesive, the SLJs were left under the pressure at room temperature for 24h. At the end of the curing process, any excess of adhesive was carefully removed using a drilling machine.

Once the curing process was over and the exceed adhesive was removed, four plates were bonded in the SJLs for the impact tests and were also bonded two plates for the static tests in order to improve grip in the impact machine and avoid the hole delamination. The ending step was to drill the holes in the SLJs to allow the assembling of the specimen to the machine holding device, as shown in figure 60.

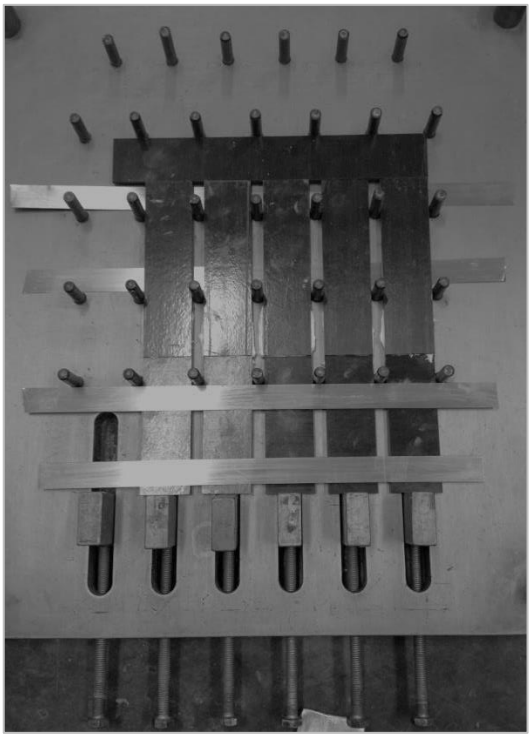

Figure 59- Mould for SLJ specimens fabrication.

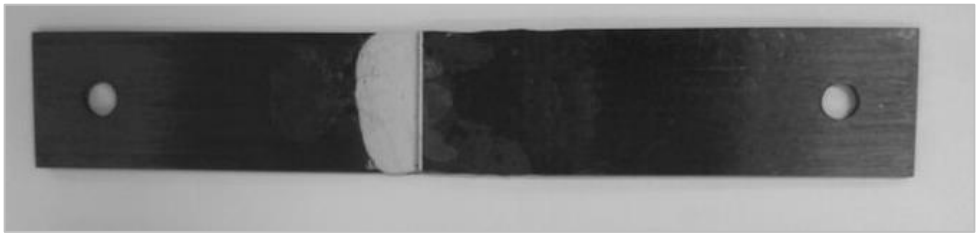

Figure 60- SLJ after to drill the holes.

3.4 Joint testing

The static tests were performed in the universal testing machine INSTRON® model 3367 (Norwood, Massachusetts, USA) with a capacity of 30 kN with a constant crosshead rate of 1mm/min at room temperature. Four joints were tested for each condition and for each joint tested load-displacement curve was produced.

The SLJs in the impact tests were tested using the machine Rosand® Instrumented Falling weight impact tester, type 5 H.V. (Stourbridge, West Midlands, U.K.). This machine drops a mass guided from a certain high until it impacts on the device that holds the specimen. The energy applied in the impact is controlled by the weight of the falling mass, and the speed can be set by the height. The load was transmitted to the SLJs thanks to the vertical guide. A load cell to keep up with the mass was used to measure load and time. After assembling the specimen, the mass (26 kg) was set to provide an impact energy of 50 J. The height was set to give an impact speed of 2 m/s. Figure 61 shows the experimental setup used for SLJ impact tests. Five SLJs were tested for each adhesive and SLJ overlap length.

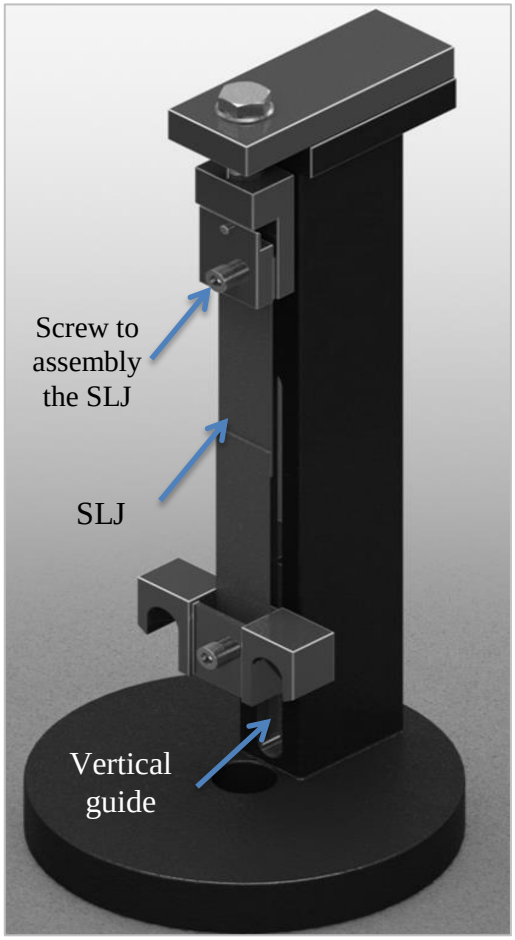

Figure 61- Setup for the impact testing of the joint [36].

Chapter 4

In this chapter, the numerical details are described as well as the properties used to the Abaqus® models for the static and impact conditions.

NUMERICAL DETAILS

The FEM software ABAQUS® was selected to perform the numerical analysis in order to predict the strength of SLJs. The mesh used for the single-lap joints can be seen in Figure 62. The mesh was particularly refined at the overlap edges to accurately capture spots of stress concentrations. The joint was modeled as two-dimensional, with plane-strain solid elements.

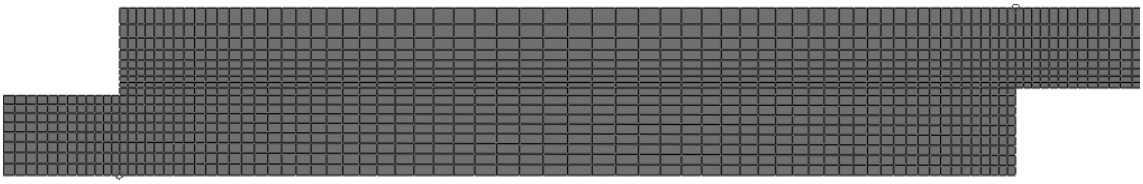

Figure 62- Detail of the mesh for the $L_0 = 25\ mm$.

4.1 Cohesive Zone Modelling (CZM)

In this work, a continuum-based approach was considered to model the finite thickness of the adhesive layer. The adhesive layer was modeled as a traction-separation law with CZM's and the adherends as elastic solids. A more detailed description of CZM can be seen in section 2.1.5. The triangular CZM (see Figure 63) formulation was chosen for this analysis because of its simplicity, large use for investigation purposes, and availability in ABAQUS including a mixed-mode formulation, which is absolutely necessary to model the single-lap joints used in this work.

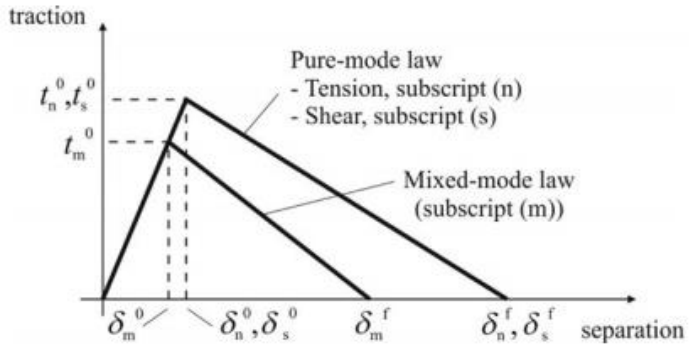

Figure 63- Traction-separation law with linear softening law available in ABAQUS®.

4.1.1 Static Analysis

Table 13 shows the values introduced in ABAQUS® for the adhesive layer damage laws. The parameters G_n^c and G_s^c (the fracture toughness in pure mode I and II) were defined by DCB and ENF tests, respectively (see section 3.1.1). The t_n^0 (normal cohesive stress) for two adhesives was determined from tensile bulk tests, while t_s^0 (shear cohesive stress) was determined from TAST tests. The elements introduced in Abaqus are shown in Figure 64.

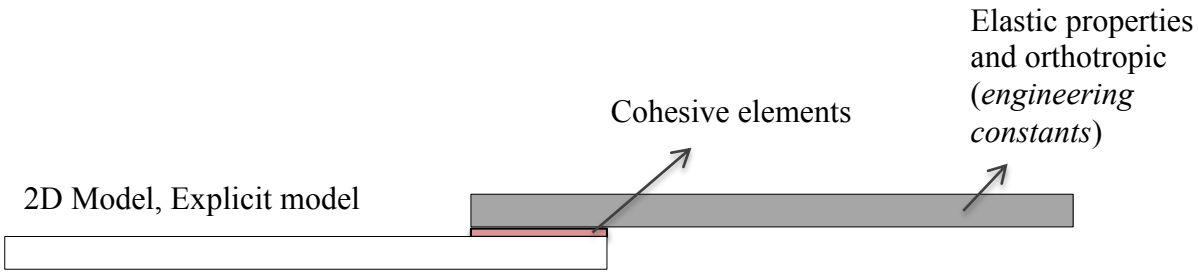

Figure 64- Elements introduced in Abaqus® simulations for the static analysis.

The joints were restrained (i.e., clamped) at one of the edges to simulate real clamping conditions in the machine grips and the other edge was subjected to a tensile displacement with transverse restraining. The G_{IIc} of SikaPower 4720 was obtained by testing various values for that found a better estimative between the numerical and experimental results.

Table 13- Cohesive parameters of the SikaPower ® 4720 and Nagase XNR ® 6852 E-2.

Property	SikaPower 4720	Nagase XNR 6852 E-2
E [MPa]	2170	1742
G[MPa]	834	640
t_n^0 [MPa]	32.0	42.9
t_s^0[MPa]	22.9	28.7
G_n^c [N/mm]	1.63	1.7
G_s^c [N/mm]	3	18

The properties used for the composite adherend were presented in the section 3.1.2. The numerical results as well as the comparison with experimental results are present in the section 5.

4.1.2 Impact analysis

In order to predict and simulate the composite to impact load, an explicit model was used. Then, the explicit model provides the capability to analyze high-speed problems, such as, drop weight tests and crash analyses of structural members. A mass was introduced in the extremity of joint, as shown in Figure 65.

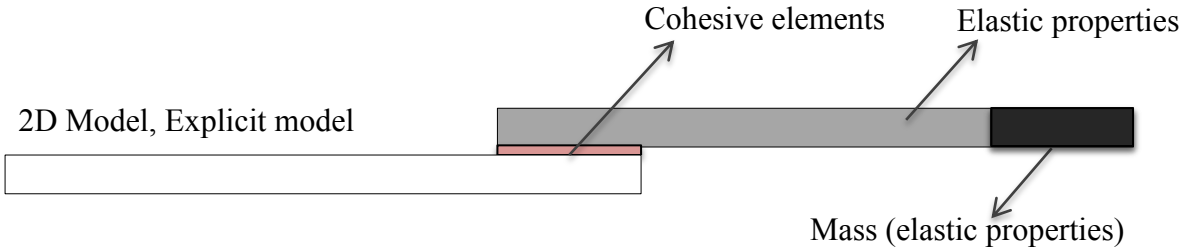

Figure 65-Elements introduced in Abaqus® simulations for the impact analysis.

The boundary conditions were the same as the ones used in the static analysis with only an exception concerning the predefined field of velocity type with the value of 2 m/s. This value was introduced in order to obtain the same conditions in drop weight tests.

For the purpose of obtaining a properties adhesive value at impact speed, extrapolation was done with experimental properties values obtained at 1 mm/min and 100 mm/min (see section 3.1.1). Then, in the Table 14, are presented the values calculated with extrapolation at 2 m/s (impact speed). A logarithmic extrapolation (see equation 30) was used in order to obtain the CZM parameters.

$$\text{Property to determine} = \text{A}\ ln(\dot{\varepsilon}) + \text{B} \qquad \text{(Eq. 14)}$$

Where A and B are constants obtained to experimental data and $\dot{\varepsilon}$ is the strain rate in s^{-1}.

In order to determine the strain rate ($\dot{\varepsilon}$) is used the following expression:

$$\dot{\varepsilon}_{impact} = \frac{v_{test}}{t} \qquad \text{(Eq. 15)}$$

In this case, the value of t is the adhesive thickness, because the elastic modulus of the adhesive is much smaller than the modulus of the adherends and in-plane length of the adhesive joint is much larger than the thickness of the adherends (see Figure 66).

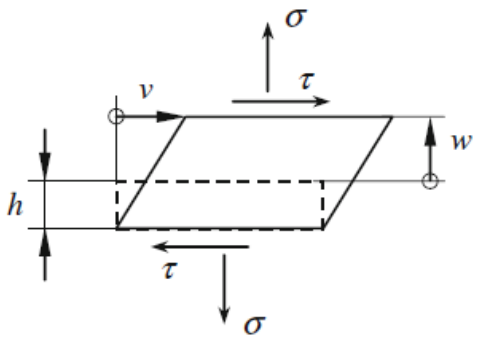

Figure 66-Deformation modes of the adhesive layer with thickness (h), peel (w), and shear (v).

Table 14- Cohesive parameters of the SikaPower® 4720 and Nagase XNR ® 6852 E-2 obtained at impact speed (2 m/s).

Property	SikaPower 4720	Nagase XNR 6852 E-2
E [MPa]	3113	1959
G*[MPa]	1198	753
t_n^0 [MPa]	45.4	54.1
t_s^0[MPa]	30	42.1

$*G = \frac{E}{2(1+\nu)}$

The critical fracture energy for mode I and mode II are also strain rate dependent. As shown in section 2.1.6, the G_{IIc} increases slightly with increasing strain rate. Therefore, this value was maintained for two adhesives from static to impact conditions. Various tests were performed in Abaqus® in order to find the better value for G_{IIc}. The results obtained are shown in section 5.3. The fracture properties used in simulations are presented in Table 15.

Table 15- Fracture properties used in simulations.

Fracture toughness	SikaPower 4720	Nagase XNR 6852 E-2
G_n^c [N/mm]	1.63	1.7
G_s^c N/mm]	4.0	19

Chapter 5

In this chapter, the experimental results obtained in static and impact tests are summarized and discussed. Moreover, the numerical results are presented as well as the conclusions taken.

RESULTS AND DISCUSSION

5.1 Experimental results - static tests

The load-displacement curves of the XNR 6852 E-2 for two overlap lengths (12.5 mm and 25 mm) are depicted in Figure 67. The load and displacement data used were extracted from the recorded files provided by the INSTRON® machine.

In the Literature Review it was mentioned how the failure load should increase as a function of the overlap length in linearly proportion in the case of adhesive joints with elastic adherends and ductile adhesive. However, although failure load increased with overlap length, in this particular case this tendency was not found (see Figure 67). Also, according to the cohesive properties obtained for this adhesive, the values are quite lower than the expected. Table 16 shows the average of the results obtained for the Nagase XNR 6852 E-2 adhesive.

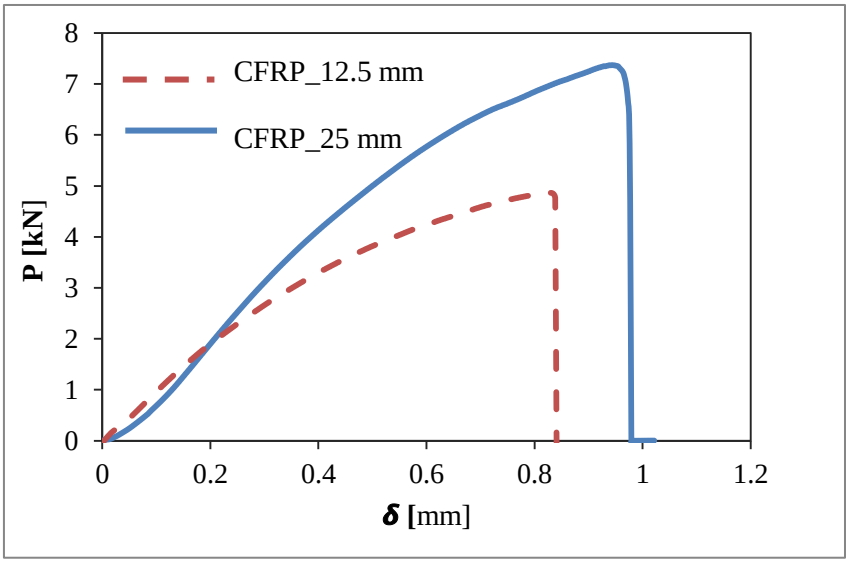

Figure 67- P-δ curve of the Nagase XNR 6852 E-2 adhesive for the two overlap lengths studied.

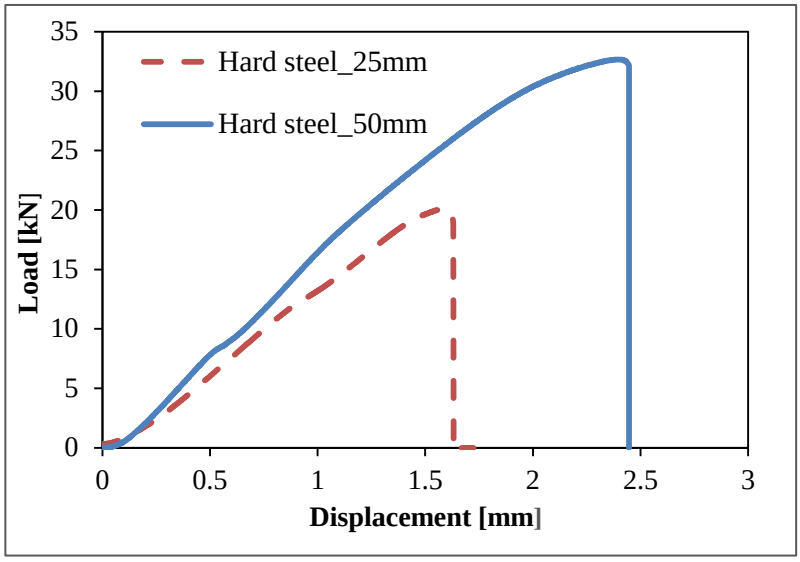

Figure 68- P-$\boldsymbol{\delta}$ curve of the Nagase XNR 6852 E-2 adhesive for hard steel adherends and the failure mode obtained, respectively.

Table 16- Average results obtained to the maximum load and displacement, respectively.

Overlap	25 mm	12.5 mm
P	**6.97** ± 0.19	**5.23** ± 0.76
$\boldsymbol{\delta}$	**1.03** ± 0.17	**0.79** ± 0.13

The reason for this can be explained by observing the failure mode obtained (see Figure 69). Even though the overlap surface could look as if there was cohesive failure in the adhesive, the adhesive layer shows a strange distribution of remaining adhesive. In first place it was though that the failure was purely in the interface of the adhesive and the CFRP but, by it observing carefully, a very thin layer of adhesive is found. Therefore, although it cannot be described as pure adhesive failure, it is considered as bad adhesion with the CFRP. Furthermore, in Figure 68 it is shown a failure mode of this adhesive in a SLJ with hard steel adherends that was tested in other work, where the results obtained for different overlap lengths followed a linear proportion and where in a good agreement with the expected values regarding the adhesive properties. All the *P*- $\boldsymbol{\delta}$ curves obtained in the experiments are shown in the appendix A.

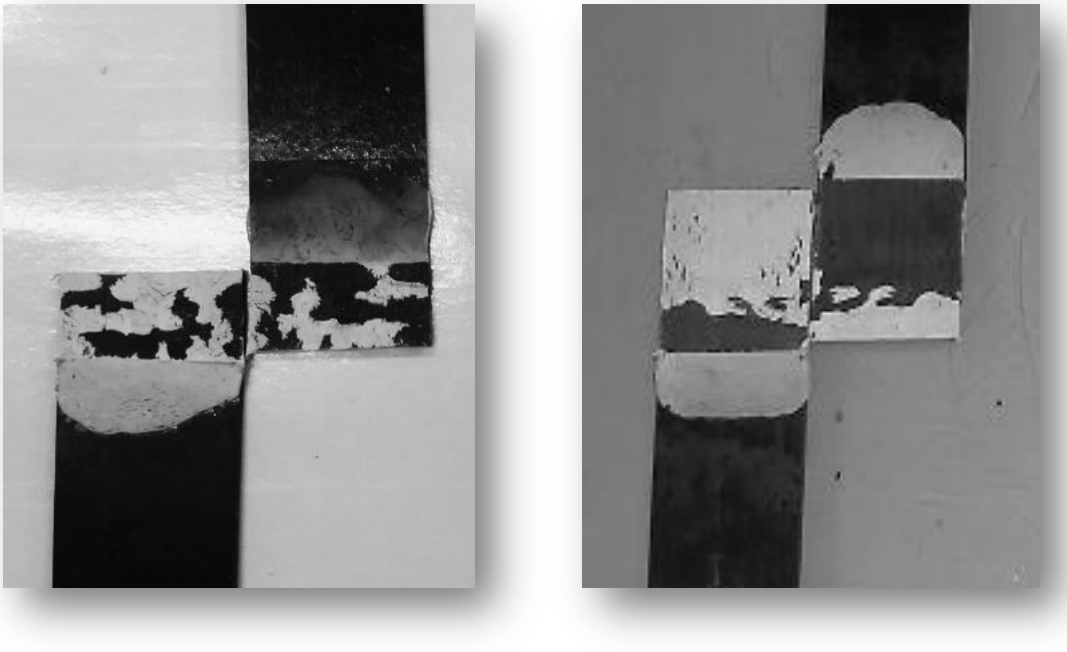

(a) **(b)**

Figure 69- Experimental fracture surfaces of Nagase XNR 6852 E-2 for two overlap lengths (a) 12.5 mm (b) 25 mm, respectively.

In the same way, the load-displacement curves for SikaPower 4720 were also obtained for two overlap lengths (12.5 mm and 25 mm). Once again, these values increase with the overlap length but, in this case, the maximum load is doubled with the 25 mm overlap (see figure 70), also agree well with the expected strength of the adhesive. The maximum displacement is also significantly higher than in the previous case. Table 17 shows the average results from the quasi-static tests for the SikaPower 4720 adhesive.

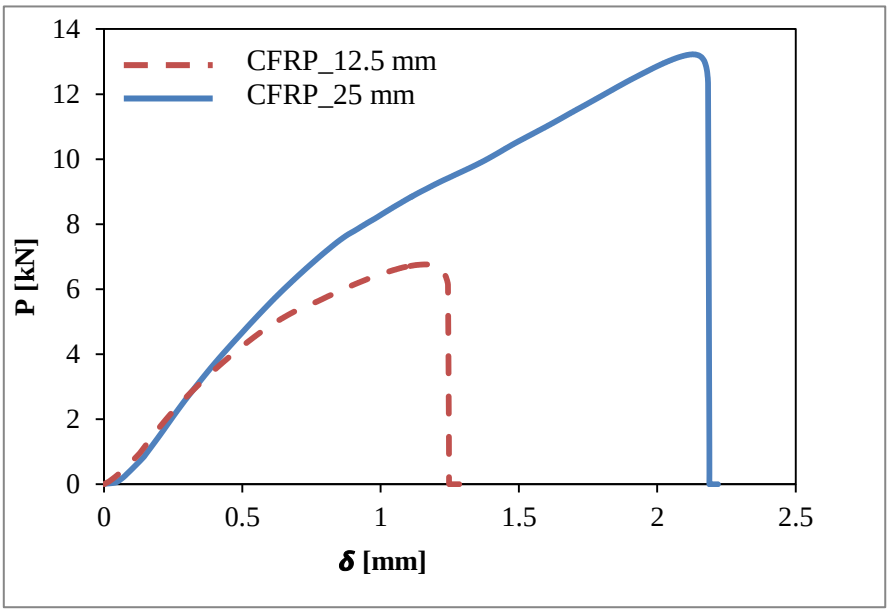

Figure 70- Quasi-static response of SikaPower 4720 SLJ for two overlap lengths .

Table 17- Average results to the maximum load (*P*) and displacement (***δ***), respectively.

Overlap	25 mm	12.5 mm
P	**12.85** ± 0.38	**6.71** ± 0.14
δ	**2.14** ± 0.10	**1.43** ± 0.34

After the tests, the failure modes of the specimens were visually evaluated. As can be observed in Figure 71, the failure in the SLJ specimens was perfectly cohesive for the two studied overlap lengths for this configuration.

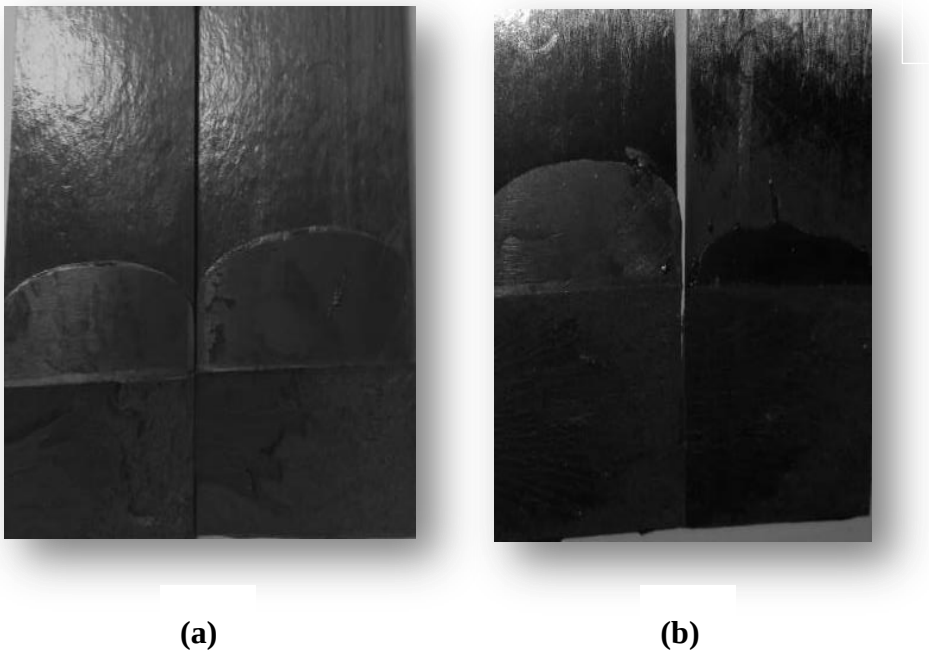

(a) **(b)**

Figure 71 - Experimental fracture surfaces of SikaPower 4720 adhesive for two overlap lengths (a) 12.5 mm (b) 25 mm, respectively.

To summarize the quasi-static tests, the average load of the Nagase XNR 6852 E-2 and SikaPower 4720 as a function of overlap length is presented in Figure 72. It can be seen more clearly the fact that the variation of the overlap affects in different ways both configurations. Moreover, according to the properties obtained in the characterisation of the adhesives, Nagase XNR 6852 E-2 was supposed to provide more strength to the joint than SikaPower 4720.

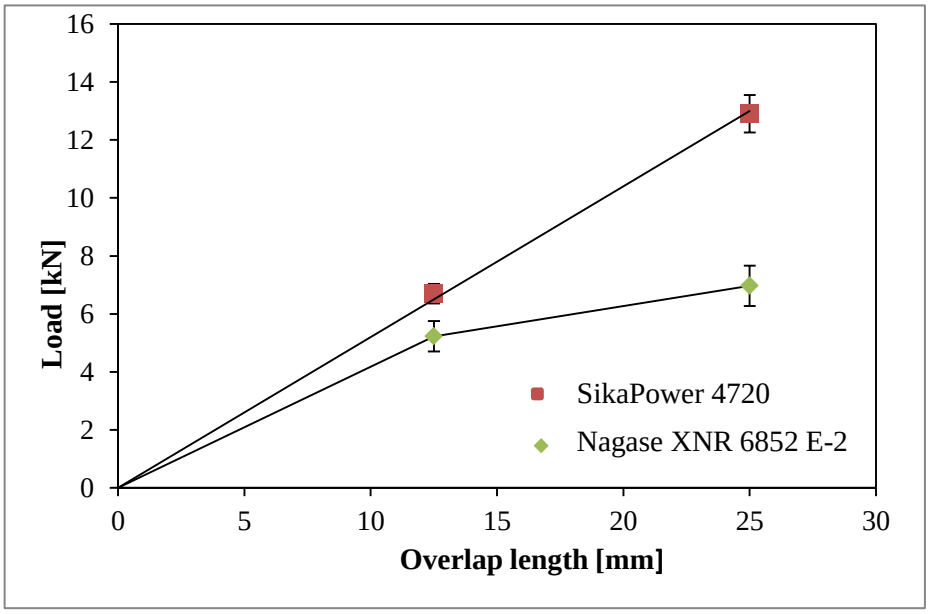

Figure 72- Failure loads of the Power 4720 and XNR 6852 E-2 with two overlap lengths studied.

- **Strength prediction**

Since all the materials of the components of the SLJ have been characterized, it should be possible to predict the joint strength by finding a suitable analysis model that explains the reason of failure. However, for the SLJ with Nagase, this prediction is expected to be inaccurate due to the reasons mentioned previously. Anyway, in order to have an idea of the strength that the joint should have, the prediction was also carried for this configuration.

Although more complex models of analysis can be found in literature, the Adams et al. model was chosen to predict failure under static conditions. The adhesive global yielding is considered for both the adhesives studied, because there is no plastic deformation in the CFRP adherends. Table 18 shows the predictions obtained compared with the experimental results. For calculations, the shear stress used for predictions are the TAST values (see section 3.1.1).

Table 18- Experimental results vs adhesive global yielding criteria of quasi-static tests.

Adhesive and Overlap length	**Avg. failure load (kN)**	**Predicted- P_y (kN)**
SikaPower 4720- 12.5 mm	6.7	7.1
SikaPower 4720- 25 mm	12.9	14.3
Nagase XNR 6852 E-2- 12.5 mm	5.2	9.0
Nagase XNR 6852 E-2- 25 mm	7.0	17.9

Figure 73 graphically represents the results in order to have a more visual comparison between the predicted curves and the experimental results.

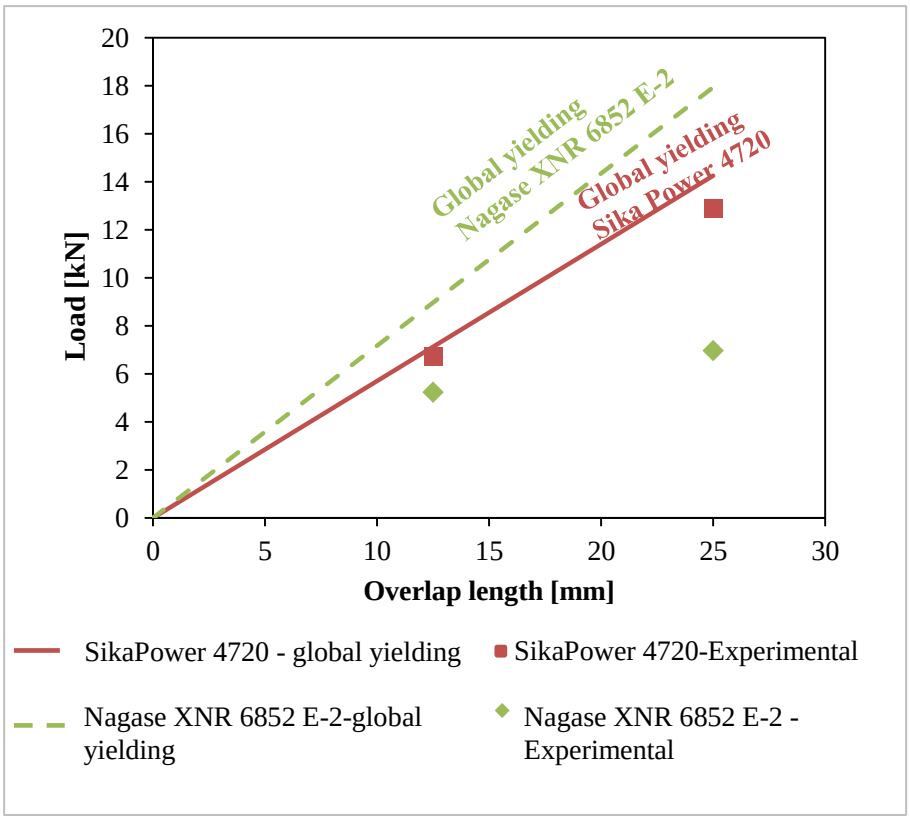

Figure 73- Global yielding criteria compared with experimental results.

As you can see in Figure 73, the results obtained for the Sika adhesive are a bit lower than the values predicted with the Global Yielding criteria, which can be explained by the fact that the adhesive has not enough strain to failure to be considered ductile and, therefore, the failure load cannot be accurately predicted with this model. On the other hand, the differences are substantially more accented with the Nagase adhesive. The maximum load for this adhesive (6.97 kN) was 45.7 % lower than the reference value calculated by the Global yielding criteria. These results can be explained due to bad adhesion existent between the adhesive and the composite.

5.2 Experimental results - impact tests

In this section, the impact results are presented and analyzed, showing the values of absorbed energy, failure load, elongation and failure mode in detail. Load and time are obtained from the load cell, which registers the values during the test and, after, the machine software calculates the displacement by integration. Then, load vs. displacement curves can be obtained. A digital filter with the value of 3 kHz (a value within the limits recommended by the machine manual) was applied to all the curves in order to filter the oscillations provided by the impact machine (drop weight) and to better estimate the effective load of each specimen.

Figure 74 shows representative load variation of the impact tests using SLJs bonded with SikaPower 4720 adhesive. As can be seen in Figure 84, every specimen showed a stable increase and the maximum filtered value before drastic decrease can be considered as the failure load of the specimens. The displacement is equivalent to the total elongation of the specimens, obtained from the load vs. elongation curve. As shown in Figure 75, all the specimens failed cohesively in the adhesive.

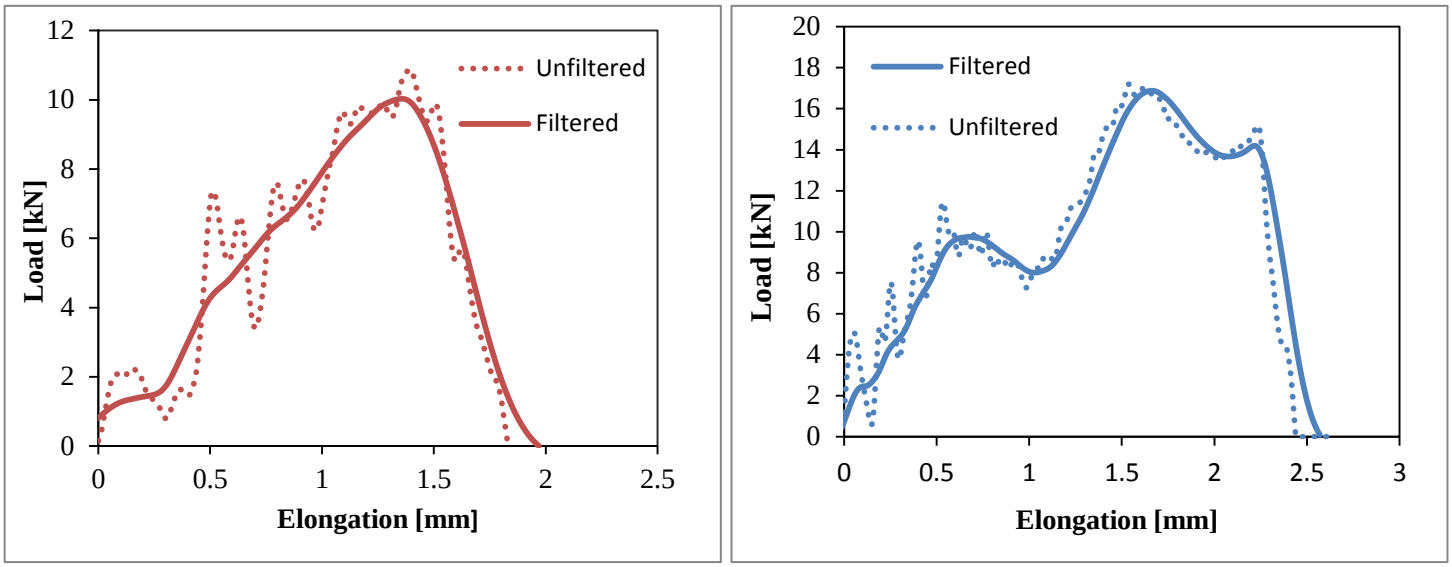

(a) **(b)**

Figure 74- Load vs. Elongation curves for SikaPower 4720 and two overlap lengths. (a) 12.5 mm (b) 25 mm

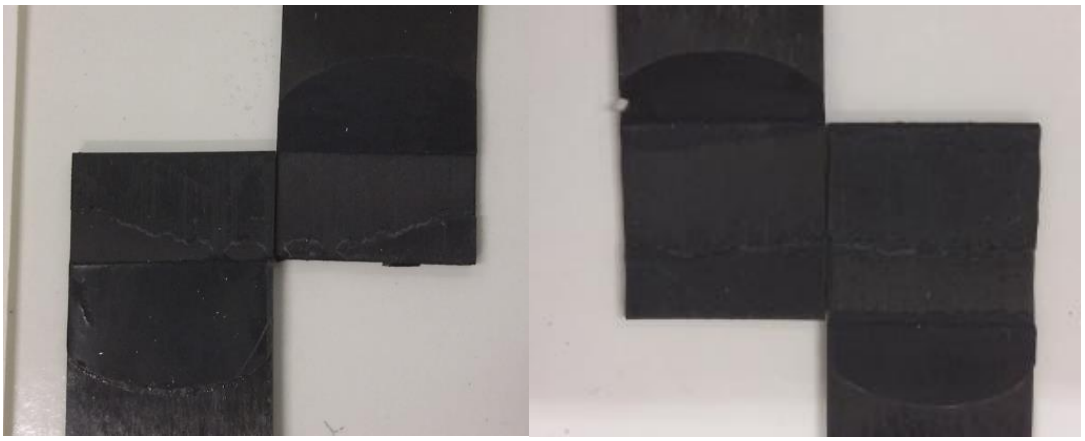

(a) **(b)**

Figure 75- Failure modes of SikaPower 4720 in impact specimens. (a) 12.5 mm (b) 25 mm.

The impact results for the Nagase adhesive are shown in Figure 76, while Figure 77 shows the fracture modes obtained. As happened under quasi-static load, the failure is controlled by a poor adhesion to the composite for two overlap lengths. Table 19 summarizes the average values and standard deviations of the impact tests for two adhesives and both 12.5 mm and 25 mm overlap lengths. The maximum failure load was obtained for the Sika adhesive and with 25 mm overlap length. Unfortunately, delamination in the composite was not obtained in either of the above cases, which was one of the objectives of this study.

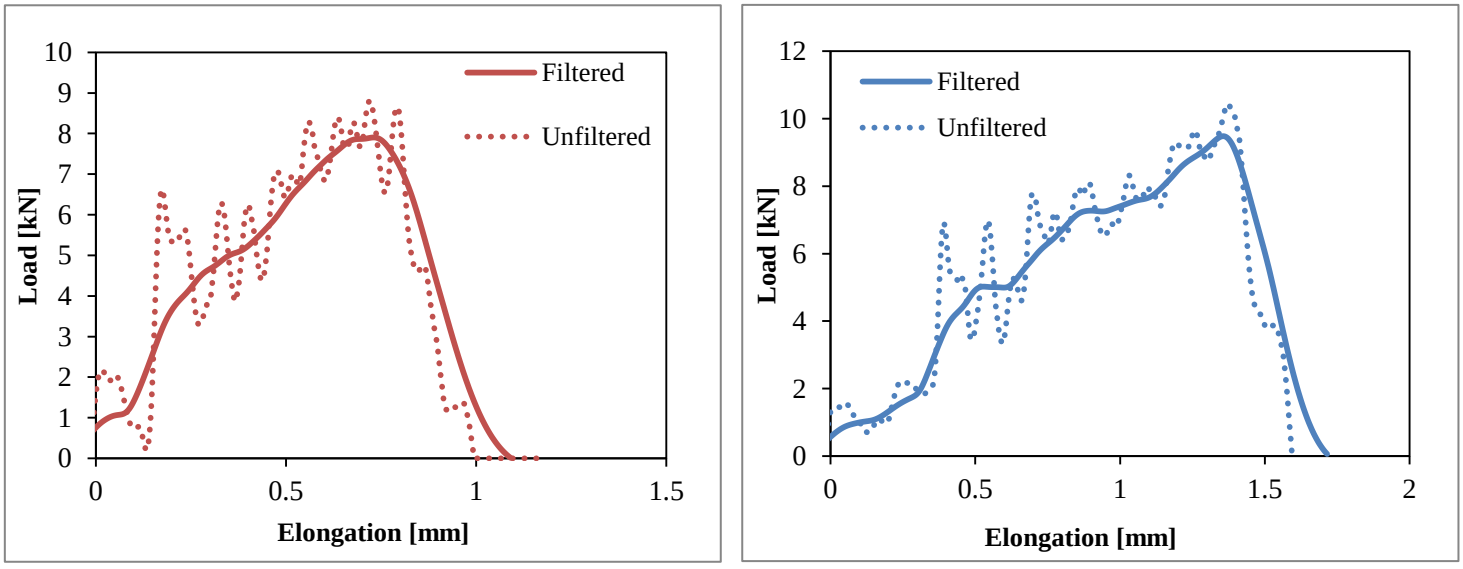

(a) **(b)**

Figure 76- Load vs. Elongation curves for Nagase XNR 6852 E-2 and two overlap lengths (a) 12.5 mm (b) 25 mm**.**

(a) **(b)**

Figure 77- Nagase XNR 6852 E-2 failure modes in impact specimens. (a) 12.5 mm (b) 25 mm.

Table 19- Summary of the impact results.

	Avg. energy absorbed (J)	**Avg. failure load (kN)**	**Avg. elongation (mm)**
SikaPower 4720_12.5 mm	10.7 ± 1.9	9.4 ± 1.1	1.7 ± 0.5
SikaPower 4720_25 mm	38.0 ± 6.2	17.3 ± 1.4	2.9 ± 0.5
Nagase XNR 6852 E-2_12.5 mm	10.4 ± 1.7	7.6 ± 1.2	1.6 ± 0.4
Nagase XNR 6852 E-2_25 mm	11.6 ± 0.9	8.9 ± 0.9	1.9 ± 0.4

The results presented above include the load vs. elongation. However, the energy absorption is a very important parameter to be measured in impact testing. Figure 78 summarizes all the absorbed energy results obtained as a function of maximum failure load.

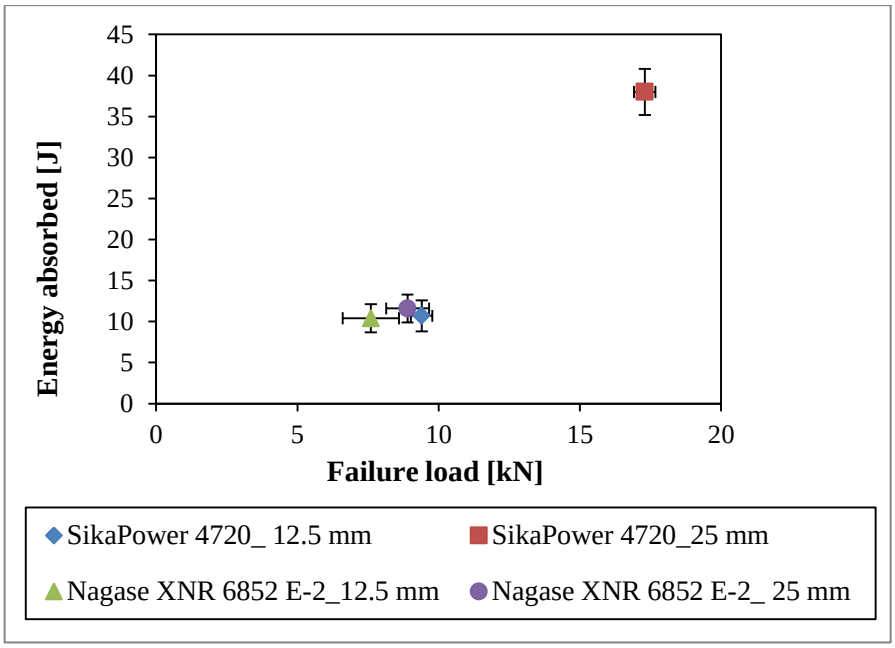

Figure 78- Energy absorbed vs. Maximum failure load results summary for the impact tests.

To conclude this section a summary of the failure loads obtained from the quasi-static and impact tests for the two studied adhesives is presented as a function of overlap length in order to compare these conditions (see Figure 79). In the case of static tests, adhesive joints under impact with SikaPower 4720 are still stronger than those with the Nagase XNR 6852 E-2 adhesive. There is an increase in joint strength from the static to the impact tests and this increase is proportional for both adhesives, which is expected due to their high strain rate sensitivity.

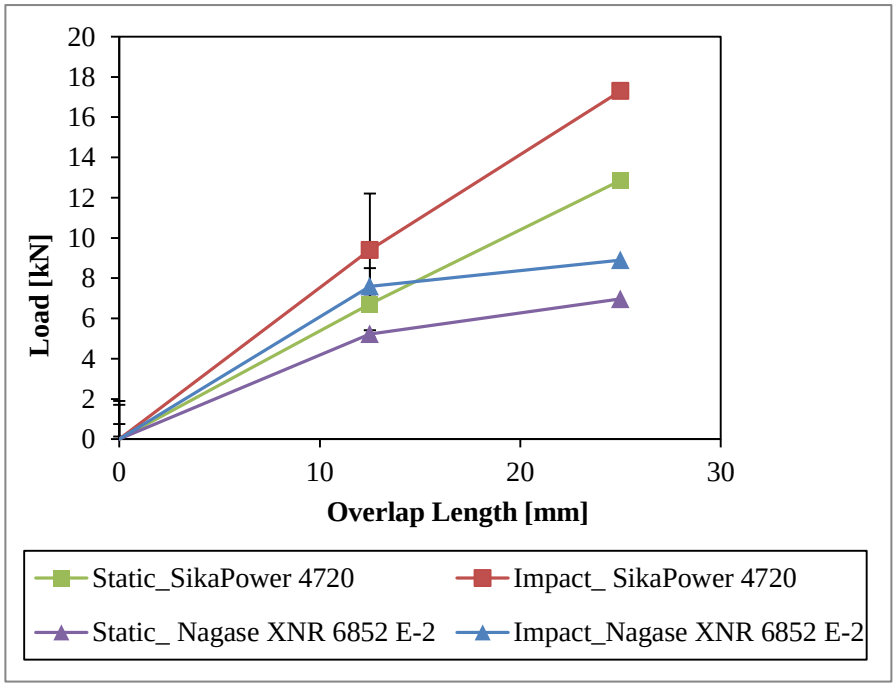

Figure 79- Comparison of the impact and static results for the two adhesives studied.

5.3 Joint strength prediction by CZM

This section focused the numerical analysis CFRP adhesive joints. Figure 80 gives an example of the overall correlation obtained between the experimental and numerical (CZM) P–δ curves for quasi-static results, by showing as an example L_0= 25 mm Power 4720® (a) and L_0= 25 mm XNR 6852 E-2 ® (b). Once again it is clear a difference between the numerical and experimental displacements. A more detailed analysis is done in section 3.1.2.

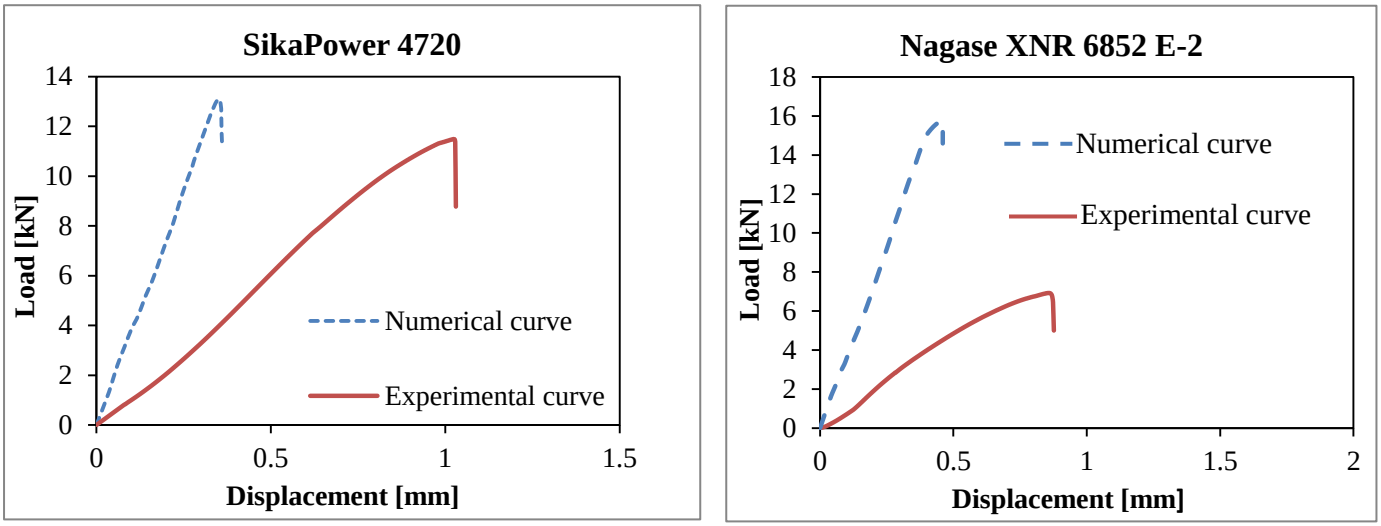

Figure 80- Experimental vs. Numerical quasi-static results for SikaPower® 4720 and Nagase ® XNR 6852 E-2, respectively.

In order to select the better value of G_{IIC} for using in the impact numerical simulations, this value was changed until a maximum force closer to the experimental value in the case of SikaPower 4720 25 mm overlap (17.3 kN). An example that was done for each value of G_{IIc} is shown in Figure 81.

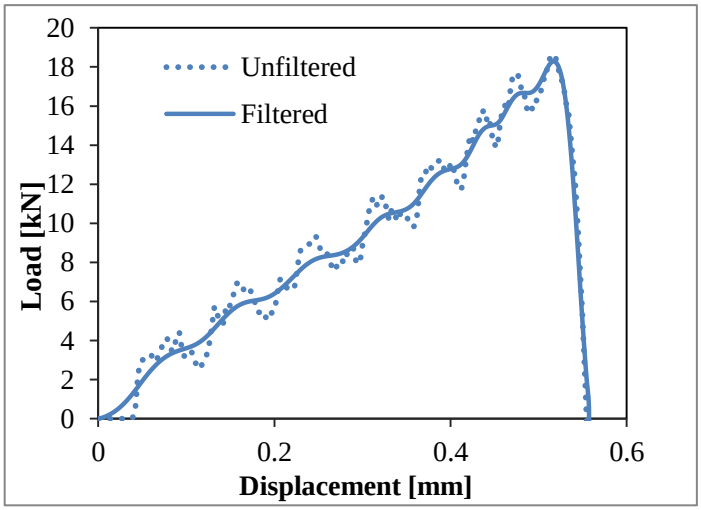

Figure 81- Impact curve obtained in Abaqus simulation for G_{IIc}=5 N/mm.

Table 20 shows the values obtained for failure load for three fracture toughness in mode II used in the numerical model. The value found for G_{IIc} that is more appropriate was 5.

Table 20- Results obtained in the numerical model for various values of G_{IIc}.

G_{IIc} (N/mm)	P_{max} (kN)
5	18.2
4	17.1
3	16.8

Figure 82 gives an example comparison between the experimental and numerical curve for SikaPower 4720 adhesive and 25 mm overlap length. It is evident a difference between the experimental and numerical displacements. In the case of experimental results, the machine measures the displacements of all their components which explain a big difference between numerical and experimental values.

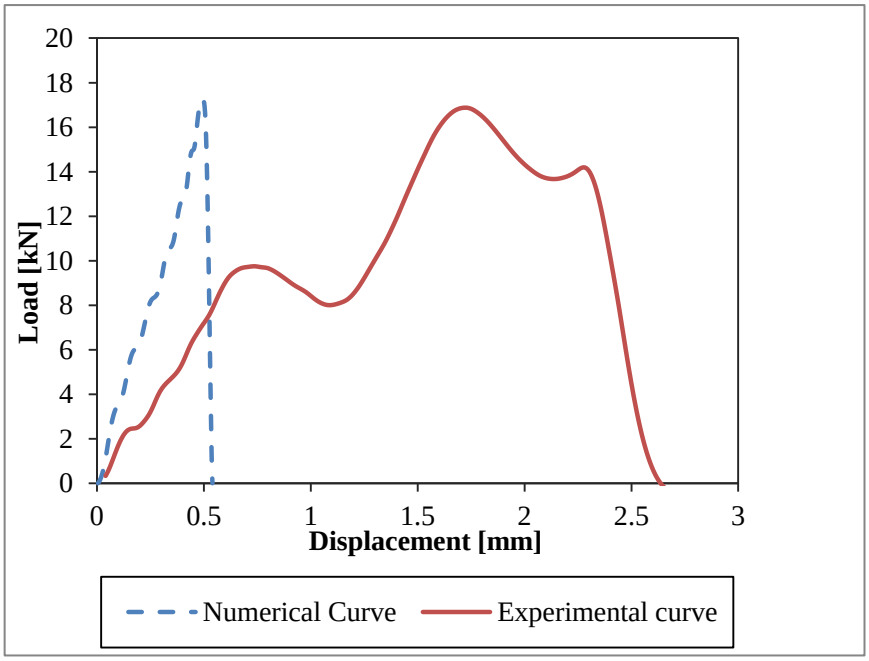

Figure 82- Experimental vs. Numerical impact results for SikaPower® 4720

Figure 83 and Figure 84 show a comparison between the experimental and numerical failure loads and the predictions using analytical method for the joints with two adhesives. For joints with SikaPower 4720 and Nagase XNR 6852 E-2, the strength prediction used was the global yielding criteria. For the joints with Nagase XNR 6852 E-2 and SikaPower 4720, the strength prediction gave reasonable values. The numerical prediction with CZM used to predict the strength of the joints with two adhesives had good results. The CZM model gives cohesive failure for two adhesives and overlap length studied as observed in the experiments.

Once again, the Nagase XNR® 6852 E-2 experimental results obtained were not as close to the numerical predictions, as referred in section 5.1.

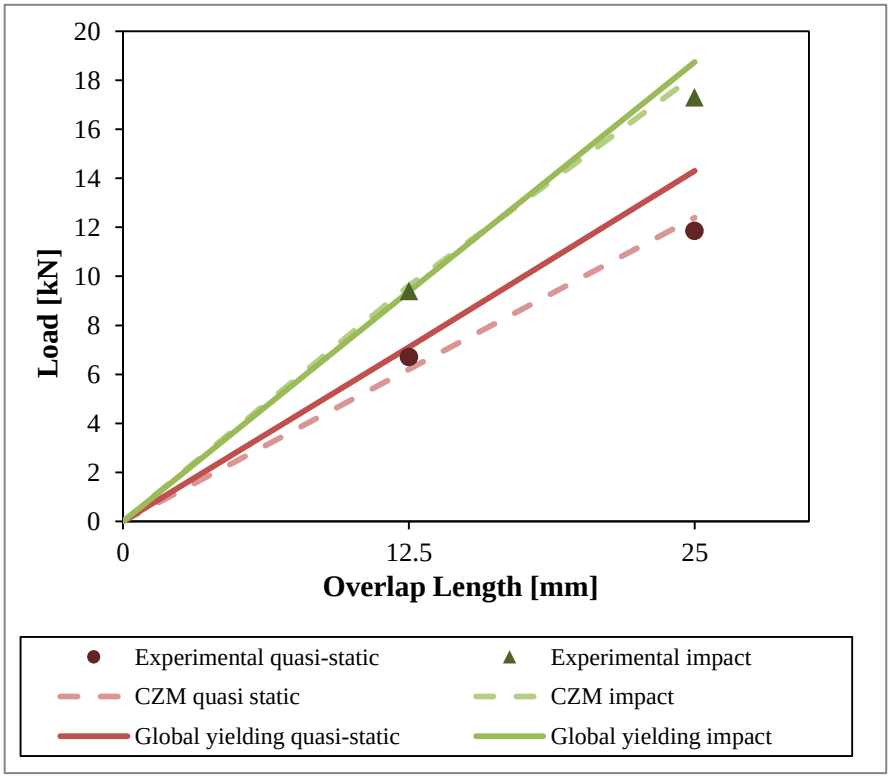

Figure 83- Experimental results vs. numerical prediction for adhesive SikaPower ® 4720.

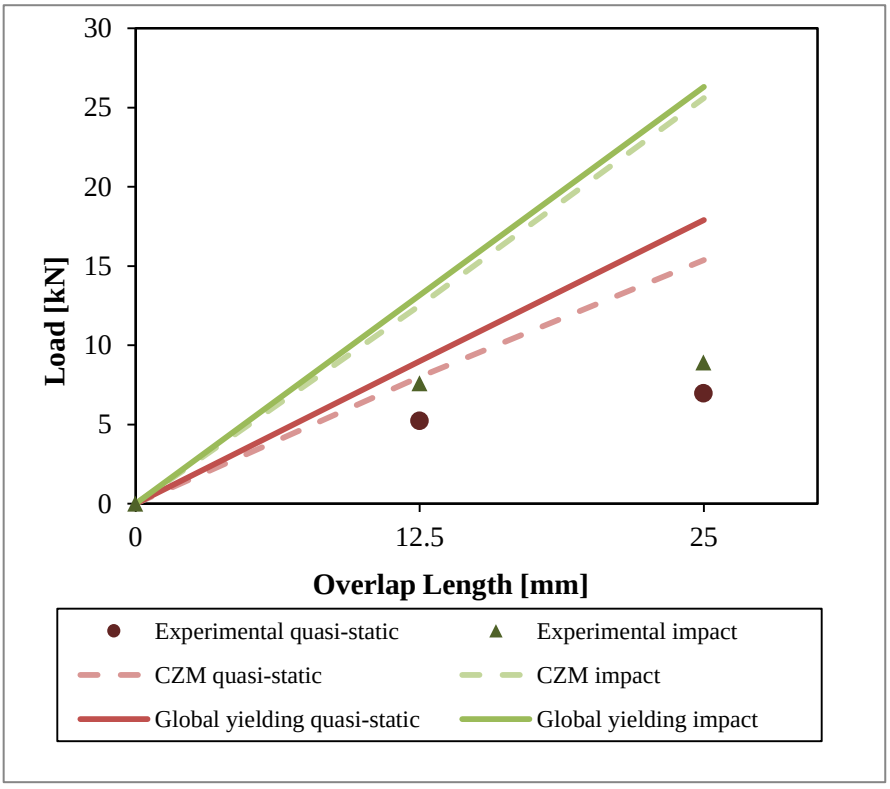

Figure 84- Experimental results vs. numerical prediction for adhesive Nagase® XNR 6852 E-2.

Chapter 6

CONCLUSIONS AND FUTURE WORK

6.1 Conclusions

In order to understand the behaviour of CFRP adhesive joints under impact conditions with applicability in the automotive industry, a theoretical and experimental analysis is required, particularly in the field of the strain rate dependence of structural adhesives. For this purpose, the basic concepts of adhesives and a state of art regarding impact and composites were firstly introduced, aiming to establish the necessary comprehension and familiarity with high strain rates and impact loads.

In order to characterize the adhesives, namely at different strain rates, different tests were performed. Tensile tests showed that the effects of strain rate can be significant on tensile and shear stresses. Regarding the toughness, only the properties of G_{IIC} were determined for both adhesives, since in mode I results can be obtained from other work. The value for Nagase was obtained experimentally while for SikaPower it was determined using the inverse method with FEM.

In line with the objective of this work, static and impact SLJ tests were performed with the same adherends but with different adhesives: SikaPower 4720 and Nagase XNR 6852 E-2. Towards the validation of the experimental results, the numerical simulations of the CFRP adhesive joints were performed. For the numerical modelling and simulation, ABAQUS® software was used. The mesh creation, boundary conditions definition and input of material properties were part of the modelling process. The numerical predictions were lastly compared with the experimental ones.

Therefore, in terms of impact tests it was concluded that the high strain rate considerably affects the responses of the SLJs when compared to static conditions. The effect of the overlap length on SikaPower 4720 was proportional to the bonded area in both quasi-static and impact tests. Although Nagase also showed high strain rate dependence, the results were unpredictable due to its bad adhesion with the composite.

Regarding the objective of obtaining delamination in the composite, it could not be achieved in any of the configurations. Increasing the overlap length and using an adhesive with better adhesion to the composite would increase the probability of finding composite delamination and, therefore, study its strain rate dependence.

The results obtained for numerical simulations agree with the experimental data and with the analytical predictions for SLJs with SikaPower 4720. The logarithmic extrapolation used in this case to obtain the adhesive properties under impact gave a good enough approximation of the adhesive strength at high strain rates.

6.2 Future work

Since the objective of obtaining failure in the composite was not accomplished, its dependence on strain rate variation could not be studied. Therefore, in future works the overlap length should be increased in order to verify if delamination occurs in the composite. Moreover, the use of an adhesive with a higher strength than the SikaPower 4720 combined with good adhesion with the composite would increase the odds of obtaining delamination.

Further studies may also be conducted to evaluate the use of the trapezoidal cohesive law for adhesive joints. This law would probably give better results on the failure load and displacement when trying to model SLJs with ductile adhesives.

In addition, fracture tests at high speed rate would also contribute to the validation of the numerical results obtained, in which G_{IIc} was determined to fit the experimental results.

REFERENCES

[1] A. J. Kinloch, *Adhesion and adhesives science and technology*. London: Chapman And Hall, 1987.

[2] L. F. M. da Silva, A. G. de Magalhães, e M. F. de S. F. de Moura, *Juntas adesivas estruturais*. Porto: Publindústria, Edições Técnicas, 2007.

[3] A. J. M. Ferreira, A. A. Fernandes, e A. T. Marques, *Modelling of sandwich structures and adhesive bonded joints*. Porto: Faculdade de Engenharia, 2000.

[4] L. da Silva, *Handbook of adhesion technology*. Heidelberg: Springer-Verlag, 2011.

[5] R. D. Adams e W. C. Wake, *Structural adhesive joints in engineering*. London: Elsevier Applied Science, 1984.

[6] S.Ebnesajjad, *Adhesives Technology Handbook*. 2008.

[7] M. Davis e D. Bond, «Principles and practices of adhesive bonded structural joints and repairs», *Int. J. Adhes. Adhes.*, vol. 19, n. 2–3, pp. 91–105, 1999.

[8] «Adhesive Bonding Workshop, October 2004, Sussex.» [Em linha]. Disponível em: https://www.niar.wichita.edu/niarworkshops/Workshops/AdhesiveBondingWorkshop, October2004,Sussex/tabid/112/Default.aspx. [Acedido: 08-Jul-2015].

[9] W. A. Lees, *Adhesives in engineering design*. London: <<The>> Design Council Springer-Verlag, 1984.

[10] M. D. Banea e L. F. M. da Silva, «Adhesively bonded joints in composite materials: an overview», *Proc. Inst. Mech. Eng. Part L J. Mater. Des. Appl.*, vol. 223, n. 1, pp. 1–18, 2009.

[11] R. D. S. G. Campilho, *Repair of composite and wood structures*. Porto: [s. n.], 2009.

[12] L. F. M. da Silva, P. J. C. das Neves, R. D. Adams, e J. K. Spelt, «Analytical models of adhesively bonded joints—Part I: Literature survey», *Int. J. Adhes. Adhes.*, vol. 29, n. 3, pp. 319–330, 2009.

[13] H. Coover, *Handbook of adhesives*, vol. 2nd ed. New York: Van Nostrand Reinhold Company, 1977.

[14] E. M. Petrie, *Handbook of adhesives and sealants*, vol. 2nd ed. New York: McGraw Hill, 2000.

[15] S.R.Hartshorn, *Structural adhesives chemistry and technology*. New York: Plenum Press, 1986.

[16] A. L. Loureiro, L. F. M. Da Silva, C. Sato, e M. A. V Figueiredo, «Comparison of the mechanical behaviour between stiff and flexible adhesive joints for the automotive industry», *J. Adhes.*, vol. 86, n. 7, pp. 765–787, 2010.

[17] C. S. Adderley, «Adhesive Bonding», *Mater. Des.*, vol. 9, n. 5, pp. 287–293, 1988.

[18] A. D. Andreas Lutz Christof Brandli, «Structural Bonding in Lightweight Vehicle Construction», 2013.

[19] L. Da Silva e A. Öchsner, *Modeling of adhesively bonded joints*. Berlin: Springer, 2008.

[20] L. F. M. da Silva, P. J. C. das Neves, R. D. Adams, A. Wang, e J. K. Spelt, «Analytical models of adhesively bonded joints—Part II: Comparative study», *Int. J. Adhes. Adhes.*, vol. 29, n. 3, pp. 331–341, 2009.

[21] M. G. and E.Reissner, «The stresses in cemented joints», *J. Appl.Mech.*, vol. 11, pp. 11–27, 1944.

[22] L. J. Hart-Smith, *Adhesive-bonded single-lap joints*. Langley Research Center Hampton, VA, 1973.

[23] U. K. Vaidya, A. R. S. Gautam, M. Hosur, e P. Dutta, «Experimental–numerical studies of transverse impact response of adhesively bonded lap joints in composite structures», *Int. J. Adhes. Adhes.*, vol. 26, n. 3, pp. 184–198, 2006.

[24] L. F. M. da Silva, R. J. C. Carbas, G. W. Critchlow, M. A. V Figueiredo, e K. Brown, «Effect of material, geometry, surface treatment and environment on the shear strength of single lap joints», *Int. J. Adhes. Adhes.*, vol. 29, n. 6, pp. 621–632, 2009.

[25] L. D. R. Grant, R. D. Adams, e L. F. M. da Silva, «Experimental and numerical analysis of single-lap joints for the automotive industry», *Int. J. Adhes. Adhes.*, vol. 29, n. 4, pp. 405–413, 2009.

[26] C. D. M. Liljedahl, A. D. Crocombe, M. A. Wahab, e I. A. Ashcroft, «Damage modelling of adhesively bonded joints», *Int. J. Fract.*, vol. 141, n. 1–2, pp. 147–161, 2006.

[27] J. P. M. Gonçalves, M. De Moura, P. De Castro, e A. T. Marques, «Interface element including point-to-surface constraints for three-dimensional problems with damage propagation», *Eng. Comput.*, vol. 17, n. 1, pp. 28–47, 2000.

[28] M. F. S. F. de Moura, J. P. M. Gonçalves, A. T. Marques, e P. M. S. T. de Castro, «Prediction of compressive strength of carbon–epoxy laminates containing delamination by using a mixed-mode damage model», *Compos. Struct.*, vol. 50, n. 2, pp. 151–157, 2000.

[29] J. Neto, R. Campilho, e L. F. M. Da Silva, «Parametric study of adhesive joints with composites», *Int. J. Adhes. Adhes.*, vol. 37, pp. 96–101, 2012.

[30] M. V Hosur, S. M. Waliul Islam, U. K. Vaidya, A. Kumar, P. K. Dutta, e S. Jeelani, «Dynamic punch shear characterization of plain weave graphite/epoxy composites at room and elevated temperatures», *Compos. Struct.*, vol. 70, n. 3, pp. 295–307, 2005.

[31] M. J. Hiley, L. Dong, e J. Harding, «Effect of strain rate on the fracture process in interlaminar shear specimens of carbon fibre-reinforced laminates», *Compos. Part A Appl. Sci. Manuf.*, vol. 28, n. 2, pp. 171–180, 1997.

[32] J. M. Lifshitz e H. Leber, «Response of fiber-reinforced polymers to high strain-rate loading in interlaminar tension and combined tension/shear», *Compos. Sci. Technol.*, vol. 58, n. 6, pp. 987–996, 1998.

[33] J. A. Harris e R. D. Adams, «An assessment of the impact performance of bonded joints for use in high energy absorbing structures», *Proc. Inst. Mech. Eng. Part C J. Mech. Eng. Sci.*, vol. 199, n. 2, pp. 121–131, 1985.

[34] L. da Silva, D. Dillard, B. Blackman, e R. Adams, *Testing adhesive joints best practices*. Weinheim: Wiley-VCH Verlag GmbH & Co. KGaA, 2012.

[35] M. Zgoul e A. D. Crocombe, «Numerical modelling of lap joints bonded with a rate-dependent adhesive», *Int. J. Adhes. Adhes.*, vol. 24, n. 4, pp. 355–366, 2004.

[36] R. Avendaño Mata, *Impact of adhesive joints for the automotive industry at low and high temperatures*. Porto: FEUP, 2014.

[37] C. M. S. Canto, *Strength and fracture energy of adhesives for the automotive industry*. Porto: FEUP, 2013.

[38] D. F. S. Saldanha, C. Canto, L. F. M. da Silva, R. J. C. Carbas, F. J. P. Chaves, K. Nomura, e T. Ueda, «Mechanical characterization of a high elongation and high toughness epoxy adhesive», *Int. J. Adhes. Adhes.*, vol. 47, n. 0, pp. 91–98, 2013.

[39] T. Carlberger, A. Biel, e U. Stigh, «Influence of temperature and strain rate on cohesive properties of a structural epoxy adhesive», *Int. J. Fract.*, vol. 155, n. 2, pp. 155–166, 2009.

[40] E. Car, F. Zalamea, S. Oller, J. Miquel, e E. Oñate, «Numerical simulation of fiber reinforced composite materials—two procedures», *Int. J. Solids Struct.*, vol. 39, n. 7, pp. 1967–1986, 2002.

[41] F. L. Matthews, G. A. O. Davies, D. Hitchings, e C. Soutis, *Finite element modelling of composite materials and structures*. Elsevier, 2000.

[42] R. D. S. G. Campilho, *Modelação da execução de reparações em materiais compósitos*. Porto: [s.n.], 2005.

[43] W. J. Cantwell e J. Morton, «The impact resistance of composite materials—a review», *composites*, vol. 22, n. 5, pp. 347–362, 1991.

[44] M. Nirbhay, A. Dixit, R. K. Misra, e H. S. Mali, «Tensile Test Simulation of CFRP Test Specimen Using Finite Elements», *Procedia Mater. Sci.*, vol. 5, pp. 267–273, 2014.

[45] M. J. Laffan, S. T. Pinho, P. Robinson, e A. J. McMillan, «Translaminar fracture toughness testing of composites: a review», *Polym. Test.*, vol. 31, n. 3, pp. 481–489, 2012.

[46] L. F M da Silva e R. D Adams, «Techniques to reduce the peel stresses in adhesive joints with composites», *Int. J. Adhes. Adhes.*, vol. 27, n. 3, pp. 227–235, 2007.

[47] T.-W. Shyr e Y.-H. Pan, «Impact resistance and damage characteristics of composite laminates», *Compos. Struct.*, vol. 62, n. 2, pp. 193–203, 2003.

[48] A. N. S. Nascimento, *Efeito da espessura do adesivo na resistência de juntas de sobreposição simples, na ligação materiais compósitos*. Porto: FEUP, 2013.

[49] J. A. B. P. Neto, *Estudo paramétrico de juntas adesivas em material compósito*. Porto: [s. n.], 2011.

[50] J. Harding e L. M. Welsh, «A tensile testing technique for fibre-reinforced composites at impact rates of strain», *J. Mater. Sci.*, vol. 18, n. 6, pp. 1810–1826, 1983.

[51] N. Taniguchi, T. Nishiwaki, e H. Kawada, «Tensile strength of unidirectional CFRP laminate under high strain rate», *Adv. Compos. Mater.*, vol. 16, n. 2, pp. 167–180, 2007.

[52] F. J. P. Chaves, *Fracture mechanics applied to the design of adhesively bonded joints*. Porto: FEUP, 2013.

[53] J. Xavier, M. Oliveira, J. J. L. Morais, e M. F. S. F. de Moura, «Determining mode II cohesive law of Pinus pinaster by combining the end-notched flexure test with digital image correlation», *Constr. Build. Mater.*, vol. 71, n. 0, pp. 109–115, 2014.

[54] A. Karac, B. R. K. Blackman, V. Cooper, A. J. Kinloch, S. Rodriguez Sanchez, W. S. Teo, e A. Ivankovic, «Modelling the fracture behaviour of adhesively-bonded joints as a function of test rate», *Eng. Fract. Mech.*, vol. 78, n. 6, pp. 973–989, 2011.

[55] H. Körber, *Mechanical response of advanced composites under high strain rates*. Porto: [s. n.], 2010.

[56] M. F. S. F. de Moura, M. A. L. Silva, A. B. de Morais, e J. J. L. Morais, «Equivalent crack based mode II fracture characterization of wood», *Eng. Fract. Mech.*, vol. 73, n. 8, pp. 978–993, 2006.

APPENDIX A

Static Results

P-δ

SikaPower® 4720 l_0=12,5 mm

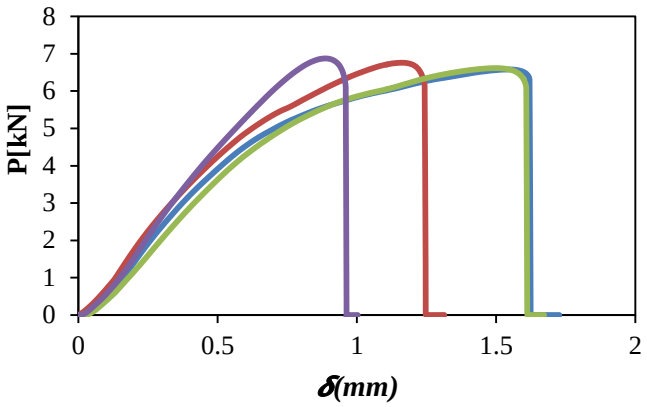

P-δ

SikaPower® 4720 l_0=25mm

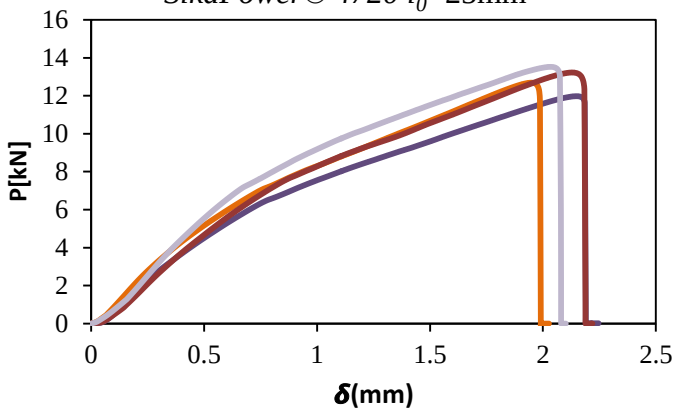

P-δ

Nagase Chemtex 4852 E-2 l_0=12.5mm

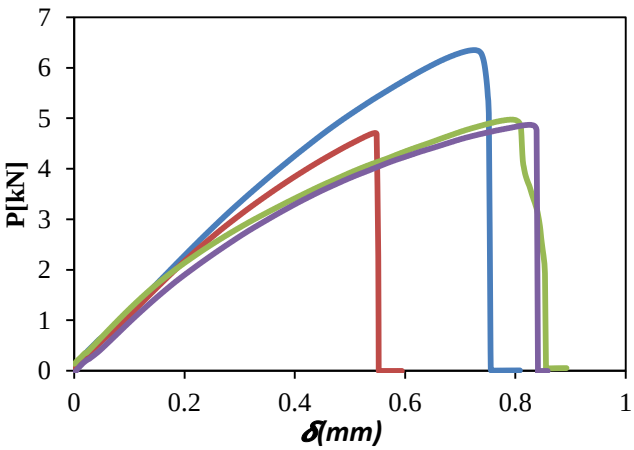

P-δ

Nagase Chemtex 4852 E-2 l_0=25mm

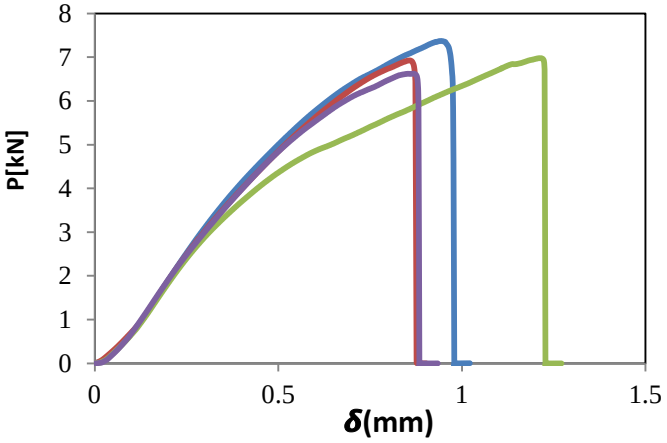

Impact Results